C.P. No. 582

C.P. No. 582

MINISTRY OF AVIATION

AERONAUTICAL RESEARCH COUNCIL

CURRENT PAPERS

Wind Tunnel Tests at Mach Numbers between 0·6 and 1·4 of a 60° Swept Wing having an Aerofoil Section Designed for Subcritical Flow at a Mach Number of 1·2

Part I: 9% Thick Section with "Triangular" Pressure Distribution

by

E. F. Lawlor

LONDON: HER MAJESTY'S STATIONERY OFFICE

1962

U.D.C. No. 533.692.1:533.693.1:533.6.011.35:533.6.011.5:533.69.048.2
533.6.011.12:533.6.071.33

C.P. No. 582

May, 1961

WIND TUNNEL TESTS AT MACH NUMBERS BETWEEN 0.6 AND 1.4 OF A 60° SWEPT WING HAVING AN AEROFOIL SECTION DESIGNED FOR SUBCRITICAL FLOW AT A MACH NUMBER OF 1.2

PART I: 9% THICK SECTION WITH "TRIANGULAR" PRESSURE DISTRIBUTION

by

E. F. Lawlor

SUMMARY

Pressures have been measured at Mach numbers between 0.6 and 1.4 around one streamwise station on a 9% thick, 60° swept wing, cambered to have a subcritical type of upper surface pressure distribution of triangular shape at a Mach number of 1.2 and a lift coefficient of 0.153. In spite of boundary layer effects which caused some loss of lift coefficient, subcritical flow conditions were achieved at the design Mach number of 1.2 with the design suction values over the forward part of the section. At all Mach numbers, the flow development was closely analogous to that over two dimensional aerofoils at subsonic speeds.

Previously issued as R.A.E. Tech. Note No. Aero.2756 - 23,177.

LIST OF CONTENTS

LIST OF APPENDICES

LIST OF TABLES

LIST OF ILLUSTRATIONS

LIST OF ILLUSTRATIONS (Contd)

1 INTRODUCTION

One possible solution to the aerodynamic problem of designing a supersonic long-range aircraft involves the use of a highly swept, high aspect-ratio wing, on the assumption that infinite-swept-wing flow conditions can be maintained all over the wing at the cruising lift coefficient. It has been predicted theoretically[1] that for a sufficiently thin and highly swept wing of infinite aspect ratio a subcritical type of flow can persist up to a supersonic free-stream Mach number, so long as the component of velocity normal to the peak suction line is less than sonic. Under these conditions the wing wave drag remains zero. By extending this concept to swept wings of finite aspect ratio, the aerodynamic outline of a supersonic transport aircraft can be determined as in Ref.2, where the design cruising Mach number is 1.2, although the actual value does not affect the design philosophy in principle.

The first stage in developing a suitable wing for this type of aircraft configuration is to choose a basic wing section shape, together with an angle of sweep, to give an essentially subcritical type of flow at the chosen cruising speed and lift coefficient on a swept wing of infinite span. Theoretical methods have been devised[3,4] for determining the geometry of aerofoil sections having a specified pressure distribution in an inviscid, incompressible flow. Methods applicable to two-dimensional wings are extended to swept wings of infinite span by the addition of a flow component parallel to the wing leading edge. There are also methods[5,6] for determining the sonic range ($M = 1$) pressure distribution from a specified two-dimensional aerofoil shape and one of these has been extended[7] to cover the Mach number range between critical and sonic. The relationship between wing sweep, thickness-chord ratio and lift coefficient for various types of upper surface pressure distribution is discussed in Ref.8.

These methods can be used in the project or early layout stages of an aircraft design to provide estimates of the inter-relation between aerofoil geometry and subcritical pressure distribution, and to predict also the Mach numbers at which drag rise begins or at which separation effects such as buffeting might be expected to appear. In general, good agreement can be obtained between experiment and theory for both moderately swept and unswept wings at low speeds, providing the characteristics of the boundary layer are determined and taken into account (see for example Refs.9 and 10).

The present series of tests is aimed at extending the comparison between experiment and theory to higher angles of sweep and higher Mach numbers, and in particular to cover the case where the free-stream Mach number is supersonic but the flow over the wing is still expected to be subcritical. There are three main objectives:-

(a) To demonstrate experimentally that a subcritical type of flow, without shocks, can exist at a supersonic free-stream Mach number on a lifting wing;

(b) to determine the extent to which viscosity and compressibility modify the theoretical pressure distribution around the aerofoil section of an infinite swept wing when the flow is subcritical; and

(c) to investigate the influence of the local supercritical region, produced by increasing Mach number or lift coefficient above the values for (a), on the drag and shock-induced boundary-layer separation characteristics of the section.

These tests are being conducted on half models (Fig.1), having untwisted and substantially untapered wings, of aspect ratio near 5 and 60° sweepback, mounted on a body. The aerofoil sections are in general designed to have a subcritical type of flow up to a Mach number of around 1.2 using the method of Ref.4 modified to take account of compressibility effects - see Appendix 2. Measurements of pressure only are made all round a streamwise section at 71% semi-span.

For the tests reported in the present note, the wing section is of basically RAE 101 thickness distribution, 9% thickness-chord ratio, and cambered to have a "triangular" or "linear" shape of upper surface pressure distribution at a C_L of 0.153 at a Mach number of 1.2 (Figs.2 and 3). The results show that, in general terms, subcritical flow conditions can be maintained at supersonic Mach numbers, for instance at M_o = 1.2 and C_L = 0.085, although at the design C_L of 0.153 a small supercritical region exists which is insufficient to cause an appreciable rise in drag. No attempt has been made in this test to determine the characteristics of the boundary layer quantitatively; this will be done later, however, for another model having a thinner section.

The tests form part of the programme of the Cruising Aerodynamics Group of the Supersonic Transport Aircraft Committee (S.T.A.C.). They were planned initially for the 8 ft × 8 ft supersonic tunnel at R.A.E. (Bedford). However, as the scope of the activities of the S.T.A.C. widened, it became desirable to transfer the actual testing to the 9 ft × 8 ft transonic tunnel of the Aircraft Research Association, Ltd., Bedford. This tunnel has a perforated-wall working section, and a flexible nozzle which together with auxiliary suction from the plenum chamber surrounding the working section enables Mach numbers of up to 1.4 to be achieved. A description of the tunnel is contained in Ref.11. The tests were made in May, 1958.

Section 2 of this note describes the design of the model and some of the problems which were encountered. The test procedure is outlined in section 3, and some comments on the accuracy of the results are given in section 4. The results are presented and discussed in section 5, which also includes a review of the expected development of the flow over an infinite sheared wing. Finally, section 6 contains the conclusions and considers certain further tests which are desirable.

2 MODEL DESIGN

2.1 Experimental approach to achieving sheared-wing conditions

Sheared-wing conditions demand that the pressures experienced by the section should be constant along lines parallel to the edges of the wing. In general these conditions are not achieved near the root of a swept wing, so that, unless the root of the wing is carefully shaped, the isobars in this region are less highly swept than the wing and unswept altogether at the root itself. Similarly, near the tip of the wing the isobars may again be insufficiently swept unless a careful choice of tip planform and camber is made. On many low aspect ratio wings these root and tip effects overlap so much that nowhere does the flow closely resemble yawed wing conditions.

In the tests reported here, the aim has been to measure the pressures at a spanwise station as far away from the root as possible while maintaining sufficient span outboard to ensure that at all supersonic speeds the Mach cone from the tip passes well downstream of this station. It was considered that sheared-wing flow was unlikely to be achieved, even approximately, inboard of the spanwise station at which the wing root trailing edge disturbance (the "rear shock" in Fig.4(a)) had passed forward of the leading edge. (This assumes it spread along a Mach wave.) It was therefore decided to design an untapered wing of the required sweepback on which measurements of pressure would be made at a single streamwise section lying aft of the root disturbance and ahead of the tip disturbance. Nevertheless, it was realised that there must be significant viscous effects since these considerations were leading to a combination of high sweep with high aspect ratio which in turn demanded a relatively thick section if model strength, and hence Reynolds number, were not to be unduly sacrificed.

Although it would have been desirable to reduce the magnitude of the wing root disturbance by having a body in which a cylindrical shape could be replaced by a "waisted" shape, it was hoped that this would not be necessary in this experiment. Provision was nevertheless made for fitting alternative body shapes, although only the cylindrical shape was used. Later tests of similar models have included "waisted" configurations.

2.2 Model layout

The basic model is sketched in Fig.1. It is a half-wing-body combination on which pressure measurements are made at 49 points on a single streamwise section on the untapered part of the wing. This configuration was preferred to a complete sting-mounted model because of the larger scale which was possible for a half model. The basic shape of the wing section to give the pressure distribution shown in Fig.2 has been determined by Weber's method given in Appendix 2.

Ordinates of the wing section at 32 pivotal points, which are relevant to the methods of Ref.4 and Appendix 2, have been determined from inspection of the model and are given in Table 1. The wing was found to be thin (8.94% instead of 9%) and to have a twist of -0.06° at the pressure measuring station; after making allowance for these considerations all ordinates were correct to within ±0.002". The ordinates of the pressure holes as determined from the inspection report are listed in Table 2.

The design of the model was arranged to ensure that the shock pattern from the wing root would not be reflected from the walls of an 8 ft × 8 ft tunnel in such a way as to strike the model in the region of the pressure plotting station above $M_o = 1.1$. This condition set limits to model size, sweepback and spanwise position of the pressure plotting station. The design was also arranged to ensure that disturbances originating at the wing root trailing edge passed (assuming they spread along a Mach wave) in front of the pressure plotting station at Mach numbers up to 1.5. This condition also set limits to the sweepback and spanwise position of the pressure plotting station. A compromise between these conflicting factors resulted in a wing of 12 ins root chord, sweepback 60°, and with a pressure measuring station 1.825 chords (21.9 inches) outboard of the effective model centreline. This in turn influenced the choice of thickness-chord ratio towards a fairly high value (9% along wind) in order to ensure adequate model strength. Since a condition of the design of wing section[2] is that nowhere over the surface of the wing should the Mach number, resolved in a direction normal to the leading edge, appreciably exceed unity ($C_p \nless C_p^*$), a limit was set to the lift coefficient which could be achieved at the design Mach number. The values finally chosen were a C_L of 0.153 at $M_o = 1.2$ with almost wholly subcritical inviscid flow. The upper surface pressure distribution (Fig.2) is of a "triangular" shape, and was obtained by adding a suitable camber line (Fig.3) to a basically RAE 101 thickness distribution. The curvature in the camber line towards the trailing edge produced a concavity in the lower surface of the section, which was "filled in" to provide a plane surface to ease manufacture. The change in camber produced by this modification was less than 0.1% at the maximum, and the effect on the upper surface pressures was not significant.

This particular combination of sweep, thickness and lift coefficient is of course only relevant in so far as it is intended to produce the desired flow conditions for the tunnel model. Further tests are being made on thinner wings which may be more relevant as a choice for an aircraft configuration.

The extent of the wing outboard of the pressure measuring station is determined by the condition that the Mach cone from the tip region should pass wholly downstream of this station when the Mach number exceeds 1.10. The actual tip shape has been chosen so as to inhibit a loss of sweep of the isobars with consequent possible spread of the disturbances inboard. The overall semispan of the model is 30.9 ins (2.575 chords) and the pressure plotting station is at 0.71 semispan.

The basic body is of 0.4 chords (4.8 ins) diameter and consists of a nose of length 4 chords (length-diameter ratio 10) plus a parallel portion which extends from 0.5 chord in front to nearly 4 chords behind the wing root leading edge, terminating in a bluff base (Fig.5). The body cross-section is D-shaped; where the body is parallel the section consists of a semicircle 2.4 ins (0.2 chord) radius displaced outwards from the wall by the addition of a 2 in. thick parallel slab, in order to minimise any effects of the tunnel boundary layer. Further forward, along the length of the nose, the body section shape is similar but decreases smoothly in area to zero at the nose; this variation is given, in units of body maximum radius, by

$$y = \left(\frac{x}{20} - 1\right)^3 + 1$$

where x = distance aft of the nose

y = local body radius.

This variation ensures that the curvature of the nose shape in plan view tends to zero at the front of the nose and again at the junction with the parallel part of the body. This type of nose was chosen to minimise the influence of the body pressure field (reflected from the walls of the tunnel) on to the pressure plotting station. The nose shock, reflected from the roof of the tunnel, clears the pressure plotting station at all Mach numbers above 1.12. Its reflection from the side walls of the tunnel, however, passes along the pressure plotting chord line between Mach numbers of 1.28 and 1.34. At the design Mach number of 1.2, the pressure plotting station is subjected to the reflected field from a region about half way along the length of the nose. This region produces a weak expansion field, which in the A.R.A. tunnel is reflected weakly as a shock; it is believed that this "second-order" disturbance does not appreciably influence the measured pressures.

The wing was made of S96 steel, heat-treated to give an ultimate tensile strength of over 70 tons/sq in. Grooves were cut in the wing to allow 0.080 in. o/d (0.053 in. i/d) copper-nickel tubes to be laid in the wing from each pressure hole (1/32 in. dia.), the pressure tubes being faired over afterwards with araldite. The body was largely constructed in light alloy.

The model was mounted on the floor of the A.R.A. 9 ft × 8 ft tunnel. Bracing wires attached to the model near the wing tip passed out through perforations in the tunnel walls and were secured at each incidence to restrain the wing from deflecting under load. The wires and attachments at the model did not exceed 0.25 in. dia. and were situated at 30% chord 6 ins. outboard (measured normal to body axis) of the pressure measuring station, this location being chosen so that the disturbances from the wires should pass wholly downstream of the pressure measuring station at all supersonic Mach numbers. Some studies of oil flow patterns at $M_0 = 1.25$ and 1.4 (Figs.27 and 28) would seem to indicate that the flow at the pressure plotting station was not significantly influenced by the wires.

3 TEST PROCEDURE AND RANGE OF TESTS

The procedure adopted was to fix the model incidence and tunnel pressure, and then vary the Mach number from 0.6 to 1.4, taking care as far as possible that the intervals of Mach number were close enough in the neighbourhood of the drag rise and separation Mach numbers to enable values of M_D and M_{SE} to be obtained. The bracing wires from the wing tip had to be re-rigged at each change of incidence, and therefore the tunnel was shut down between incidence runs.

The theoretical design incidence α_T for the wing of infinite span was $1.83°$; in order to investigate the flow over a wide range of conditions, tests were made at a range of incidences from $0°$ to $5°$. A carborundum strip (particles 0.002 to 0.003" high) was applied around the leading edge and extending back to 5% chord on both surfaces but with a small gap in the immediate proximity of the pressure holes) in order to fix transition. Figs.27 and 28 show that there is a striated flow pattern behind the carborundum strip which is consistent with turbulent flow; whereas at the extreme wing tip, outboard of the carborundum strip, the pattern is not striated so strongly forward of the turbulent "wedge" springing from the end of the strip. On this evidence it would appear that turbulent flow was successfully achieved over most of the wing.

At each Mach number, complete pressure readings of the section were recorded by photographing a multi-tube mercury manometer. Most of the tests were made at atmospheric stagnation pressure, so that the Reynolds number (based on wing chord) varied from 3.8×10^6 at $M = 0.6$ to 5×10^6 at $M = 1.0$, remaining close to 5×10^6 at all supersonic speeds. In addition, however, one run was carried out at an incidence of $2.6°$ at a stagnation pressure of 36" mercury. For this run the Reynolds number varied from 4.5×10^6 to 6×10^6. The variation of Reynolds number with Mach number and stagnation pressure is shown in Fig.19.

4 ACCURACY

The mercury manometer readings were recorded on film which was subsequently projected on to a screen from which the readings were recorded manually. It was possible to read the height of the mercury columns to ±0.02 in. and this results in an error of ±0.002 in p/H_{eff} (see para.5.1). When integrating pressures around the section to determine force coefficients, the trapezium rule has been used for simplicity and convenience, thus enabling coefficients to be compared on a consistent basis, even though there is some loss of absolute accuracy. Because of the large number of pressure holes and their close spacing (approx. 0.005c) around the nose, the force coefficients are always correct to within ±2%, and in all but a few cases to within ±1%.

For Fig.12 to 15 the values of pressure coefficient (C_p) have been obtained by a process of "smoothing" the experimental results, as described in para.5.3. It is therefore necessary to take into account the accuracy of the smoothing process in assessing the accuracy of the data plotted on these figures.

5 RESULTS AND DISCUSSION

5.1 Presentation of results

It is convenient to present the pressures measured at each pressure plotting hole in the form of p/H_{eff}, where p is the local pressure and H_{eff} is a "reduced" form of the total head which effectively corresponds to the two-dimensional value at a free stream Mach number of $M_o \cos \Lambda$ (Λ = sweepback angle). The value of H_{eff} is determined from the actual total head H_o by the following relation:-

$$\frac{H_{eff}}{H_o} = \left(\frac{1 + \frac{\gamma - 1}{2} M_o^2 \cos^2 \Lambda}{1 + \frac{\gamma - 1}{2} M_o^2} \right)^{\frac{\gamma}{\gamma - 1}} .$$

A derivation of this relation is given in Appendix 1.

Provided that yawed wing conditions have been achieved these values of p/H_{eff} are directly comparable with the values of p/H_o in two-dimensional flow at $M_o \cos \Lambda$.

5.1.1 Pressure distributions

The pressure distributions measured at various Mach numbers are plotted in the form of p/H_{eff} for each incidence in Figs.6 to 11. The pressures are shown in carpet form plotted against x/c (chordwise position) and Mach number. The values of p/H_{eff} at each pressure hole, and the position of each hole as determined by inspection of the model after manufacture, are given in Table 3. Figs.12 to 15 show comparisons of theoretical and experimental pressure distributions at Mach numbers near 0.6 and 1.2 - the pressures in this case being in the form of C_p since the theoretical distributions determined by the method of Appendix 2 are in this form. In Figs. 12 to 15 only, however, some adjustments have been made to the measured pressures which have the effect of smoothing the variation of pressure at any pressure hole with variation of Mach number. This procedure is discussed in greater detail in para.5.3.

5.1.2 Integrated loads

The pressure distributions around the section have been integrated normal to and along the chord at each Mach number and incidence, and the results are tabulated in coefficient form as $\overline{C_Z}$ and $\overline{C_X}$ in Table 4. The coefficients are plotted against Mach number for various incidences in Figs.16 and 17, while $\overline{C_Z}$ is plotted against incidence for a Mach number near 1.2 and compared with theory for inviscid flow and infinite aspect ratio in Fig.18.

5.2 Effect of Reynolds number

An additional run at an incidence of 2.6° only was made at a stagnation pressure of 36 ins. mercury, the Reynolds number varying from 4.5×10^6 at $M_o = 0.6$ to about 6×10^6 at supersonic speeds (Fig.19). The corresponding run at the lower Reynolds number (30 ins. mercury) was only made at Mach numbers from 0.98 upwards. It was found that nowhere did this admittedly small variation in Reynolds number cause any significant variation in either upper or lower surface pressure distributions (Table 3). The curves of Fig.6, 7, 9, 10 and 11 are all for 30 ins. mercury stagnation pressure. However, the curves of Fig.8 ($\alpha_E = 2.6^o$) are for 36 ins. mercury, except for $M_o = 1.405$ which is for 30 ins.

5.3 Disturbances in flow development

5.3.1 Disturbances affecting pressure distribution

Figs.6 to 11 show that the development of pressure distribution with Mach number is not entirely regular. In general, the pressures around 40% chord seem to be slightly greater (less suction) than expected. Inspection of the model revealed nothing likely to account for this, but it is possible that a leak may have developed during the test in the appropriate pressure tube.

More significantly, there are areas over which the rate of decrease of pressure with Mach number is temporarily reduced, as for example near $M_o = 0.98$ over the rearmost 20% of the chord. Because of the high sweep and aspect ratio of the model, the trailing edge of the pressure plotting station was located 14 inches further downstream in the tunnel working section than would have been recommended[11] for a complete model. However, any deterioration of the flow near this region is mainly associated with the complete-model support strut, which of course was not present for these tests. It seems more probable that the local high pressure region near the trailing edge at $M_o = 0.98$ is due to a simple blockage effect.

Over the most forward 30% of the chord a similar local high pressure region occurs at all incidences near $M_o = 1.02$. Application of a blockage correction does not account satisfactorily for this effect. Some tests at close intervals of Mach number on a later wing in the series have shown that a similar region moves rearwards over the section as M_o is increased from 1.02 to 1.04. The rate of movement suggests a disturbance originating from the forward part of the model and being reflected from the tunnel sidewalls. The source of this disturbance is probably the suction region expected to occur at this Mach number over the rear part of the section at the wing root. At the sidewalls this suction would be reflected as a compression[12]. A properly waisted body would thus be expected to improve matters. Some disturbance would also be expected from the bow shock associated with the bracing wire near the tip, but the chordwise extent of the disturbance (about 0.3 c) seems rather large for it to be accounted for entirely by the wire.

Another region of relatively high pressure occurs over the upper surface of the wing between 25% and 50% chord at $M_o = 1.19$. The cause in this case appears to be a disturbance originating from the saw-tooth junction in the tunnel floor and being reflected from the roof. Moreover, the analysis in the next section (5.3.2) reveals that on the lower surface there is a low pressure region further aft (45% to 70% chord) which could arise from a different part of the same disturbance (Fig.25). Other deviations in pressure between 50% and 80% chord near $M_o = 1.35$ on the lower surface have probably arisen from the disturbance due to the other saw-tooth junction in the roof being reflected from the floor.

At low incidences (0° and 2°) the suction at 6% chord seems to be slightly low over most of the Mach number range; at 2.6° this "trough" has moved back to 8% and is more noticeable. Also, at high incidences (up to 4°) the pressure distributions near the nose are rather "wavy", especially between Mach numbers of 0.9 and 1.0, and there appears to be a "double peak suction" at 3% and 10% chord at $M_0 = 0.9$ and 0.94. On a later model in the series, similar effects have been found to arise from the discontinuity in the transition strip near the pressure plotting station, suggesting that the boundary layer may be laminar within a limited region between the transition strips. This may be giving rise to a local laminar bubble separation, with subsequent reattachment as a turbulent layer, at the higher incidences.

5.3.2 Disturbances affecting integrated loads

The variation of $\overline{C_X}$ with Mach number for various incidences (Fig.17) shows that a sudden change in $\overline{C_X}$ is observable near $M_0 = 1.02$ followed by some deviations at higher Mach numbers. The similarity of the curves for various incidences suggests that the source of these deviations is probably external to the wing section, and may arise from disturbances spreading out from the root, or from the tunnel flow itself. These disturbances need only be very localised; for instance, if only the first 10% of the chord is affected on both surfaces, there may be a substantial effect on $\overline{C_X}$ and yet not on $\overline{C_Z}$.

The curves of p/H_{eff} against M_0 and x/c (Figs.6 to 11) show that the pressure over the front 30% of the chord is relatively high at $M_0 = 1.02$ which accounts for much of the high value of $\overline{C_X}$. Also, at $M_0 = 1.19$ there is a further band of high pressure between 25% and 50% chord; however, in this region it does not significantly affect $\overline{C_X}$. On the other hand, the region of high pressure aft of 55% chord at $M_0 = 1.10$ contributes to a reduction in $\overline{C_X}$ at that Mach number. Since the results are believed to be affected in this way, it has been thought worthwhile to attempt to correct them. To do this, the experimental pressures for one incidence ($\alpha_E = 2.6^\circ$) for both upper and lower surfaces have been plotted as a ratio of tunnel stagnation pressure (i.e. in the form p/H_0) in Figs.20 and 21 in carpet form against chordwise position and Mach number, together with the curve of p_0/H_0 for free stream conditions. An attempt is made on these figures to draw "smooth"* curves through the pressures measured at each pressure hole. The deviation of each value of p/H_0 from its appropriate "smooth" curve has been integrated around the chord in the same manner as the pressures themselves and used to provide a deviation in $\overline{C_X}$, plotted as ΔC_X in Fig.22. For Mach numbers above 1.2 this method could not be used for the upper surface due to the onset of supercritical flow with shock waves. In this region, therefore, ΔC_X has been taken as twice the value appropriate to the lower surface. The curves of Fig.22 show that below M = 1.2 this procedure would in general give a reasonable estimate of ΔC_X. The values of ΔC_X so obtained have been taken to apply at all incidences. When applied to $\overline{C_X}$, and resolved together with $\overline{C_Z}$ to provide C_D, a fairly plausible variation of

---

* Smooth - defined here as being of the same general shape as the curve of p_0/H_0 against M_0.

C_D with Mach number and incidence is obtained (Fig.23). These values of C_D also include an allowance for skin friction drag under tunnel conditions. This has been estimated by the method of Refs.17a and 21 and is shown in Fig.19. Comparison of the values of total C_D with those of ΔC_X help to put into better perspective the scatter in the experimental results.

The assumed corrections to the flow, in terms of the deviations in p/H_o used for the construction of Fig.23, are shown as a plot of local Mach number in Figs.24 and 25. The reduction of Mach number near the nose at $M_o = 1.02$ occurs on both surfaces. The low Mach number aft of 55% at $M_o = 1.10$ is seen to be more marked on the upper than the lower surface. The reduction in Mach number at about 40% chord at $M_o = 1.19$ seems to be confined to the upper surface, while there is an increase in Mach number (and hence suction) around 50% to 70% chord on the lower surface which will also be contributing to the increase in $\overline{C_X}$ observed at this M_o; these deviations are unfortunate in so far as they occur near the design Mach number. On the other hand the deviation near the nose is not considered to be a spurious effect but is associated with the imminent development of a local supersonic region.

5.4 Predicted flow pattern over sheared wing

Before discussing the results in detail, it may be worth briefly reviewing the physical principles underlying the concepts of subcritical and supercritical flow over an infinite sheared wing.

In considering the inviscid flow pattern expected to develop over the wing, it is suggested that only the component of flow normal to the wing leading edge is significant. Thus the onset of critical flow conditions, with the associated drag rise and separation effects, is governed solely by the magnitude of the Mach number component normal to the wing and is independent of the component parallel to the wing, irrespective of magnitude. The parallel component serves merely to influence the resultant (i.e. free-stream) Mach number and the absolute magnitude of the pressures. On simple assumptions such as these, there is no theoretical limit to the magnitude of this parallel component, and no significance is necessarily attached, therefore, to a free-stream Mach number of unity or greater.

Defining now the critical Mach number M_{CR} as the Mach number at which the flow component normal to the isobars first reaches a sonic value somewhere over the section, it is found that above M_{CR} the flow expands rapidly from the attachment line (equivalent to the stagnation line on a two dimensional wing) so that the component normal to the isobars is supersonic over an appreciable part of the section. Behind this region, the pressure recovers to a value which differs little from that given by the appropriate subcritical distribution. The manner of recovery is at first almost isentropic but, at supercritical Mach numbers, soon develops into a shock which in plan view will be fully swept, if sheared wing conditions are being maintained. With further increase of Mach number, the shock moves back along the section and increases in strength, producing in due course an increase in section drag. Eventually, as Mach number is increased still further the pressure rise across the shock becomes sufficient to cause the boundary layer to separate forward of the trailing edge, producing non-linear changes in lift and drag. If the drag rise Mach number is defined as M_D, and the Mach number at which separation effects become noticeable is defined as M_{SE}, the significance of these Mach numbers is broadly that M_D sets a limit to the aerodynamic efficiency of the wing section and hence to the cruising economy of the aircraft, and M_{SE} sets a limit to the usable speed of the aircraft, due to effects such as buffeting and possibly loss of control effectiveness.

The problem is therefore to achieve as high a Mach number as possible for the onset of drag rise while retaining an adequate margin between this Mach number and the Mach number for the onset of separation effects.

As in the two-dimensional case, several basically different types of pressure distribution suggest themselves, for example:-

(a) a distribution which at lift has a peak suction well forward (i.e., ahead of, say, 0.2 chord) followed by approximately linearly increasing pressure to the trailing edge. The shape of this distribution is thus roughly "triangular",

(b) a distribution which, after an initial rapid fall near the leading edge, has approximately constant pressure over part of the chord (back to 0.5 chord, say), followed by a more rapid increase in pressure to the trailing edge, i.e. of "rooftop" shape at its design lift coefficient.

For a given lift and thickness the peak suction for the "triangular" type will in general be greater than for the "rooftop" type, so that M_{CR} will be lower. However, as Mach number is increased above M_{CR} the supersonic region for the triangular type will initially be confined to forward-facing parts of the section, i.e. ahead of the crest (defined as the chordwise station where the upper surface slope is parallel to the undisturbed stream), whereas for the rooftop type the supersonic region will quickly extend to the back of the rooftop, i.e., well behind the crest. Tests by Nitzberg and Crandall[13] suggest that M_D is closely associated with the Mach number at which the shock moves aft of the crest, so that for the triangular type the margin $M_D - M_{CR}$ may be greater than for the rooftop. It is not, therefore, immediately apparent which type will have the greater value of M_D. Moreover, with the triangular type there is a less severe adverse pressure gradient aft of the maximum suction so that the margin $M_{SE} - M_D$ may also be greater for this type, since the corresponding strength of shock needed to cause the boundary layer to separate will also be greater. Thus the value of M_{CR} alone is not necessarily a reliable guide to the merits of different wing sections from the viewpoint of drag rise and separation effects.

In the tests reported here, the upper surface pressure distribution is of the "triangular" type. Further tests on other sections of "rooftop" type are in progress and will be reported in due course.

5.4.1 Three dimensional effects

Departures from infinite sheared wing flow occur in general on finite wings in the neighbourhood of the tips and of any abrupt changes in sweep, as for instance at the root of a wing of V planform. In this experiment the influence of the tip is confined at supersonic speeds to a conical region which always passes well downstream of the pressure measuring station. However, the compressions which arise near the wing root leading edge and the wing root trailing edge may give rise to shocks spreading outboard along the wing at sufficiently high Mach numbers (Fig.4b). These shocks, which are sometimes called the forward and rear shocks, tend to approach and coalesce somewhere along the span, thereafter forming a single shock called the outboard shock. By placing the pressure plotting station well outboard these root effects are minimised but may not be entirely negligible; later tests of other section shapes incorporate shaping of the body at the root in order to try to reduce these effects still further.

5.5 Compressibility and viscosity effects

The theoretical estimates of pressure distribution given in Refs.3 and 4 do not include compressibility or viscosity effects. In Appendix 2, however, an extension of these methods is given which allows the effect of compressibility to be estimated; this extension has been used to provide the theoretical estimates for these tests. The experimental results include both compressibility and viscosity effects, and differ (as might be expected) from the inviscid theoretical estimates.

It has been shown (in Refs.9 and 10 for example) that the incompressible inviscid theory can be used to give good estimates of pressure distributions at low speeds on both unswept and swept wings of symmetrical section, providing that allowance is made for the displacement thickness of the boundary layer. For example, Ref.10 gives the loss in loading, due to boundary layer effects, along a chord at 0.41 semispan on a 12% thick RAE 101 section wing of 45° sweep. In this case, measurements of the boundary layer profile were made just behind the trailing edge, and the displacement thickness estimated. The theoretical pressure distribution was then re-calculated for the aerofoil profile as modified by the addition of the displacement thickness, and it was found to agree well with the experimental results.

In the tests reported here, the wing section is no longer symmetrical, compressibility effects are present, and the high sweepback and aspect ratio would be expected to produce a substantial boundary-layer displacement thickness. No measurements have been made, however, of the boundary layer profile in this test and hence no allowance for it appears in the theoretical estimates. It is therefore not possible to devise a wholly satisfactory criterion for comparing theory and experiment. The provisional criterion chosen has been the simple one of equal level of peak suction. This at least shows to some extent the differences between the general shapes of the theoretical and the experimental upper surface pressure distributions without significantly affecting the Mach number for the onset of critical flow conditions.

For later tests in the series, boundary layer profiles are being measured at the trailing edge of the pressure plotting station, and it is hoped that this will enable comparisons to be made in future between the theory for inviscid flow and experiment so that the viscosity effects can be shown up and studied in more detail.

In much of the discussion which follows, the conditions of subcritical flow and supercritical flow have been treated separately. However, in those figures in which parameters are plotted against Mach number, the whole Mach number range has been covered. It follows, therefore, that the reader may be referred to different parts of the same figure on different occasions.

5.6 Subcritical flow conditions

5.6.1 Comparison with theory

At the lowest subsonic Mach number of 0.6, the theoretical (inviscid, compressible, and for infinite aspect ratio) and experimental pressure distributions are shown in Fig.12, which is a carpet plot of C_p against x/c and incidence. By comparing the distributions for equal levels of peak suction it has been found possible to relate the theoretical and experimental wing incidences (α_T and α_E) by an empirical equation of the form

$$\alpha_E = N \alpha_T + K$$

and for this Mach number the best agreement is obtained by putting N = 1.2 and K = 0.7 (degrees). The value of N of 1.2 is partly accounted for by the finite aspect ratio. Extrapolation from the results of Ref.14 for wings of somewhat similar planform suggests a value of 1.1 for incompressible flow. No tunnel constraint corrections have been applied to the results. The normal Glauert correction would not be significant but there is some uncertainty as to the precise nature of the boundary condition at the wing root. Experience at A.R.A. suggests that a small part (perhaps 10%) of the deficiency in lift curve slope might be attributed to root effects. Much of the remaining discrepancy may be due to the influence of viscosity.

The reason for the additional shift of 0.7° is not understood; it appears at other Mach numbers and at zero lift (as noted in para.5.6.3) but does not seem to be accounted for by deviations in the tunnel flow or twist of the wing. Since it occurs at zero lift, where the pressure gradient on the lower surface is more adverse than that on the upper surface, it does not seem likely that its origin is due solely to viscous effects, although on a later model the addition of vortex generators to the upper surface only has been found to decrease the zero lift angle by up to 0.3°.

In Fig.13 the theoretical and experimental pressure distributions on both surfaces at $M_o = 0.6$ are compared at closely corresponding levels of peak suction, and shows satisfactory agreement over the forward 30% of the chord. Further aft, where the pressure gradients are unfavourable, there is some loss of loading so that C_L is about 17% less experimentally (0.100 as compared with 0.120), possibly because of viscous effects. In addition, the predicted positive pressure coefficient near the trailing edge is not achieved, as is commonly observed.

Turning now to the design Mach number of 1.2, the theoretical and experimental pressure distributions (Fig.14 and 15) show that, for equal levels of peak suction, there is a greater loss of loading over the rear of the section than at a Mach number of 0.6. Fig.14 shows that the theoretical (again inviscid, compressible, and for infinite aspect ratio) and experimental wing incidences are now related by the equation

$$\alpha_E = \alpha_T + 0.7$$

and in this case α_E is varying at the same rate as α_T (N = 1.00), instead of 20% more rapidly as at $M_o = 0.6$. Some calculations of the spanwise variation of twist at $M_o = 1$ in Ref.15 suggest that for wings having triangular (linear) chordwise loadings the incidence at the pressure measuring station would only be about 6% greater than the infinite sheared wing value (N = 1.06). The discrepancy in N is probably partly due to the fact that near locally critical conditions the peak suction pressure coefficients in practice tend to change more rapidly with incidence than the subcritical theory predicts. It is however noteworthy that the other discrepancy of 0.7° persists. In Fig.15 the pressure distributions on both surfaces are compared at closely corresponding levels of peak suction near to the design value. Although agreement is still good in the regions of favourable pressure gradient, these are confined to the forward 10% of the upper surface and the forward 30% of the lower surface, and behind these regions both surfaces, but particularly the upper, contribute to a considerable loss of loading.

It appears that, although the level of peak suction has risen rapidly with Mach number, the suction well aft of the peak (for instance at 60% chord) actually falls, in terms of C_p, so that overall there is also a fall in C_L (from 0.100 at M_o = 0.6 to 0.085 at $M_o \doteqdot 1.2$) instead of a gain as predicted for inviscid flow (from 0.120 at M_o = 0.6 to 0.153 at M_o = 1.2). Thus at M_o = 1.2 the experimental lift coefficient is 44% less than the theoretical value; some of this effect may be attributable to the low value of N as discussed above, but even if the value of N were taken to be 1.2 (as at M_o = 0.6) the loss in C_L would still be 34% (C_L = 0.100). For equal C_L the value of N would have to be 1.8. It is not clear how a discrepancy of this magnitude arises, unless it is due to much more severe viscous effects than those encountered at M_o = 0.6. The increase in M_o, in spite of (or perhaps even together with) the increase in Reynolds number from 3.8 to 5.0×10^6 may possibly be producing a more rapid and non-linear thickening of the boundary layer on the upper surface. It was found in Ref.10 that even at low speed and a lower sweep (45°), at a station 0.41 semi-span outboard from the root of an aspect ratio 3 wing, that the flow direction was parallel to the trailing edge (i.e. "spanwise") at the trailing edge and for a height of nearly 0.01 chord above it at a C_L of 0.57. The resultant loss in C_L compared with an inviscid estimate neglecting boundary layer thickness was 14%. However, by determining and adding the displacement thicknesses on both surfaces of the aerofoil, and treating the resultant "modified" aerofoil by the inviscid theory, it was found that the loss in C_L could be accounted for fully. It was also found[10] that this loss of lift increases with angle of sweep. Later tests in the present series will include measurements of boundary layer profiles at the trailing edge, as well as the addition of vortex generators, in an endeavour to assess quantitatively the nature and magnitude of viscous effects.

5.6.2 <u>Normal force and drag</u>

The variation of $\overline{C_Z}$ with M_o for various incidences (Fig.16) shows that very little change in $\overline{C_Z}$ occurs with Mach number, except at high incidence and Mach number where a flow separation behind a shock becomes established. The nature of this separation is discussed in more detail in para.5.7.3. Its effect on the pressure distribution is to increase the suction over the rear part of the upper surface (Fig.11 shows this happening at 5° incidence at all Mach numbers above 1.15) and hence to increase both $\overline{C_Z}$ and $\overline{C_X}$.

The comparison of theoretical and experimental values of $\overline{C_Z}$ as a function of incidence show (Fig.18) that at zero lift the experimental angle of incidence α_E is about 0.8° greater than the theoretical value α_T, corresponding closely to the discrepancy of 0.7° found when comparing theoretical and experimental pressure distributions (para.5.6.1). The loss of loading discussed in para.5.6.1 appears in Fig.19 as a reduction in the slope of the experimental curve.

The drag coefficient, corrected by the method of paragraph 5.3.2, is plotted against Mach number for various incidences in Fig.23. As predicted by the yawed wing analogy, there is no significance in a Mach number of unity. Thus, in spite of the shortcomings of the experimental pressure distributions, the flow conditions predicted in Ref.1 have been achieved - i.e., an effectively shock free flow has been obtained - with lift - at a supersonic Mach number, without incurring any penalty in wave drag.

No detailed comparison between theory and experiment has been made at the design lift coefficient ($C_L = 0.153$) and Mach number (1.2), since the experimental pressure distribution includes an appreciable supercritical region well forward, and an incipient separation near the trailing edge. Instead, the approach preferred here has been to make comparisons for similar values of pressure coefficient over regions of favourable pressure gradient, and to look for possible reasons to account for the loss in loading over the remaining regions. However, it is worth noting that at the design lift coefficient there is no great increase in drag over the subcritical value, so that although the flow is no longer shock free the design conditions of Mach number and lift have been achieved without appreciable penalty (except that the margin $M_{SE} - M_D$ is virtually zero, since both M_{SE} and M_D are close to 1.2 at this incidence).

5.6.3 Trailing edge pressure recovery

In Fig.26 the pressure coefficient (C_p) has been plotted for the upper surface at 95% chord. This figure shows that, except for Mach numbers between 0.9 and 1.0, the pressure coefficient at this position was never greater than 0.032. This is rather less than, for example, the pressure coefficients measured at 90% chord on a tapered wing of 59° sweepback[16] in which the value of C_p, everywhere outboard of 40% semispan, was around 0.06, at low speed and at a Reynolds number of 1.6×10^6 (the Reynolds number for the tests reported here was at least 3.8×10^6). At 5° incidence, C_p at 95% chord is negative at all Mach numbers. Figs.6 to 11 also show that the pressure distribution is somewhat uneven between 80% and 95% on the upper surface at most incidences and Mach numbers for which the flow has not separated farther upstream. This suggests that the thickness of the boundary layer may be great enough to affect the comparison between theoretical and experimental pressure distributions.

5.7 Supercritical flow conditions

The analogy with two-dimensional flow would suggest that above a certain Mach number which depends on incidence, a shock would form near the nose of the aerofoil. Further increase of Mach number and incidence would cause the shock to move aft and strengthen, followed by an increase in the drag of the section, and leading ultimately to separation of the flow everywhere aft of the shock.

5.7.1 Pressure distribution

The pressure distributions shown in Fig.6 to 11 suggest that in general a recognizable shock (shown by the dotted part of the lines) first appears soon after the value of p/H_{eff} falls below about 0.52 anywhere on the surface. This corresponds to the onset of a region of locally supersonic flow over a two-dimensional section. As Mach number is increased, the position of the shock corresponds approximately to the more aft of the two chordwise positions at which the local value of p/H_{eff} would have been 0.52 if the pressure distribution had remained of subcritical shape. Further aft the distribution follows the subcritical shape, while in front of the shock the pressure distribution becomes of a typically supersonic form, and in particular the local value of p/H_{eff} no longer decreases with increase of free stream Mach number. (Near the nose p/H_{eff} actually increases somewhat.) There is thus a strong "Mach-number-component freeze", analogous to the corresponding Mach number freeze observed in many experiments on two dimensional wings, and discussed by Sinnott[6] and predicted by Randall's theory[5].

Oil flow patterns observed at an incidence of 2.6° and a Mach number of 1.25 are illustrated in Fig.27. The upper part of the figure shows the outboard two-thirds of the span and the shock wave can be seen crossing the pressure measuring station near 20% chord. In this region it is some 5° less swept than the wing, and further inboard it is tending towards the wing root trailing edge, as well as becoming less sharply defined. It appears therefore that the root is still exerting some influence on the flow conditions at the pressure measuring station. To this extent then the experiment has not succeeded in creating yawed wing flow in the required region, although the correlations with two dimensional flow discussed above suggest that at this station the root effects may not be very significant. Shaping the body at the root would be expected to lessen these effects.

If the Mach number and incidence are further increased the pressure distributions of Figs.8 to 11 suggest that flow separation begins to occur aft of the shock which then ceases to move rearwards and may even move forwards again. The flow pattern was therefore observed at an incidence of 2.6° and a Mach number of 1.40, and is shown in Fig.28. The shock is now passing over the pressure measuring station near the 30% chord position. Behind the shock the oil pattern indicates a large region of separated flow. Inboard of the pressure measuring station the shock moves back and becomes less clearly defined, again suggesting that its origin lies near the wing root trailing edge (compare the "rear shock" of Fig.4(b)). There is another disturbance, however, which is visible well inboard in front of the main shock, and which is more highly swept than the wing; this appears to be the forward shock (Fig.4(b)) which coalesces with the rear shock to form the outboard shock at a point on the span roughly half a chord inboard of the pressure measuring station.

It has been suggested[18] that for flows with a high supersonic leading edge suction peak the bulk of the subsequent pressure recovery may take place isentropically rather than through a shock, under the influence of the reflection of the leading edge supersonic expansion waves as compression waves from the sonic line. The nearest approach to a high supersonic leading edge suction in this experiment occurs at an incidence α_E of 5° (Fig.11). Subcritically the pressure distribution is peaky near the nose, while supercritical values of p/H_{eff} (i.e. less than 0.528) occur down to a Mach number of as little as 0.9. However, up to Mach numbers of at least 1.2 the shape of the pressure distributions suggests a less abrupt pressure recovery than one would expect from a shock, even though the flow has completely separated further aft along the section. This effect is illustrated in Fig.29 where the Mach number for which p/H_{eff} first falls below 0.515 anywhere on the upper surface, and the Mach number for which a recognizable shock appears, are plotted against incidence. It will be noted that at the higher incidences these Mach numbers diverge by an amount which may bear some relation to the extent to which the pressure recovery takes place isentropically.

5.7.2 Comparison with theory

The theoretical prediction of the transonic characteristics of two-dimensional round nosed aerofoils in a sonic stream has been considered by Sinnott[6] and Randall[5]. Sinnott's method is semi-empirical and applies over the region behind the crest of the aerofoil. Randall's treatment is purely theoretical (inviscid) but deals also with the region forward of the crest almost up to the nose of the aerofoil. Sinnott has also extended his method[7,18,20] to deal with Mach numbers below unity for which a shock wave is present on the wing surface aft of the crest. He further suggests that this method may be used to estimate drag rise and separation Mach number (M_D, M_{SE}), at any rate for comparative purposes.

Some calculations of pressure distributions have been made using both Sinnott's and Randall's methods. These estimates are compared with the experimental results in Fig.30. Some caution is necessary in interpreting this comparison, however. First of all, estimates for two dimensional wings are being compared with experimental results on a three dimensional wing. Secondly, Sinnott's method is intended for use on fairly thin sections having a value of the parameter χ not greater than 0.9. The parameter χ, introduced in Ref. 6, is defined as

$$\chi = \frac{\left(\frac{z}{c}\right) \quad \text{at} \quad \frac{x}{c} = 0.02}{\Delta\left(\frac{x}{c}\right) \quad \text{for} \quad \theta = 2^{\circ} \quad \text{to} \quad \theta = 4^{\circ}}$$

(where θ is the surface slope of the wing section, in the region forward of the wing crest). For this wing $\chi = 1.01$ at $\alpha_T = 1.9^{\circ}$ (corresponding to $\alpha_E = 2.6^{\circ}$) so that extrapolation beyond Sinnott's recommended limits is necessary. Thirdly, Randall's sonic range theory cannot strictly be used to treat sections whose shape is defined by a polynomial in $\frac{x}{c}$ which contains terms in both $\left(\frac{x}{c}\right)^{\frac{1}{2}}$ and $\left(\frac{x}{c}\right)$. In the case considered here, a polynomial expansion in $\left(\frac{x}{c}\right)^{\frac{1}{2}}$ was derived from the inspection report* of the aerofoil shape, and the coefficient of $\left(\frac{x}{c}\right)$ was found to be small, although not zero. In any case, the effect of incidence appears as a change in the coefficient of $\frac{x}{c}$. Randall has suggested an approximation for overcoming this difficulty for small incidences; in this experiment the incidence normal to the leading edge (3.8°) is possibly large enough to introduce significant errors.

Using Sinnott's method[18], the pressure distributions downstream of the shock have been derived from the experimental distribution at the highest shock-free Mach number (in this case 1.20) by application of the Prandtl-Glauert rule. In this way, the effects of compressibility and viscosity can be included approximately. The shock position along the chord is then given by the intercept of this pressure distribution for the appropriate Mach

* To avoid any possible differences due to deviations between the nominal (design) and the achieved aerofoil shape.

number with the locus of $\frac{p_{2_G}}{H}$ (the subcritical pressure just downstream of the shock position). $\frac{p_{2_G}}{H}$ is a function of $\frac{p_1}{H}$ (pressure just upstream of the shock) but varies very slowly - in this case it always lies between 0.52 and 0.53. The value of $\frac{p_1}{H_o}$ is obtained for the appropriate Mach number and shock position. The pressure at the crest (which must be forward of the shock) and the variation of pressure from crest to shock is then estimated. The pressure distribution at sonic conditions has also been calculated by both Sinnott's and Randall's methods; the latter method is of interest here since it deals with the forward part of the aerofoil ahead of the crest.

In Fig.30 the various estimated pressure distributions described above are plotted as full lines. For comparison, experimental values of $\frac{p}{H_{eff}}$ are also shown as symbols, joined by dotted lines. The experimental value for $M_o = 1.26$ (where the shock is theoretically at the crest) has, however, been obtained by interpolation between experimental results at nearby Mach numbers.

It is interesting to observe that, downstream of the shock, agreement is reasonably good at all Mach numbers except 1.40 where in any case the flow had separated completely behind the shock. Further, the predictions of shock wave position are in fair agreement in that the shock always lies between the same pressure holes as found experimentally (except again at $M_o = 1.40$), although it is clear from oil flow pictures (Figs.27 and 28) that the flow field was to some extent influenced by conditions at the wing root.

Just upstream of the shock however, the experimental value of $\frac{p_1}{H_{eff}}$ is sometimes up to 0.02 greater than predicted, while at the crest this discrepancy increases to 0.04 to 0.05 at the highest Mach number. This effect has also been observed in recent unpublished N.P.L. tests; the cause is at present unresolved.

5.7.3 Drag rise and separation effects

The curves of Fig.23 show that a rapid rise in drag coefficient begins when the Mach number and incidence is sufficiently high. Considering initially the case where no flow separation occurs downstream of the shock, the pressure distributions of Figs.6 to 11 show how the shock forms initially well forward on the aerofoil, and gains in strength as it moves back with increase of Mach number and incidence. Initially it is ahead of the aerofoil crest, but as it passes behind the crest the drag of the section starts to rise rapidly. For incidences of 2° or less the shock does not pass significantly behind the crest at Mach numbers up to 1.4, but at $\alpha_E = 2.6°$ the crest is close to 22% chord and the shock passes over this position at just over $M_o = 1.25$. From Fig.23 the drag rise is seen to begin at around $M_c = 1.25$ at this incidence. This correlation between Mach numbers for shock-on-crest and for drag-rise has been observed in two dimensions by Nitzberg and Crandall[13] while Sinnott[18] suggests that the Mach number for shock on crest will be given by the condition that $\frac{p_{2_G}}{H}$ (for a two dimensional wing) at the crest is 0.515, a value obtained by analysis of experimental results with a fairly weak shock[7]. For the shock strengths observed in this case a more appropriate value of $\frac{p_{2G}}{H}$ might be 0.52 to 0.53 but this does not introduce significant errors. The experimentally observed values of Mach number for shock-on-crest and for drag rise are compared in Fig.31 with estimates using the above criterion*. It will be seen that good agreement is obtained between the estimates and the experimental values, except at $\alpha_E = 0°$ where the experimental value has been derived by taking into account a single rather high drag value at M = 1.408 (Fig.23), and at $\alpha_E = 4°$ and $5°$ where some of the drag rise is due to flow separation.

Further increase of Mach number causes the shock to increase in strength until the flow downstream of it separates completely. The condition of practical interest is the onset of the effects of this separation, such as buffeting. Pearcey[19] has suggested that for two-dimensional aerofoils this condition is observed to correspond to the stage at which the separation bubble behind the shock fails to reattach upstream of the trailing edge. When this happens the pressure at the trailing edge decreases abruptly. In the experiment described in this note, the pressures observed at 95% chord have been plotted against Mach number for various incidences in Fig.26, and it will be seen that above $\alpha_E = 2°$ the trailing edge pressure decreases, fairly rapidly, above a certain Mach number which varies with incidence. Thus again an analogous behaviour with two-dimensional wings has been observed. Sinnott[18] suggests a relation between the pressure immediately ahead of the shock at the separation Mach number and the parameter χ which depends on leading edge geometry. This parameter, as pointed out in para. 5.7.2, has a value of 1.01 for this section at $\alpha_E = 2.6°$, which is higher than the upper limit (0.9) recommended by Sinnott; however, by extrapolation from Fig.12 of Ref.18 a value of $\frac{p_1}{H}$ (pressure just upstream of the shock) of 0.31 has been estimated. Experimentally, the value of $\frac{p_1}{H_{eff}}$ is between 0.33 and 0.34 at $\alpha_E = 2.6°$ when the trailing edge pressure diverges, which is at a Mach number between 1.35 and 1.40.

At higher incidences (higher values of χ) Fig.12 of Ref.18 suggests that the value of $\frac{p_1}{H}$ should remain nearly constant at around 0.31; the experimental value of $\frac{p_1}{H_{eff}}$ is in fact found to remain constant near 0.33. The discrepancy of 0.02 in $\frac{p_1}{H_{eff}}$ is probably partly due to the addition of a spanwise component of flow which causes a thicker boundary layer to form so that separation begins slightly earlier. However, with this adjustment the analysis of Sinnott offers a reasonable guide to the separation Mach number of a yawed wing, and in Fig.31 the actual values of M_{SE} for various incidences are plotted together with the curve for $\frac{p_1}{H_{eff}} = 0.33$.

From Fig.31 the margin of Mach number between drag rise and the onset of separation effects ($M_{SE} - M_D$) has been derived and is plotted in Fig.32. This shows that above an incidence of about 3.7 degrees the margin is zero or negative, and that even at the design incidence ($\alpha_E = 2.6°$), the margin is

---

* M_D has been taken here as the Mach number for which the actual drag coefficient exceeds the subcritical value (extrapolated to the same Mach number) by 0.0015.

only 0.07. This margin is smaller than would be expected on inviscid considerations; some form of boundary layer control may be required if these viscous effects persist at full scale Reynolds numbers.

6 CONCLUSIONS

Pressure distributions have been measured around the section of a 60° swept wing at Mach numbers from 0.6 to 1.4. The section was basically a 9% thick RAE 101 thickness distribution, cambered to provide an approximately triangular upper surface pressure distribution, which was subcritical almost everywhere, at a Mach number of 1.2 and a lift coefficient of 0.153 in inviscid flow. The wing was substantially untapered and had an aspect ratio near 5. Pressures were measured all round one streamwise station at 0.71 semi-span.

It is concluded that:-

(1) A subcritical type of flow, without shocks, has been achieved at a supersonic free stream Mach number on a lifting wing, as predicted theoretically in Ref.1, without incurring any significant wave drag.

(2) At the design Mach number of 1.2, the theoretical (inviscid) and experimental pressure distributions, compared on a basis of equal peak suction, are in good agreement wherever the pressure gradient is favourable. Elsewhere, agreement is less good, both upper and lower surfaces contributing to a loss in loading sufficient to reduce lift curve slope by around 40%. Substantial boundary layer outflow is observed which would be expected to account for much of this effect. At the design lift coefficient, a region of supercritical flow, terminated by a shock, develops well forward on the aerofoil, without causing any great increase in drag. However, the boundary layer is at this stage on the point of separating completely over the rear of the section.

(3) As Mach number or lift coefficient is increased above the design value, there appears on the upper surface a shock which in plan view is nearly as highly swept as the wing itself. No drag penalty is evident until the shock moves aft of the crest of the aerofoil. Eventually the flow separates everywhere behind the shock. Rather small margins between the Mach numbers for drag rise and for the onset of separation effects were found but the relatively thick boundary layer may be largely responsible for this.

(4) Some estimates of supercritical pressure distributions for two-dimensional wings have been extended to the swept wing case and compared with the experimental results. In general quite good agreement is found. The Mach number for which the shock first appears, the subsequent movement of the shock, the drag-rise Mach number and the Mach number for the onset of separation effects can all be predicted with reasonable accuracy from knowledge of the just-subcritical pressure distribution. Ahead of the shock the component of local Mach number normal to the leading edge "freezes" in an analogous manner to the two-dimensional case.

(5) No significant variations in pressure distributions were found due to increasing Reynolds number from 5×10^6 to 6×10^6 at supersonic speeds.

Future testing will include models having design pressure distributions of roof-top shape, a thinner (6%) section, body shaping to help reduce root effects still further, and devices which are intended to reduce the effective boundary layer thickness, as well as measurements of total head distributions in the region of the trailing edge.

7 ACKNOWLEDGMENTS

The author wishes to acknowledge the help and co-operation of Mr. Haines, Mr. Wingfield and many other members of the staff of the Aircraft Research Association, Limited, especially during the actual testing which took place in the A.R.A. 9 ft x 8 ft tunnel at Bedford.

LIST OF SYMBOLS

C_Z	normal force coefficient
C_X	chord force coefficient
ΔC_X	error in C_X due to tunnel flow (para.5.3)
C_L	lift coefficient
C_D	drag coefficient
C_f	skin friction drag coefficient
C_p	pressure coefficient $\dfrac{p - p_o}{0.7\, p_o\, M_o^2}$
C_p^*	pressure coefficient when local Mach number component normal to leading edge is equal to unity
c	local wing chord
H	stagnation pressure
H_{eff}	stagnation pressure for equivalent unswept wing (see para.5.1)
M	Mach number
N	$\dfrac{\partial \alpha_E}{\partial \alpha_T}$ (para.5.6.1)
p	local static pressure
x,y,z	orthogonal co-ordinates defining wing surface
α	angle of incidence
γ	ratio of specific heats (taken as 1.4)
θ	surface slope of aerofoil measured forward from crest
Λ	angle of sweepback
χ	$\left(\left(\frac{z}{c}\right)_{x=0.02c}\right) \Big/ \left(\Delta \frac{x}{c} \text{ between } \theta = 2^\circ \text{ and } \theta = 4^\circ\right)$ (a function of aerofoil geometry near leading edge)

LIST OF SYMBOLS (Contd)

Suffices

o	free stream conditions
1	immediately upstream of shock
2	immediately downstream of shock
2_G	used in p_{2_G} to denote value of p_2 given by appropriate sub-critical pressure distribution at position of shock
CR	critical value
D	value at onset of drag rise
E	experimental value
SE	value at onset of separation effects
T	theoretical value

LIST OF REFERENCES

No.	Author	Title, etc.
1	Küchemann, D. Weber, J.	The subsonic flow past swept wings of zero lift without and with body. A.R.C. R. & M.2908. March, 1953.
2	Bagley, J.A.	An aerodynamic outline of a transonic transport aeroplane. A.R.C. 19,205. October, 1956.
3	Weber, J.	The calculation of the pressure distribution over the surface of two-dimensional and swept wings with symmetrical aerofoil sections. A.R.C. R. & M.2918. July, 1953.
4	Weber, J.	The calculation of the pressure distribution on the surface of thick cambered wings and the design of wings with given pressure distribution. A.R.C. R. & M.3026. June, 1955.
5	Randall, D.G.	Transonic flow over two-dimensional round-nosed aerofoils. A.R.C. C.P.456. September, 1958.
6	Sinnott, C.S.	On the flow of a sonic stream past an aerofoil surface. Journal Aero/Space Sciences, Vol.26, No.3. March, 1959.
7	Sinnott, C.S.	On the prediction of mixed, subsonic/supersonic pressure distributions. Journal Aero/Space Sciences, Vol.27, No.10. October, 1960.
8	Bagley, J.A.	Wing section design for a transonic aeroplane. Unpublished M.O.A. Report.

LIST OF REFERENCES (Contd)

No.	Author	Title, etc.
9	Brebner, G.G. Bagley, J.A.	Pressure and boundary layer measurements on a two dimensional wing at low speed. A.R.C. R. & M.2886. February, 1952.
10	Küchemann, D.	Boundary layers on swept wings - their effects and their measurements. AGARD Paper No. AG 19/P9. April, 1955.
11	Haines, A.B. Jones, J.C.M.	The centre line Mach number distributions and auxiliary suction requirements for the ARA 9 ft × 8 ft transonic wind tunnel. A.R.C. R. & M.3140. April, 1958.
12	O'Hara, F. Squire, L.C. Haines, A.B.	An investigation of interference effects on similar models of different size in various transonic tunnels in the U.K. A.R.C. 21,094. February, 1959.
13	Nitzberg, G.E. Crandall, S.	A study of flow changes associated with air-foil section drag rise at supercritical speeds. N.A.C.A. Tech. Note No. 1813. February, 1949.
14	Blake, M.	Results of some calculations on camber and twist distributions for swept wings at M = 0. Vickers Armstrongs (Aircraft) Ltd. Report No. A.570.2. September, 1959.
15	Bagley, J.A. Beasley, J.A.	The shapes and lift-dependent drags of some sweptback wings designed for $M_0 = 1.2$. A.R.C. C.P.512. June, 1959.
16	Tunnel Staff of Aero Dept.	Pressure and boundary layer measurements on a 59° sweptback wing at low speed and comparison with high speed results on a 45° swept wing. A.R.C. C.P.86. August, 1950.
17	Monaghan, R.J.	A review and assessment of various formulae for turbulent skin friction in compressible flow. A.R.C. C.P.142. August, 1952.
18	Sinnott, C.S.	Theoretical prediction of the transonic characteristics of aerofoils. Report No. NPL/Aero/369. January, 1959.
19	Pearcey, H.H.	Some effects of shock induced separation of turbulent boundary layers in transonic flow past aerofoils. Proc. Symposium on boundary layer effects in aerodynamics. A.R.C. R. & M.3108. June, 1955.
20	Sinnott, C.S.	The design of two dimensional cambered aero-foil sections for the supersonic transport project. Report No. NPL/Aero/332. July, 1957.
21	Monaghan, R.J.	Formulae and approximations for aerodynamic heating rates in high speed flight. A.R.C. C.P.360. October, 1955.

APPENDIX 1

RELATION BETWEEN PRESSURE AND MACH NUMBER COMPONENT NORMAL TO THE LEADING EDGE OF A SWEPT WING

In the case of two-dimensional wings, it is sometimes convenient to express pressures around the wing section in the form p/H_o, where H_o is the stagnation pressure. For swept wings of infinite span, there is an analogous expression for pressure which may be written p/H_{eff}, where H_{eff} is defined as the pressure at the attachment line, i.e., the line where the local component of flow normal to the leading edge is zero. Thus the value of p/H_o for an unswept wing will be the same as the value of p/H_{eff} for the same wing yawed through an angle Λ, if the free stream Mach number is increased by a factor equal to the secant of the angle of yaw.

Let V = velocity

a = velocity of sound

M = Mach number $\left(\frac{V}{a}\right)$

Λ = sweepback angle

γ = ratio of specific heats for air

p = static pressure

H = stagnation pressure

Suffix o = free stream conditions

n = normal to wing leading edge

t = parallel to wing leading edge.

We assume that the velocity component parallel to the leading edge is constant, i.e.

$$V_t = V_o \sin \Lambda = \text{constant} .$$

We express the value of p/H_o in the two following ways:-

$$\frac{p}{H_o} = \left(1 + \frac{\gamma - 1}{2} M^2\right)^{\frac{\gamma}{1-\gamma}} \tag{1}$$

$$\frac{p}{H_o} = \left(1 - \frac{\gamma - 1}{2} \left(\frac{V}{a_o}\right)^2\right)^{\frac{\gamma}{\gamma-1}} . \tag{2}$$

Now

$$\left(\frac{V_o}{a_o}\right)^2 = \frac{M_o^2}{1 + \frac{\gamma - 1}{2} M_o^2}, \quad \text{so that, when} \quad V_n = 0$$

$$\frac{p}{H_o} = \frac{H_{eff}}{H_o}$$

$$= \left\{1 - \frac{\gamma - 1}{2} \left(\frac{V_t}{a_o}\right)^2\right\}^{\frac{\gamma}{\gamma - 1}} .$$

But

$$\left(\frac{V_t}{a_o}\right)^2 = \frac{M_o^2 \sin^2 \Lambda}{1 + \frac{\gamma - 1}{2} M_o^2}, \quad \text{whence}$$

$$\frac{H_{eff}}{H_o} = \left\{\frac{1 + \frac{\gamma - 1}{2} M_o^2 \cos^2 \Lambda}{1 + \frac{\gamma - 1}{2} M_o^2}\right\}^{\frac{\gamma}{\gamma - 1}} . \tag{3}$$

$$\frac{p}{H_{eff}} = \frac{p}{H_o} \cdot \frac{H_o}{H_{eff}}$$

so that, from (1) and (3)

$$\frac{p}{H_{eff}} = \left(1 + \frac{\gamma - 1}{2} M^2 \cos^2 \Lambda\right)^{\frac{\gamma}{1 - \gamma}} \tag{4}$$

which is the isentropic relation with an "effective" stagnation pressure.

APPENDIX 2

DESIGN OF AEROFOIL SECTIONS WITH LINEARLY VARYING PRESSURE DISTRIBUTION ON THE UPPER SURFACE

by

J. Weber, Dr.rer.nat.

The task is to design for infinite sheared wings with given thickness distribution a camber line such that the wing has at the design incidence a given lift coefficient and on its upper surface a pressure distribution which varies nearly linearly along the chord (no requirement is made for the lower surface). It is required that these conditions are satisfied at a given Mach number for which the flow is subcritical. The latter condition imposes certain limits on the thickness of the wing and on the design lift coefficient.

In designing the wing which has been the subject of these tests, we have relaxed these conditions somewhat by allowing the velocity to be slightly supersonic forward of the crest but have performed the calculations as if the flow were subcritical throughout.

The symbols are defined as follows:-

A	see equation (2)
C_{p_i}	pressure coefficient as defined in equation (3)
h	see equation (6)
M	Mach number
$S^{(n)}(x)$	functions given in Refs.2 and 3
V	velocity
x	distance aft of leading edge (in units of wing chord)
z	distance above chord line (in units of wing chord)
z_c	ordinate of camber line of section
z_t	ordinate of thickness distribution of section
α	angle of incidence
$\Gamma(x)$	load distribution
γ	ratio of specific heats (taken as 1.4)
Λ	angle of sweep

Suffices:-

o	free stream conditions
D	design
n	component normal to leading edge
us	upper surface
μ, ν	as defined in Ref.3

The pressure distribution on an infinite sheared wing in subcritical flow can be calculated from the following equation:-

$$\left(\frac{V}{V_o}\right)^2 = \cos^2\alpha\,\sin^2\Lambda + \frac{1}{1 + \left[\dfrac{S^{(2)}(x) \pm S^{(5)}(x)}{A\cos\Lambda}\right]^2}$$

$$\times\left\{\cos\alpha\left[\cos\Lambda + \frac{S^{(1)}(x)}{A} \pm \frac{S^{(4)}(x)}{\sqrt{1 - M_o^2\cos^2\Lambda}}\right]\right.$$

$$\left.\pm\frac{\sin\alpha}{\sqrt{1 - M_o^2\cos^2\Lambda}}\sqrt{\frac{1-x}{x}}\left[1 + \frac{S^{(3)}(x)}{A\cos\Lambda}\right]\right\}^2 \tag{1}$$

where

$$A = \sqrt{1 - M_o^2\left(\cos^2\Lambda - C_{pi}\right)} \tag{2}$$

and

$$C_{pi} = \cos^2\Lambda - \frac{\{\cos\Lambda + S^{(1)}(x)\}^2}{1 + \left[\dfrac{S^{(2)}(x)}{\cos\Lambda}\right]^2}\,. \tag{3}$$

$S^{(1)}(x)$, $S^{(2)}(x)$ and $S^{(3)}(x)$ are functions of the ordinates $z_t(x)$ of the thickness distribution and $S^{(4)}(x)$ and $S^{(5)}(x)$ are functions of the ordinates $z_c(x)$ of the camber line. The relations between $S^{(\nu)}(x)$ and $z_t(x)$ and $z_c(x)$ are given in Refs.2 and 3.

The pressure coefficient is determined from the velocity distribution by the relation:-

$$C_p = \frac{2}{\gamma M_o^2}\left(\left\{1 + \frac{\gamma-1}{2}M_o^2\left[1 - \left(\frac{V}{V_o}\right)^2\right]\right\}^{\frac{\gamma}{\gamma-1}} - 1\right). \tag{4}$$

The local Mach number M_n of the velocity component normal to the isobars is related to the pressure coefficient by the equation:-

$$C_p(M_n, M_o, \Lambda) = \frac{2}{\gamma M_o^2}\left\{\left[\frac{2}{2+(\gamma-1)M_n^2}\right]^{\frac{\gamma}{\gamma-1}}\left[1+\frac{\gamma-1}{2}M_o^2\cos^2\Lambda\right]^{\frac{\gamma}{\gamma-1}}-1\right\}. \qquad \dots (5)$$

For the present test programme, aerofoil sections were required for wings of 60° sweep which had a design lift coefficient of 0.15 and which satisfied the conditions mentioned above at a free stream Mach number of 1.2. The further condition was imposed that the difference between the upper and lower surface pressures tends to zero at the trailing edge.

Thickness distributions of the type RAE 100 and RAE 101 were considered. According to linear theory, these sections have at zero incidence pressure distributions of the form

$$C_{p_t}(x) = \begin{cases} A & 0 < x < h \\ A + B(x-h), & h < x < 1 \end{cases}. \qquad (6)$$

(h = 0 for RAE 100, h = 0.3 for RAE 101). A linear pressure distribution on the upper surface

$$C_p(x) = A + B(1-h) + C(1-x)$$

is obtained according to linear theory if the load distribution is

$$C_{p_{US}} - C_{p_{LS}} = \begin{cases} 2B(1-h) + 2C(1-x), & 0 < x < h \\ 2(B+C)(1-x), & h < x < 1 \end{cases}. \qquad (7)$$

If we consider these first order terms only, then we find that a wing thickness of 9% is possible. This implies that the wing section normal to the leading edge is 18% thick and that therefore the second-order terms in equation (1) have a significant effect on the pressure distribution.

To determine the required camber-line, we need to know the linear order term of the chordwise load distribution in incompressible flow:-

$$\frac{\Gamma(x)}{2V_o} = S^{(4)}(x) + \tan\alpha_D\sqrt{\frac{1-x}{x}} \qquad (8)$$

where α_D is the design incidence. The relation between the shape of the camber-line, z_c, and the load distribution is:-

$$\frac{dz_c(x)}{dx} - \tan\alpha_D = -\frac{1}{\pi}\int_0^1 \frac{\Gamma(x')}{2\,V_0}\frac{dx'}{x - x'} .$$

This relation can be approximated by:-

$$\frac{dz_c(x)}{dx} - \tan\alpha_D = \sum_{\mu=1}^{N-1} S^{(22)}_{\mu\nu}\frac{\Gamma_\mu}{2\,V_0} + S^{(22)}_{N\nu}\lim_{x\to 0}\frac{\Gamma(x)}{2\,V_0}\sqrt{x} \; ; \qquad (9)$$

the coefficients $S^{(22)}_{\mu\nu}$ are tabulated in Ref.3.

In view of the relatively large second order terms in equation (1), we have not attempted to obtain a first approximation to $\Gamma(x)$ from the linear order terms given in equations (6) and (7). Instead, we have estimated an upper surface pressure distribution and have determined an approximation to $\Gamma(x)$ from:-

$$\frac{\Gamma(x)}{2\,V_0} = S^{(4)}(x) + \tan\alpha_D\sqrt{\frac{1-x}{x}}$$

$$= -\left[C_{p_{US}} - C_p(\alpha = 0,\ z_c = 0)\right]\sqrt{1 - M_0^2\cos^2\Lambda}\;\frac{1 + \left[\dfrac{S^{(2)}(x)}{\Lambda\cos\Lambda}\right]^2}{2\left[\cos\Lambda + \dfrac{S^{(1)}(x)}{\Lambda}\right]} \qquad \ldots (10)$$

where $C_p(\alpha = 0,\ z_c = 0)$ is the pressure coefficient of the uncambered section at zero lift.

With the $\Gamma(x)$ of equation (10) the slope of the skeleton line was determined by equation (9). By graphical integration of the slopes the incidence α_D and the ordinates of the camber-line were found. Then the pressure distribution can be determined from equations (1), (2) and (3), taking account of all higher order terms. If a modification to the resulting pressure distribution is then required, the procedure is to estimate the required alteration of the camber-line and of the incidence and determine $S^{(4)}(x)$ and $S^{(5)}(x)$ and $C_p(x)$. This procedure does not, of course, lead to explicit expressions for the load distribution and the camber line.

The results of the calculations are shown in Figs.2 and 4, which show the surface pressure distributions, and the shape of the camber line respectively. The required pressure distribution has been substantially achieved, except over the first 10% of the chord.

TABLE 1

Ordinates of aerofoil at 32 pivotal points

(from inspection of model)

$\frac{x}{c}$	$\frac{z}{c}$ upper	$\frac{z}{c}$ lower
1.0000	0	0
0.9976	0	0
0.9904	0.00078	0.00085
0.9785	0.00181	0.00185
0.9619	0.00333	0.00317
0.9410	0.00521	0.00484
0.9157	0.00763	0.00689
0.8865	0.01033	0.00926
0.8536	0.01320	0.01189
0.8172	0.01621	0.01480
0.7778	0.01946	0.01799
0.7357	0.02288	0.02134
0.6913	0.02598	0.02488
0.6451	0.02915	0.02852
0.5975	0.03213	0.03231
0.5490	0.03457	0.03621
0.5000	0.03668	0.04010
0.4510	0.03789	0.04386
0.4025	0.03879	0.04712
0.3549	0.03925	0.04954
0.3087	0.03908	0.05050
0.2643	0.03852	0.04979
0.2222	0.03748	0.04766
0.1828	0.03571	0.04474
0.1464	0.03338	0.04112
0.1135	0.03058	0.03693
0.0843	0.02704	0.03226
0.0590	0.02300	0.02741
0.0381	0.01850	0.02233
0.0215	0.01402	0.01718
0.0096	0.00892	0.01190
0.0024	0.00379	0.00575
0	0	0

TABLE 2

Ordinates of pressure holes

Upper Surface		Lower Surface	
$\frac{x}{c}$	$\frac{z}{c}$	$\frac{x}{c}$	$\frac{z}{c}$
0	0	0	0
0.0044	0.00558	0.0034	0.00743
0.0101	0.00923	0.0115	0.01290
0.0197	0.01332	0.0184	0.01607
0.0300	0.01653		
0.0399	0.01904	0.0408	0.02307
0.0598	0.02333	0.0618	0.02796
0.0803	0.02625	0.0819	0.03183
0.1005	0.02900	0.1016	0.03518
0.1502	0.03367	0.1516	0.04168
0.2003	0.03650	0.2016	0.04625
0.2499	0.03818	0.2516	0.04926
0.2998	0.03896	0.3016	0.05050
0.3498	0.03925	0.3516	0.04968
0.4000	0.03896	0.4016	0.04714
0.4498	0.03803	0.4507	0.04390
0.4997	0.03673	0.5012	0.03999
0.5496	0.03454	0.5510	0.03606
0.5997	0.03191	0.6012	0.03202
0.6498	0.02887	0.6514	0.02807
0.6998	0.02541	0.7012	0.02409
0.7503	0.02182	0.7514	0.02010
0.7999	0.01779	0.8018	0.01601
0.8503	0.01358	0.8515	0.01202
0.9003	0.00895	0.9010	0.00809
0.9493	0.00457		

WT.2078. C.P.582.K3 - Printed in England.

TABLE 3 - Values of p/H_{eff}

(a) Stagnation pressure 30 in. mercury

Upper surface

$\alpha_E = 0^\circ$

Mach Number (Values of p/H_{eff})

x/c	z/c	·609	·803	·855	·904	·943	·983	1·026	1·063	1·107	1·145	1·193	1·253	1·304	1·356	1·408
0.000	+ 0.00000	1.000	1.002	1.000	1.005	1.003	1.004	1.017	1.005	·999	·998	1.002	1.002	1.003	·997	1.008
0.004	+ 0.00558	·975	960	955	959	952	950	962	942	936	929	926	926	924	898	899
0.010	+ 0.00923	·960	936	929	927	919	915	926	898	891	886	877	866	857	823	823
0.020	+ 0.01332	·942	905	895	888	879	873	878	857	851	827	812	797	786	741	734
0.030	+ 0.01653	·933	890	877	867	858	849	852	814	796	775	756	740	725	677	672
0.040	+ 0.01904	·926	877	863	853	842	832	838	798	779	758	741	720	706	661	655
0.060	+ 0.02333	·922	869	854	842	829	816	823	782	767	736	711	684	670	625	621
0.080	+ 0.02625	·915	856	839	826	813	793	798	761	744	717	698	662	644	588	579
0.100	+ 0.02900	·912	851	834	819	804	787	782	745	727	699	685	642	627	559	547
0.150	+ 0.03367	·911	847	830	817	803	783	782	751	724	694	675	629	610	613	511
0.200	+ 0.03650	·911	850	831	818	803	787	787	746	720	693	674	632	611	589	488
0.250	+ 0.03818	·910	847	826	809	798	778	782	746	718	687	674	635	612	597	479
0.300	+ 0.03896	·913	853	835	821	804	791	786	763	731	700	688	645	621	610	591
0.350	+ 0.03925	·913	854	835	822	809	792	786	764	736	705	700	652	621	608	591
0.400	+ 0.03896	·919	861	845	834	820	807	799	776	752	719	707	677	635	619	618
0.450	+ 0.03803	·917	860	842	830	816	802	794	769	753	713	696	669	634	613	616
0.500	+ 0.03673	·915	857	840	826	813	797	787	766	753	717	699	674	639	621	617
0.550	+ 0.03454	·919	861	845	831	819	806	790	766	758	729	712	687	656	633	628
0.600	+ 0.03191	·922	869	851	840	827	817	797	774	772	744	722	701	673	655	640
0.650	+ 0.02887	·923	871	854	844	832	823	801	780	784	755	729	716	680	662	644
0.700	+ 0.02541	·927	878	863	852	843	832	813	791	799	767	743	733	696	682	666
0.750	+ 0.02182	·930	881	866	856	847	839	818	797	804	777	750	735	708	691	672
0.800	+ 0.01779	·932	886	872	864	853	848	825	807	808	786	762	742	722	706	688
0.850	+ 0.01358	·932	887	873	865	857	852	829	812	808	791	773	745	729	713	695
0.900	+ 0.00895	·939	900	887	880	872	871	845	832	828	812	795	775	753	733	725
0.949	+ 0.00457	·943	904	892	887	880	880	852	839	834	820	805	782	761	736	718

$\alpha_E = 2^\circ$

Mach Number (Values of p/H_{eff})

x/c	z/c	·601	·797	·850	·900	·941	·979	1·020	1·062	1·101	1·142	1·190	1·252	1·306	1·355	1·409
0.000	+ 0.00000	·981	·967	·965	·964	·964	·962	·974	·957	956	·945	·949	·934	·941	·953	·965
0.004	+ 0.00558	·923	870	860	846	836	823	827	803	794	778	774	753	760	773	781
0.010	+ 0.00923	·907	841	829	813	801	792	795	855	733	708	696	666	668	680	691
0.020	+ 0.01332	·889	813	792	774	764	744	738	685	662	635	618	575	574	584	590
0.030	+ 0.01653	·887	804	784	763	740	717	710	662	632	602	580	528	524	533	540
0.040	+ 0.01904	·885	802	781	758	741	718	714	672	639	606	578	510	504	507	509
0.060	+ 0.02333	·887	804	782	759	731	712	720	668	632	595	560	507	489	493	500
0.080	+ 0.02625	·885	800	777	753	724	709	711	666	630	590	548	491	467	466	471
0.100	+ 0.02900	·886	799	777	754	735	695	694	661	624	588	540	472	444	442	444
0.150	+ 0.03367	·891	809	787	766	745	725	710	672	639	608	566	559	398	394	393
0.200	+ 0.03650	·895	817	795	775	754	745	726	683	661	626	607	560	517	381	365
0.250	+ 0.03818	·896	820	798	777	759	740	733	690	671	634	619	569	578	378	360
0.300	+ 0.03896	·903	831	809	793	776	748	747	718	696	660	644	595	586	554	362
0.350	+ 0.03925	·905	836	817	797	783	764	752	730	707	676	666	616	593	589	513
0.400	+ 0.03896	·913	849	829	812	800	792	765	750	725	696	685	635	614	617	574
0.450	+ 0.03803	·912	848	829	812	800	784	765	743	733	699	681	648	620	627	608
0.500	+ 0.03673	·912	848	829	812	800	781	765	741	737	708	688	667	632	630	618
0.550	+ 0.03454	·915	854	836	821	809	796	774	753	750	727	704	683	651	648	638
0.600	+ 0.03191	·920	863	847	831	820	805	789	768	767	745	722	706	672	664	650
0.650	+ 0.02887	·923	867	851	838	829	819	799	779	782	758	734	720	689	683	658
0.700	+ 0.02541	·928	876	862	847	840	830	813	794	798	775	751	741	707	699	674
0.750	+ 0.02182	·930	880	866	854	847	839	822	805	806	785	761	752	721	710	685
0.800	+ 0.01779	·934	887	875	865	856	850	831	814	815	798	774	760	734	720	696
0.850	+ 0.01358	·935	889	876	867	860	855	834	813	814	799	778	759	738	724	699
0.900	+ 0.00895	·943	900	890	880	875	870	849	834	831	815	797	773	757	741	717
0.949	+ 0.00457	·945	904	895	884	880	878	855	837	832	815	803	774	759	744	719

TABLE 3(a) (Cont'd.) - Values of p/H_{eff}

(a) Stagnation pressure 30 in. mercury

Upper surface

$\alpha_E = 2.6^o$

Mach Number

Values of p/H_{eff}

x/c		z/c	·982	1·022	1·064	1·103	1·143	1·194	1·216	1·226	1·252	1·302	1·355	1·405
0.000	+	0.00000	·941	·950	935	·935	·920	·929	·920	·920	·912	·924	·937	·953
0.004	+	0.00558	·763	769	738	734	709	712	692	692	688	702	722	738
0.010	+	0.00923	·740	737	692	677	643	644	622	621	614	625	643	656
0.020	+	0.01332	·683	677	624	607	567	561	531	530	521	529	547	555
0.030	+	001653	·661	660	602	582	536	532	489	487	474	484	496	503
0.040	+	0.01904	·686	676	614	588	534	531	478	474	462	466	478	485
0.060	+	0.02333	·696	677	619	584	539	512	442	433	421	423	430	434
0.080	+	0.02625	·692	676	624	583	551	511	474	454	429	427	434	437
0.100	+	0.02900	·680	671	625	585	552	499	519	454	422	411	414	416
0.150	+	0.03367	·698	689	650	614	580	526	526	551	398	370	373	371
0.200	+	0.03650	·717	707	675	645	609	570	564	553	561	353	354	348
0.250	+	0.03818	·733	719	682	658	621	607	588	582	569	528	348	333
0.300	+	003896	·753	735	705	687	645	633	622	612	590	572	524	485
0.350	+	0.03925	·760	743	719	698	664	649	635	634	614	624	557	540
0.400	+	0.03896	·770	759	741	715	685	678	656	661	634	613	588	555
0.450	+	003803	·778	761	749	727	699	690	666	672	646	627	616	564
0.500	+	0.03673	·782	759	749	737	705	691	675	674	667	634	620	569
0.550	+	0.03454	·793	769	760	750	724	706	688	691	686	653	642	584
0.600	+	0.03191	·810	785	772	768	745	726	712	710	707	672	659	594
0.650	+	0.02887	·817	796	777	784	761	744	728	725	724	689	671	604
0.700	+	002541	·830	810	791	798	775	756	749	742	740	708	687	617
0.750	+	0.02182	·840	820	800	808	786	768	760	751	748	717	693	623
0.800	+	0.01779	·853	833	811	819	796	778	771	764	759	729	706	638
0.850	+	0.01358	·856	835	813	815	797	779	772	766	755	731	700	632
0.900	+	0.00895	·871	846	830	826	809	793	783	775	767	749	722	667
0.949	+	000457	·878	849	831	827	810	797	849	776	768	751	724	675

$\alpha_E = 3^o$

Mach Number

Values of p/H_{eff}

x/c		z/c	·600	·803	·848	·901	·942	·979	1·023	1·064	1·105	1·145	1·195	1·213	1·244	1·298	1·328	1·352	1·407
0.000	+	0.00000	·959	·930	·926	·921	·921	·911	·926	·904	904	·905	·893	·889	·886	·907	·915	·914	·936
0.004	+	000558	·886	803	785	763	747	729	734	702	701	687	663	659	663	685	696	704	722
0.010	+	000923	·871	781	762	741	725	693	693	643	632	614	587	581	581	597	609	616	630
0.020	+	001332	·858	757	734	709	680	638	635	576	561	529	502	492	491	505	516	518	534
0.030	+	001653	·858	753	728	693	661	628	626	558	538	497	460	450	446	459	468	471	482
0.040	+	001904	·861	758	732	711	675	660	645	570	544	491	454	439	433	443	452	456	462
0.060	+	002333	·867	767	742	704	693	679	656	589	555	499	424	418	409	410	413	418	423
0.080	+	0.02625	·869	768	742	711	691	678	663	603	555	503	436	405	389	391	395	398	398
0.100	+	002900	·871	772	746	717	683	661	669	604	556	510	487	404	377	377	392	386	392
0.150	+	0.03367	·880	788	762	737	729	687	686	639	596	568	518	528	352	352	352	344	351
0.200	+	0.03650	·886	800	777	757	727	709	703	665	632	602	550	568	512	335	342	340	334
0.250	+	0.03818	·888	804	782	762	749	729	715	671	652	623	585	584	567	492	438	478	416
0.300	+	0.03896	·896	820	799	779	760	750	733	697	683	650	624	621	592	547	538	536	531
0.350	+	003925	·901	824	806	787	774	756	739	715	695	665	643	635	610	578	561	553	546
0.400	+	0.03896	·910	840	824	802	788	771	758	739	718	693	666	658	642	611	592	568	554
0.450	+	0.03803	·910	842	825	807	793	777	763	748	729	706	687	670	653	630	616	587	557
0.500	+	0.03673	·910	844	826	807	795	782	764	749	735	717	694	679	661	637	630	591	560
0.550	+	003454	·912	849	833	817	806	795	774	756	753	736	711	699	689	658	648	602	571
0.600	+	003191	·918	858	843	829	819	809	788	766	770	754	726	716	707	672	666	620	579
0.650	+	002887	·924	866	853	839	829	820	798	778	787	773	749	732	719	688	682	629	584
0.700	+	002541	·928	875	865	850	842	833	812	795	804	788	759	750	737	703	701	642	588
0.750	+	0.02182	932	881	868	856	849	842	822	804	810	796	763	760	744	713	705	645	580
0.800	+	0.01779	·936	889	878	865	859	853	831	814	816	802	773	769	753	724	712	662	587
0.850	+	001358	·939	890	879	866	859	853	831	814	813	803	769	767	746	719	708	651	565
0.900	+	000895	·943	898	889	877	871	868	846	827	822	812	781	777	758	738	728	685	619
0.949	+	000457	·945	902	889	880	876	873	848	828	823	815	785	779	761	741	728	699	619

TABLE 3(a) (Cont'd.) - Values of p/H_{eff}

(a) Stagnation pressure 30 in. mercury

Upper surface

$\alpha_E = 4^\circ$

x/c	z/c	·596	·797	·847	·903	·941	·981	1·023	1·062	1·101	1·145	1·196	1·251	1·301	1·357	1·403
		Mach Number														
		Values of p/H_{eff}														
0.000	+ 0.00000	·924	·878	·870	·861	·854	·840	·845	·831	·825	·820	·830	·847	·863	·873	·892
0.004	+ 0.00558	·837	721	688	662	648	620	618	593	581	569	570	589	611	628	650
0.010	+ 0.00923	·827	708	678	638	610	567	564	525	509	498	499	510	526	541	554
0.020	+ 0.01332	·821	690	657	601	567	510	504	452	427	413	408	418	434	443	459
0.030	+ 0.01653	·825	695	651	603	569	510	508	430	393	372	363	372	387	399	412
0.040	+ 0.01904	·835	712	682	639	602	536	541	437	393	362	349	358	370	377	390
0.060	+ 0.02333	·845	730	688	667	630	588	593	489	408	358	340	342	355	362	370
0.080	+ 0.02625	·851	737	702	663	651	638	612	533	465	369	338	339	345	354	360
0.100	+ 0.02900	·855	746	711	661	650	650	614	543	521	354	330	323	330	337	339
0.150	+ 0.03367	·869	769	741	706	681	662	668	603	555	531	500	454	298	301	295
0.200	+ 0.03650	·879	788	762	736	717	682	677	647	604	572	549	510	493	498	460
0.250	+ 0.03818	·883	800	771	745	725	693	696	660	636	601	589	529	507	516	500
0.300	+ 0.03896	·895	814	791	768	750	723	721	685	672	632	627	548	518	523	514
0.350	+ 0.03925	·897	823	801	781	758	749	734	708	692	653	649	570	529	529	524
0.400	+ 0.03896	·906	837	818	798	786	773	754	738	715	687	676	593	545	543	539
0.450	+ 0.03803	·908	842	824	803	792	782	764	754	734	710	687	609	562	552	551
0.500	+ 0.03673	·910	846	827	808	796	787	768	756	743	716	690	603	562	551	546
0.550	+ 0.03454	·916	855	837	821	811	800	785	772	763	737	703	609	573	552	552
0.600	+ 0.03191	·920	864	850	835	826	813	799	781	779	752	716	613	576	556	548
0.650	+ 0.02887	·926	873	860	846	836	823	807	788	789	763	724	619	583	551	541
0.700	+ 0.02541	·932	881	869	855	846	836	818	797	797	772	734	636	594	548	542
0.750	+ 0.02182	·934	884	872	858	851	839	820	801	800	777	724	636	596	538	527
0.800	+ 0.01779	·937	890	878	865	857	849	828	806	803	780	718	665	615	548	523
0.850	+ 0.01358	·937	890	877	865	857	849	825	804	797	778	709	657	597	534	504
0.900	+ 0.00895	·942	895	885	871	864	859	834	814	809	787	731	702	659	570	533
0.949	+ 0.00457	·944	898	886	872	866	860	833	811	800	778	734	713	665	600	558

$\alpha_E = 5^\circ$

x/c	z/c	·605	·795	·848	·904	·944	·983	1·022	1·062	1·105	1·143	1·185	1·252	1·308	1·357	1·403
		Mach Number														
		Values of p/H_{eff}														
0.000	+ 0.00000	·885	·818	·801	·799	·794	·779	·783	·769	·771	·792	·775	·800	·823	·833	·851
0.004	+ 0.00558	·783	626	593	571	551	530	522	506	504	527	499	527	548	566	588
0.010	+ 0.00923	·780	627	579	536	507	477	466	443	436	457	425	450	469	486	507
0.020	+ 0.01332	·780	622	560	504	462	417	401	370	364	384	345	369	383	395	409
0.030	+ 0.01653	·789	630	576	524	480	422	387	336	328	352	332	326	333	342	360
0.040	+ 0.01904	·805	666	620	569	516	445	420	326	315	342	349	305	315	325	344
0.060	+ 0.02333	·820	693	643	624	576	479	539	340	314	333	400	288	298	310	320
0.080	+ 0.02625	·829	706	680	643	611	550	560	415	345	339	531	288	288	298	310
0.100	+ 0.02900	·837	719	679	636	625	571	574	528	488	371	568	401	282	289	297
0.150	+ 0.03367	·854	750	721	698	669	633	638	602	564	541	573	514	473	486	466
0.200	+ 0.03650	·868	775	748	727	697	685	665	650	617	599	588	540	500	512	504
0.250	+ 0.03818	·875	787	762	746	727	717	695	672	658	627	601	567	522	534	530
0.300	+ 0.03896	·886	808	786	776	752	730	727	702	689	650	616	570	549	559	546
0.350	+ 0.03925	·892	819	801	787	772	747	746	722	705	664	632	606	571	574	561
0.400	+ 0.03896	·903	837,	819	810	795	772	770	753	727	685	644	613	590	588	571
0.450	+ 0.03803	·907	846	829	824	808	783	779	761	740	702	644	617	595	592	565
0.500	+ 0.03673	·910	850	835	828	813	794	781	767	749	706	646	624	597	578	540
0.550	+ 0.03454	·916	862	848	839	826	808	790	775	762	718	658	632	603	563	530
0.600	+ 0.03191	·922	871	855	849	833	818	796	780	772	727	668	646	597	545	516
0.650	+ 0.02887	·926	875	860	854	841	823	803	782	777	732	670	642	579	523	500
0.700	+ 0.02541	·930	879	865	858	845	832	806	784	780	740	676	639	562	502	489
0.750	+ 0.02182	·930	880	866	859	846	832	806	780	776	751	656	599	521	479	470
0.800	+ 0.01779	·934	883	870	862	848	834	808	781	780	763	644	579	507	480	464
0.850	+ 0.01358	·934	882	866	860	845	826	799	767	760	745	604	546	496	486	455
0.900	+ 0.00895	·935	885	870	863	850	838	807	781	775	742	634	586	565	546	491
0.949	+ 0.00457	·935	884	868	861	847	837	800	774	769	711	644	596	593	587	519

TABLE 3 - Values of p/H_{eff}

(b) Stagnation pressure 30 in. mercury

Lower surface

$\alpha_E = 0^\circ$

Mach Number — Values of p/H_{eff}

x/c	z/c	·609	·803	·855	·904	·943	·983	1·026	1·063	1·107	1·145	1·193	1·253	1·304	1·356	1·408
0.003	– 0.00743	·968	·950	·943	·942	·938	·933	·938	·926	·924	·922	·919	·902	·902	·895	·902
0.012	– 0.01290	·951	923	913	911	903	897	909	890	873	862	857	838	833	826	833
0.018	– 0.01607	·938	900	887	881	872	866	867	835	806	795	788	769	767	757	768
0.041	– 0.02307	·919	869	853	842	829	820	829	797	778	759	749	722	711	697	702
0.062	– 0.02796	·910	852	833	819	804	793	798	760	743	722	709	677	663	648	649
0.082	– 0.03183	·909	847	829	814	799	782	787	748	726	702	685	654	637	618	625
0.102	– 0.03518	·902	837	817	799	784	766	766	726	702	677	659	625	607	583	592
0.152	– 0.04168	·896	823	801	782	766	746	743	702	673	645	621	581	557	522	518
0.202	– 0.04625	·891	815	792	771	753	733	732	688	662	621	600	549	525	489	479
0.252	– 0.04926	·886	806	781	760	738	714	717	667	638	593	570	522	481	450	430
0.302	– 0.05050	·885	804	779	756	734	714	705	664	639	581	565	505	418	381	357
0.352	– 0.04968	·892	818	794	775	754	735	721	693	667	619	602	550	517	494	518
0.402	– 0.04714	·902	833	812	794	778	761	745	723	698	664	643	612	583	573	555
0.451	– 0.04390	·909	846	827	812	798	781	768	748	732	698	675	650	627	612	571
0.501	– 0.03999	·916	859	840	827	814	801	787	766	754	724	702	681	653	640	577
0.551	– 0.03606	·922	868	850	838	827	816	801	780	773	743	724	703	672	667	585
0.601	– 0.03202	·926	873	858	846	835	824	809	788	787	757	735	714	690	678	591
0.651	– 0.02807	·928	878	863	853	843	833	818	796	796	770	748	728	705	688	599
0.701	– 0.02409	·931	884	868	860	849	842	825	803	804	783	761	747	716	702	611
0.751	– 0.02010	·933	887	872	865	855	848	830	811	811	793	774	756	729	713	625
0.802	– 0.01601	·935	891	877	871	861	856	836	818	820	801	780	762	739	726	648
0.852	– 0.01202	·939	896	884	877	868	863	842	827	827	808	789	771	767	737	671
0.901	– 0.00809	·939	896	885	879	871	869	845	830	826	813	795	775	772	746	708

$\alpha_E = 2^\circ$

Mach Number — Values of p/H_{eff}

x/c	z/c	·601	·797	·850	·900	·941	·979	1·020	1·062	1·101	1·142	1·190	1·252	1·306	1·355	1·409
0.003	– 0.00743	·997	·995	·996	·997	·997	999	1.013	·998	·992	·980	·986	·981	·983	·980	·983
0.012	– 0.01290	·988	983	982	981	980	981	995	978	971	960	962	949	943	930	934
0.018	– 0.01607	·975	959	956	952	949	947	962	941	934	918	912	887	880	864	863
0.041	– 0.02307	·956	926	918	911	905	902	911	886	879	862	859	839	828	808	806
0.062	– 0.02796	·944	906	895	884	875	869	876	850	839	820	815	792	776	757	748
0.082	– 0.03183	·940	898	885	875	866	857	862	834	817	797	790	765	748	732	720
0.102	– 0.03518	·933	885	872	858	848	838	840	807	793	769	760	735	714	696	681
0.152	– 0.04168	·921	863	847	832	818	806	803	769	754	724	714	686	653	640	611
0.202	– 0.04625	·914	851	833	815	801	783	781	752	732	695	686	646	604	589	563
0.252	– 0.04926	·907	838	819	798	782	766	759	730	707	666	649	603	558	531	501
0.302	– 0.05050	·903	832	811	789	773	753	740	716	691	653	625	581	533	479	429
0.352	– 0.04968	·908	839	819	801	784	767	751	721	708	672	640	601	566	510	416
0.402	– 0.04714	·914	850	832	815	800	783	769	737	729	697	670	640	608	580	551
0.451	– 0.04390	·920	859	843	827	814	800	785	758	752	722	698	672	635	620	592
0.501	– 0.03999	·925	868	852	839	827	814	797	778	771	745	720	692	663	652	619
0.551	– 0.03606	·928	876	862	847	837	824	808	791	783	763	734	707	684	675	645
0.601	– 0.03202	·931	880	866	853	843	833	818	795	791	775	739	725	695	685	658
0.651	– 0.02807	·933	884	869	857	849	838	822	806	799	782	760	740	703	694	670
0.701	– 0.02409	·935	886	874	862	854	843	827	810	808	788	766	747	716	699	677
0.751	– 0.02010	·937	890	876	866	857	849	831	813	813	791	772	753	730	707	689
0.802	– 0.01601	·938	891	879	869	861	853	835	815	811	791	776	759	732	715	696
0.852	– 0.01202	·940	896	884	875	866	860	842	825	821	803	785	763	738	720	700
0.901	– 0.00809	·939	894	881	872	865	859	838	821	815	803	785	759	739	725	696

TABLE 3(b) (Cont'd.) - Values of p/H_{eff}

(b) Stagnation pressure 30 in. mercury

Lower surface

$\alpha_E = 2.6$

Mach Number

Values of p/H_{eff}

$^x/c$	$^z/c$	·982	1·022	1·064	1·103	1·143	1·194	1·216	1·226	1·252	1·302	1·355	1·405
0.003	- 0.00743	1·008	1·020	1·006	1·005	·992	1·001	·996	·997	·987	·993	·995	·999
0.012	- 0.01290	·998	1·008	991	989	976	985	980	979	965	960	954	953
0.018	- 0.01607	·963	975	958	955	941	942	934	933	911	901	892	886
0.041	- 0.02307	·921	926	907	900	883	886	879	878	859	847	836	829
0.062	- 0.02796	·888	894	869	860	840	838	833	830	813	831	782	768
0.082	- 0.03183	·879	877	852	838	819	818	808	804	788	767	757	742
0.102	- 0.03518	·856	856	825	813	790	786	775	775	756	731	719	704
0.152	- 0.04168	·820	820	790	773	744	739	720	724	706	674	661	638
0.202	- 0.04625	·798	796	762	748	714	706	685	687	665	625	605	583
0.252	- 0.04926	·776	767	740	721	682	670	648	641	625	584	561	525
0.302	- 0.05050	·765	750	724	703	666	643	620	609	597	554	512	456
0.352	- 0.04968	·775	758	735	717	683	654	638	626	612	577	532	499
0.402	- 0.04714	·791	775	755	739	705	682	672	659	646	613	589	555
0.451	- 0.04390	·808	788	771	757	727	707	693	687	674	638	627	592
0.501	- 0.03999	·818	801	782	775	747	729	721	714	694	667	655	630
0.551	- 0.03606	·828	811	791	790	763	739	738	729	710	682	677	647
0.601	- 0.03202	·836	815	798	794	775	750	746	741	729	690	689	658
0.651	- 0.02807	·841	821	803	799	783	759	751	751	739	702	696	662
0.701	- 0.02409	·846	828	808	808	789	770	757	758	747	715	700	682
0.751	- 0.02010	·851	830	812	814	791	775	765	764	753	724	705	693
0.802	- 0.01601	·853	832	814	813	790	776	769	762	755	725	713	699
0.852	- 0.01202	·858	840	820	815	798	781	775	769	760	729	719	701
0.901	- 0.00809	·860	836	819	814	799	783	772	769	759	733	721	696

$\alpha_E = 3^{\circ}$

Mach Number

Values of p/H_{eff}

$^x/c$	$^z/c$	·600	·803	·848	·901	·942	·979	1·023	1·064	1·105	1·145	1·195	1·213	1·244	1·298	1·328	1·352	1·407
0.003	- 0.00743	1·001	1·002	1·003	1·003	1·006	1·006	1·025	1·003	1·007	1·010	·996	·992	·984	·994	1·000	1·000	1·005
0.012	- 0.01290	1·000	999	998	999	1·000	1·003	1·019	995	997	998	987	985	968	973	972	963	968
0.018	- 0.01607	989	980	977	974	974	973	989	966	967	968	955	946	922	918	918	911	907
0.041	- 0.02307	·970	948	943	937	933	931	943	917	914	911	894	894	870	865	862	849	852
0.062	- 0.02796	·957	926	917	910	904	900	910	879	874	867	850	847	823	814	809	798	787
0.082	- 0.03183	953	916	908	899	891	888	895	864	854	841	824	818	801	783	780	773	756
0.102	- 0.03518	945	903	893	881	872	866	873	838	828	814	796	787	768	746	733	735	723
0.152	- 0.04168	·933	880	867	852	840	831	836	800	788	767	748	734	717	692	691	677	655
0.202	- 0.04625	·923	866	851	834	821	808	809	776	759	736	712	698	678	643	639	624	602
0.252	- 0.04926	·916	851	833	816	800	785	779	752	731	700	674	659	633	599	590	576	541
0.302	- 0.05050	910	841	823	804	789	770	762	735	712	682	650	630	606	568	559	527	477
0.352	- 0.04968	914	847	831	812	797	781	770	743	724	698	660	647	617	585	570	542	508
0.402	- 0.04714	·918	857	840	822	809	796	782	755	742	718	686	672	646	623	616	595	565
0.451	- 0.04390	·923	865	849	833	821	810	795	767	763	741	709	697	673	642	642	631	600
0.501	- 0.03999	928	872	858	844	833	821	806	782	781	760	731	724	692	668	662	656	636
0.551	- 0.03606	933	880	866	851	841	832	814	793	789	773	743	740	709	681	683	680	653
0.601	- 0.03202	·934	883	868	856	847	837	819	799	795	783	748	746	728	694	687	692	663
0.651	- 0.02807	·935	885	872	860	851	841	824	805	800	791	756	751	738	703	699	700	668
0.701	- 0.02409	·938	889	875	862	855	847	828	810	811	798	764	756	745	717	705	706	688
0.751	- 0.02010	·938	890	879	865	858	850	832	814	811	801	771	765	752	724	716	710	699
0.802	- 0.01601	·938	891	879	866	859	852	831	814	810	801	771	767	752	724	719	718	698
0.852	- 0.01202	·940	894	882	871	866	858	838	820	816	804	775	773	755	729	730	722	695
0.901	- 0.00809	·938	890	879	866	861	855	832	813	809	802	773	767	750	727	728	720	680

TABLE 3(b) (Cont'd.) - Values of p/H

(b) Stagnation pressure 30 in. mercury

Lower surface

$\alpha_E = 4^{\circ}$

Mach Number

Values of p/H_{eff}

x/c	z/c	·596	·797	·847	·903	·941	·981	1·023	1·062	1·101	1·145	1·196	1·251	1·301	1·357	1·403
0.003	-0.00743	·999	1·000	1·004	1·003	1·013	1·001	1·019	1·005	1·002	·999	1·003	·995	1·009	1·004	1·016
0.012	-0.01290	1·003	1·005	1·009	1·008	1·007	1·011	1·028	1·009	1·008	999	1·003	991	995	989	989
0.018	-0.01607	·995	994	995	993	993	991	1·009	989	988	979	981	962	960	944	942
0.041	-0.02307	·982	967	965	960	957	954	971	947	941	926	930	910	907	893	879
0.062	-0.02796	·972	947	943	934	930	926	939	910	906	898	887	863	850	837	826
0.082	-0.03183	·966	937	930	923	917	912	925	895	888	864	862	840	825	810	796
0.102	-0.03518	·956	922	916	905	898	892	904	870	861	835	834	807	789	771	761
0.152	-0.04168	·942	899	888	876	865	858	865	833	819	792	781	752	734	718	702
0.202	-0.04625	·934	882	869	854	842	831	833	807	788	755	745	714	684	669	640
0.252	-0.04926	·924	866	850	832	821	806	803	779	756	722	702	672	639	610	582
0.302	-0.05050	·918	856	839	820	806	790	785	758	739	704	676	639	610	571	537
0.352	-0.04968	·920	860	843	824	811	796	787	761	743	709	682	642	614	580	550
0.402	-0.04714	·924	862	850	833	820	806	798	768	759	725	699	667	642	621	590
0.451	-0.04390	·928	872	859	840	829	816	804	777	773	743	724	686	665	653	631
0.501	-0.03999	·932	878	864	850	837	828	814	789	789	762	742	708	690	680	660
0.551	-0.03606	·936	885	871	856	846	834	820	799	794	777	756	735	704	708	672
0.601	-0.03202	·936	886	874	860	849	838	825	805	800	786	765	746	708	723	688
0.651	-0.02807	·937	889	876	861	852	842	826	808	806	790	772	754	734	726	694
0.701	-0.02409	·938	890	878	862	854	844	826	810	809	787	779	763	739	727	693
0.751	-0.02010	·939	891	878	865	857	847	828	811	807	786	782	768	742	721	682
0.802	-0.01601	·938	890	878	865	856	846	826	810	800	780	781	763	741	708	672
0.852	-0.01202	·941	895	882	870	859	851	831	811	803	787	785	770	746	704	666
0.901	-0.00809	·937	887	875	861	854	845	820	802	792	778	774	763	734	672	645

$\alpha_E = 5^{\circ}$

Mach Number

Values of p/H_{eff}

x/c	z/c	·605	·795	·848	·904	·944	·983	1·022	1·062	1·105	1·143	1·185	1·25.2	1·308	1·357	1·403
0.003	-0.00743	·991	·987	·988	·994	·995	·994	1·008	·992	·994	·998	·990	·991	1·008	1·005	1·018
0.012	-0.01290	1·002	1·004	1·005	1·012	1·013	1·012	1·030	1·010	1·012	1·008	1·001	1·003	1·009	1·005	1·009
0.018	-0.01607	1·001	1·000	1·001	1·008	1·008	1·006	1·022	1·002	1·001	999	995	983	987	973	972
0.041	-0.02307	·989	978	977	978	977	974	988	965	963	948	946	936	931	921	921
0.062	-0.02796	·978	959	956	956	951	948	960	928	930	911	907	890	884	873	862
0.082	-0.03183	·972	950	944	944	939	931	946	925	911	892	882	867	858	851	839
0.102	-0.03518	·962	937	929	927	921	912	924	900	890	862	852	835	821	811	799
0.152	-0.04168	949	911	902	894	885	873	884	862	846	817	802	777	764	753	736
0.202	-0.04625	·938	893	879	872	860	850	855	834	815	782	763	742	716	699	679
0.252	-0.04926	·928	875	861	850	838	826	827	806	788	750	726	698	670	641	626
0.302	-0.05050	·922	864	847	835	822	808	803	778	768	732	704	664	639	610	583
0.352	-0.04968	·922	866	850	838	825	812	805	776	772	734	713	668	640	626	592
0.402	-0.04714	·925	871	855	844	828	819	810	786	783	750	735	692	672	663	643
0.451	-0.04390	·927	875	860	850	836	825	817	797	795	769	748	714	696	694	666
0.501	-0.03999	·930	880	866	859	845	833	825	806	807	790	766	745	716	721	687
0.551	-0.03606	934	884	870	863	851	841	827	813	814	800	782	771	734	731	692
0.601	-0.03202	·934	886	873	863	853	844	828	814	815	805	788	771	750	725	692
0.651	-0.02807	·934	887	874	866	853	844	830	814	815	804	795	776	750	721	689
0.701	-0.02409	·935	887	874	867	855	845	832	812	807	799	795	777	742	709	679
0.751	-0.02010	·935	888	874	868	855	847	833	813	803	799	794	769	733	699	670
0.802	-0.01601	·935	886	872	866	851	844	827	809	791	792	788	751	723	685	660
0.852	-0.01202	·937	888	874	868	855	848	825	808	789	786	776	743	709	670	653
0.901	-0.00809	·932	879	864	858	844	836	808	791	777	748	745	708	675	645	634

TABLE 3 - Values of p/H_{eff}

(c) Stagnation pressure 36 in. mercury

$\alpha_E = 2.6^{\circ}$ Upper Surface

Mach Number

Values of p/H_{eff}

x/c	z/c	.598	.797	.851	.896	.938	.976	1.022	1.063	1.103	1.144	1.192	1.215	1.226	1.250	1.303	1.355
0.000	+ 0.000[illegible]	968	.945	.942	.944	.944	.944	.953	.932	.934	.916	.930	.919	.919	.916	.924	.938
0.004	+ 0.00558	898	830	815	801	781	766	769	738	735	711	714	692	690	694	707	726
0.010	+ 0.00923	886	807	791	777	766	749	740	695	678	646	650	622	620	621	632	648
0.020	+ 0.01332	.870	778	756	743	726	692	680	625	607	568	566	530	529	527	536	548
0.030	+ 0.01653	.869	776	753	729	697	671	662	603	578	538	537	486	485	475	483	495
0.040	+ 0.01904	870	776	750	726	706	677	680	620	589	542	523	478	476	468	473	478
0.060	+ 0.02333	874	782	756	728	706	684	683	625	584	547	513	442	431	423	424	426
0.080	+ 0.02625	.875	780	753	728	712	684	683	625	584	551	510	475	454	434	431	435
0.100	+ 0.029[illegible]	.877	784	757	735	693	675	677	625	586	547	496	500	450	424	416	416
0.150	+ 0.03367	.882	794	769	745	727	697	691	658	612	580	524	525	549	402	375	376
0.200	+ 0.03650	.889	807	783	762	748	734	711	676	643	603	572	560	551	563	358	354
0.250	+ 0.03818	.890	809	785	765	747	734	722	678	656	616	602	585	578	571	537	343
0.300	+ 0.03896	.898	826	801	783	771	749	736	704	685	646	630	618	609	591	573	519
0.350	+ 0.03925	.901	830	811	791	775	748	742	720	694	664	647	626	626	608	596	554
0.400	+ 0.03896	.910	843	822	806	794	778	760	742	716	686	684	653	655	636	622	584
0.450	+ 0.038[illegible]3	.910	845	824	809	797	786	765	750	730	696	686	664	668	645	628	613
0.500	+ 0.03673	.909	845	824	807	796	784	759	748	736	703	686	672	669	662	633	619
0.550	+ 0.03454	.913	851	832	817	807	792	769	755	746	724	702	692	686	686	651	637
0.600	+ 0.03191	.919	859	842	829	818	803	784	766	767	743	726	710	704	706	674	659
0.650	+ 0.02887	.923	866	848	838	828	817	795	776	782	757	739	724	722	721	689	671
0.700	+ 0.02541	927	875	859	849	840	833	808	792	799	773	752	745	740	741	709	689
0.750	+ 0.02182	930	880	866	855	847	843	821	803	806	782	765	757	746	750	721	697
0.800	+ 0.01779	935	887	873	863	858	852	831	813	817	793	705	770	760	758	730	710
0.850	+ 0.01358	936	889	875	865	860	855	834	815	816	793	778	770	760	755	733	705
0.900	+ 0.00895	942	901	887	880	875	872	848	831	828	807	792	779	778	769	747	726
0.949	+ 0.00457	944	903	891	884	880	877	850	834	828	807	794	781	778	771	758	728

$\alpha_E = 2.6^{\circ}$ Lower Surface

Mach Number

Values of p/H_{eff}

x/c	z/c	.598	.797	.851	.896	.938	.976	1.022	1.063	1.103	1.144	1.192	1.215	1.226	1.250	1.303	1.355
0.003	- 0.00743	1.002	1.002	1.002	1.004	1.006	1.011	1.023	1.004	1.006	991	999	.994	.994	.991	.999	.999
0.012	- 0.01290	.996	993	992	993	994	1.002	1.010	992	988	976	983	978	975	966	967	955
0.018	- 0.016[illegible]7	984	973	967	966	965	966	976	956	953	939	939	930	931	913	908	893
0.041	- 0.02307	965	941	931	924	923	920	928	906	898	882	888	878	873	863	856	838
0.062	- 0.02796	953	920	908	900	894	889	895	869	857	838	839	830	833	813	800	784
0.082	- 0.03183	948	910	899	890	882	876	880	852	837	816	815	804	802	792	769	757
0.102	- 0.03518	939	899	884	871	864	856	859	826	812	788	784	771	771	758	734	717
0.152	- 0.04168	928	874	858	846	834	825	823	790	775	746	737	721	722	709	677	662
0.202	- 0.04625	921	861	842	827	814	801	798	764	747	716	704	683	685	668	631	605
0.252	- 0.04926	911	847	826	809	794	778	769	745	721	683	668	645	641	629	590	560
0.302	- 0.05050	907	838	816	797	783	765	750	727	702	667	641	619	607	599	561	510
0.352	- 0.04968	912	845	824	807	793	777	760	739	716	681	653	637	623	613	584	532
0.402	- 0.04714	917	853	834	820	806	792	776	752	736	705	679	667	656	649	614	589
0.451	- 0.04390	.922	863	844	829	819	807	789	764	758	727	707	691	680	671	643	628
0.501	- 0.03999	927	872	854	842	831	819	802	778	776	748	726	726	710	695	671	654
0.551	- 0.036[illegible]6	.930	878	862	850	841	830	813	791	788	768	731	735	724	713	686	678
0.601	- 0.032[illegible]2	.931	882	868	855	846	836	818	799	793	776	746	744	738	730	695	689
0.651	- 0.028[illegible]7	934	886	869	859	850	842	819	806	799	783	760	749	746	740	704	695
0.701	- 0.024[illegible]9	.936	887	873	862	855	846	822	811	809	786	767	756	753	748	721	701
0.751	- 0.02010	.938	891	876	866	859	852	830	814	811	786	773	763	762	756	727	705
0.802	- 0.016[illegible]1	.939	892	876	866	860	853	832	813	810	788	773	765	758	756	729	714
0.852	- 0.012[illegible]2	940	897	882	872	867	861	839	820	817	801	778	773	766	761	734	720
0.901	- 0.008[illegible]9	939	891	878	869	864	859	834	817	809	796	781	770	764	757	736	718

TABLE 4 - Values of $\overline{C_Z}$ and $\overline{C_X}$

(a) Stagnation pressure 30 in. mercury

α_E	M	$\overline{C_Z}$	$\overline{C_X}$
0.0	0.609	- 0.027	+ 0.0011
	0.803	- 0.028	+ 0.0015
	0.855	- 0.028	+ 0.0015
	0.904	- 0.030	+ 0.0014
	0.943	- 0.030	+ 0.0012
	0.983	- 0.030	+ 0.0006
	1.026	- 0.028	+ 0.0040
	1.063	- 0.030	+ 0.0022
	1.107	- 0.029	+ 0.0003
	1.145	- 0.029	+ 0.0008
	1.193	- 0.029	+ 0.0016
	1.253	- 0.028	+ 0.0010
	1.304	- 0.026	+ 0.0019
	1.356	- 0.024	+ 0.0011
	1.408	- 0.037	+ 0.0040
2.0	0.601	+ 0.060	- 0.0002
	0.797	+ 0.060	+ 0.0000
	0.850	+ 0.059	+ 0.0003
	0.900	+ 0.059	+ 0.0001
	0.941	+ 0.058	- 0.0003
	0.979	+ 0.059	- 0.0006
	1.020	+ 0.060	+ 0.0025
	1.062	+ 0.061	+ 0.0008
	1.101	+ 0.061	- 0.0010
	1.142	+ 0.061	- 0.0014
	1.190	+ 0.060	- 0.0003
	1.252	+ 0.060	- 0.0013
	1.306	+ 0.057	- 0.0004
	1.355	+ 0.058	- 0.0002
	1.409	+ 0.055	+ 0.0017
4.0	0.596	+ 0.139	- 0.0066
	0.797	+ 0.136	- 0.0062
	0.847	+ 0.139	- 0.0063
	0.903	+ 0.139	- 0.0065
	0.941	+ 0.138	- 0.0066
	0.981	+ 0.138	- 0.0075
	1.023	+ 0.138	- 0.0036
	1.062	+ 0.141	- 0.0061
	1.101	+ 0.145	- 0.0074
	1.145	+ 0.150	- 0.0078
	1.196	+ 0.166	- 0.0048
	1.251	+ 0.198	- 0.0015
	1.301	+ 0.204	+ 0.0013
	1.357	+ 0.193	+ 0.0044
	1.403	+ 0.169	+ 0.0066
5.0	0.605	+ 0.166	- 0.0102
	0.795	+ 0.166	- 0.0102
	0.848	+ 0.167	- 0.0103
	0.904	+ 0.163	- 0.0105
	0.944	+ 0.164	- 0.0101
	0.983	+ 0.177	- 0.0112
	1.022	+ 0.177	- 0.0067
	1.062	+ 0.183	- 0.0086
	1.105	+ 0.182	- 0.0087
	1.143	+ 0.190	- 0.0063
	1.185	+ 0.216	- 0.0001
	1.252	+ 0.224	+ 0.0008
	1.308	+ 0.225	+ 0.0037
	1.357	+ 0.206	+ 0.0059
	1.403	+ 0.195	+ 0.0085
2.6	0.982	+ 0.084	- 0.0030
	1.022	+ 0.085	+ 0.0011
	1.064	+ 0.085	- 0.0009
	1.103	+ 0.086	- 0.0024
	1.143	+ 0.087	- 0.0029
	1.194	+ 0.086	- 0.0015
	1.216	+ 0.081	- 0.0027
	1.226	+ 0.087	- 0.0020
	1.252	+ 0.089	- 0.0031
	1.302	+ 0.085	- 0.0012
	1.355	+ 0.091	+ 0.0000
	1.405	+ 0.101	+ 0.0034
3.0	0.600	+ 0.100	- 0.0027
	0.803	+ 0.100	- 0.0024
	0.848	+ 0.100	- 0.0023
	0.901	+ 0.098	- 0.0023
	0.942	+ 0.098	- 0.0028
	0.979	+ 0.099	- 0.0034
	1.023	+ 0.100	+ 0.0003
	1.064	+ 0.100	- 0.0023
	1.105	+ 0.101	- 0.0036
	1.145	+ 0.104	- 0.0040
	1.195	+ 0.103	- 0.0033
	1.213	+ 0.101	- 0.0036
	1.244	+ 0.104	- 0.0038
	1.302	+ 0.105	- 0.0015
	1.328	+ 0.106	- 0.0007
	1.352	+ 0.122	+ 0.0013
	1.407	+ 0.125	+ 0.0050

TABLE 4 - Values of $\overline{C_Z}$ and $\overline{C_X}$

(b) Stagnation pressure 36 in. mercury

α_E	M	$\overline{C_Z}$	$\overline{C_X}$
2.6	0.598	+ 0.088	- 0.0016
	0.797	+ 0.087	- 0.0013
	0.851	+ 0.085	- 0.0010
	0.896	+ 0.084	- 0.0011
	0.938	+ 0.084	- 0.0015
	0.976	+ 0.086	- 0.0020
	1.022	+ 0.084	+ 0.0015
	1.063	+ 0.085	- 0.0008
	1.103	+ 0.086	- 0.0023
	1.144	+ 0.089	- 0.0027
	1.192	+ 0.086	- 0.0013
	1.215	+ 0.089	- 0.0022
	1.226	+ 0.087	- 0.0018
	1.250	+ 0.090	- 0.0028
	1.303	+ 0.087	- 0.0012
	1.355	+ 0.090	+ 0.0000

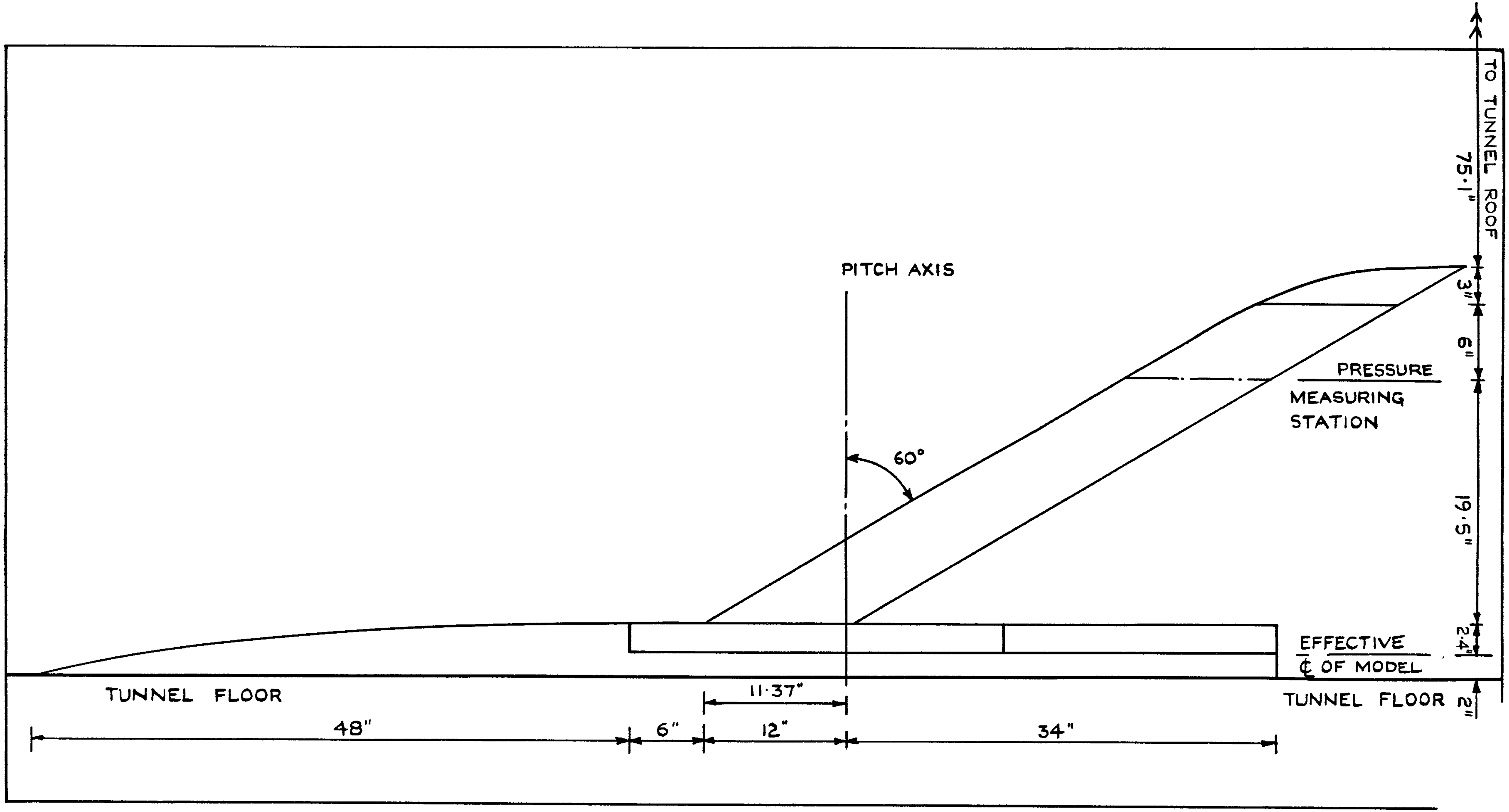

FIG.1. LAYOUT OF MODEL.

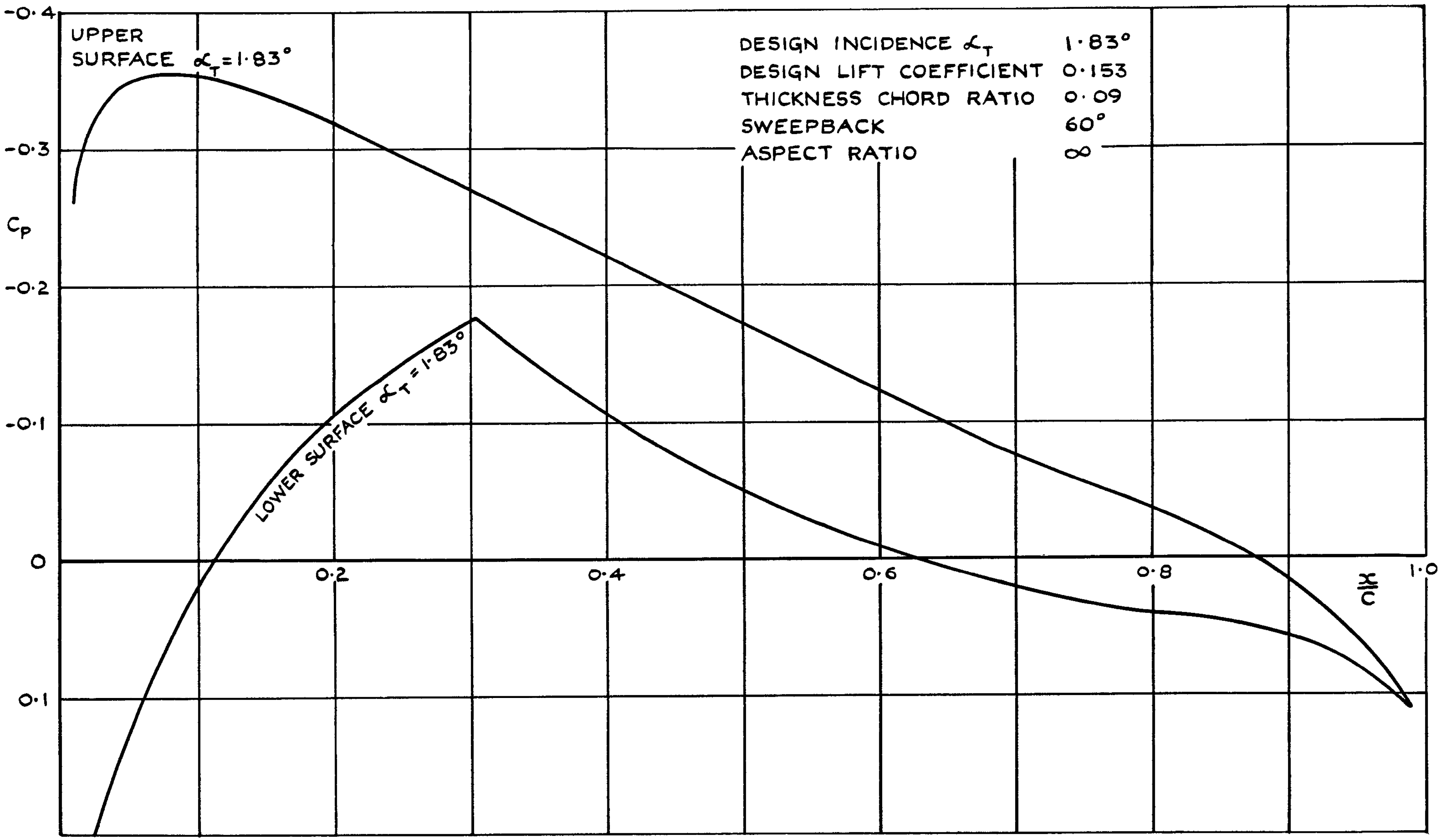

FIG. 2. CALCULATED INVISCID SUBCRITICAL PRESSURE DISTRIBUTIONS AROUND AEROFOIL AT $M_0 = 1{\cdot}2$.

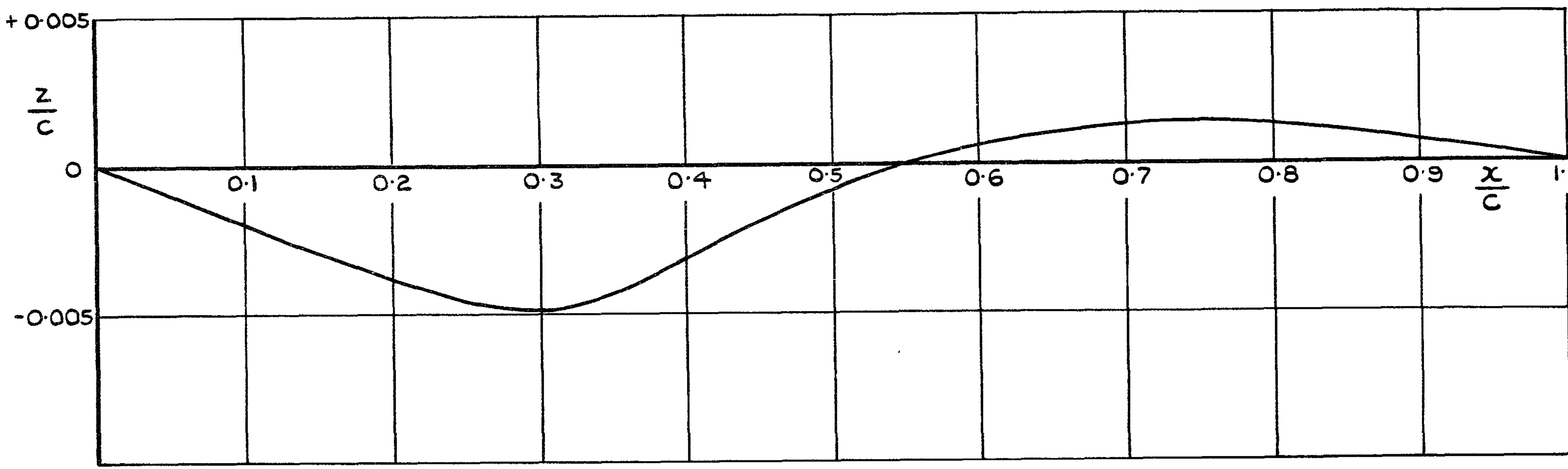

FIG. 3. CAMBER LINE (ALONG WIND) FOR AEROFOIL.

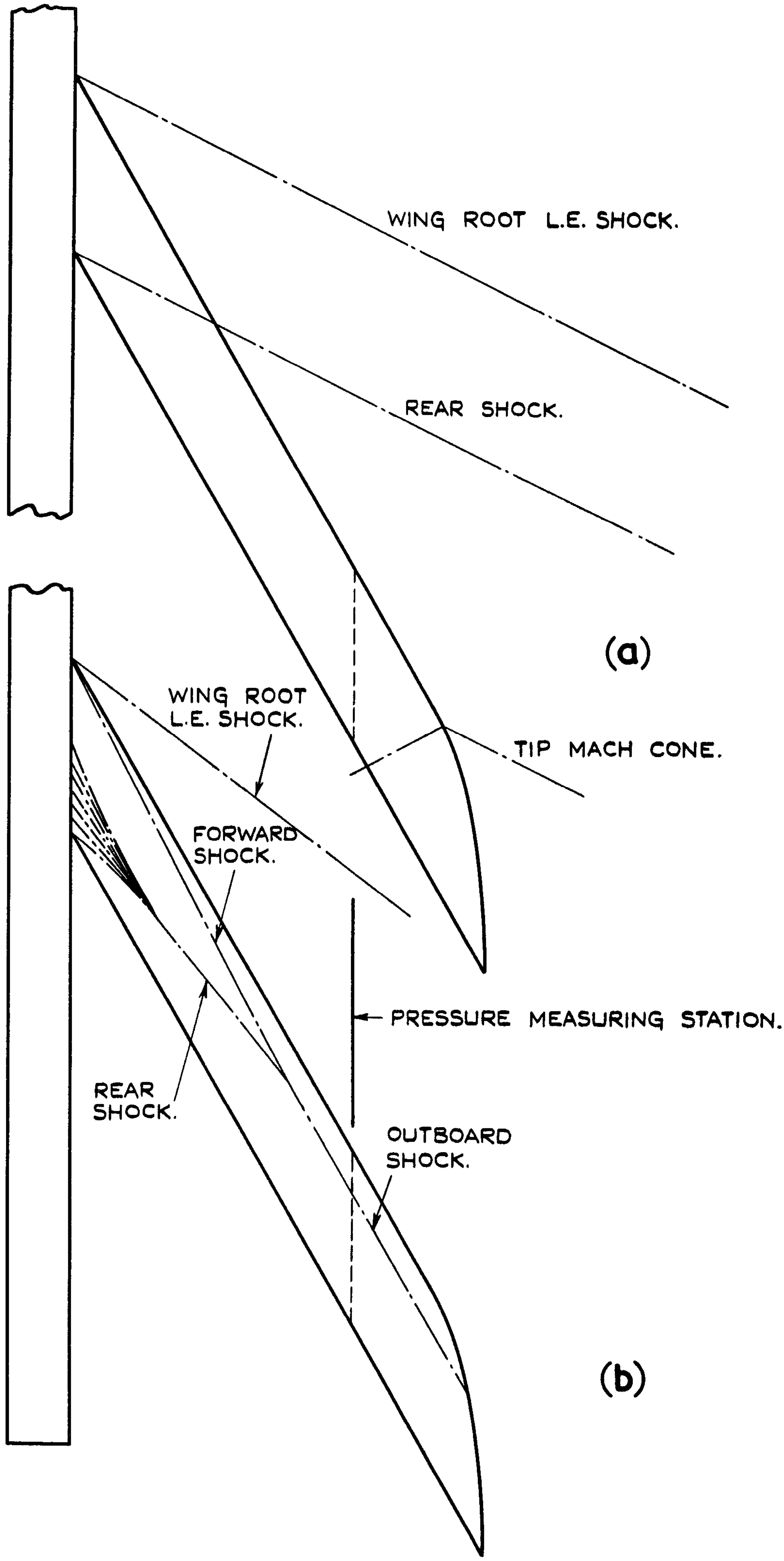

FIG. 4. SKETCH OF POSSIBLE SHOCK PATTERNS FROM ROOT WHEN FLOW AT PRESSURE MEASURING STATION IS (a) SUBCRITICAL AND (b) SUPERCRITICAL.

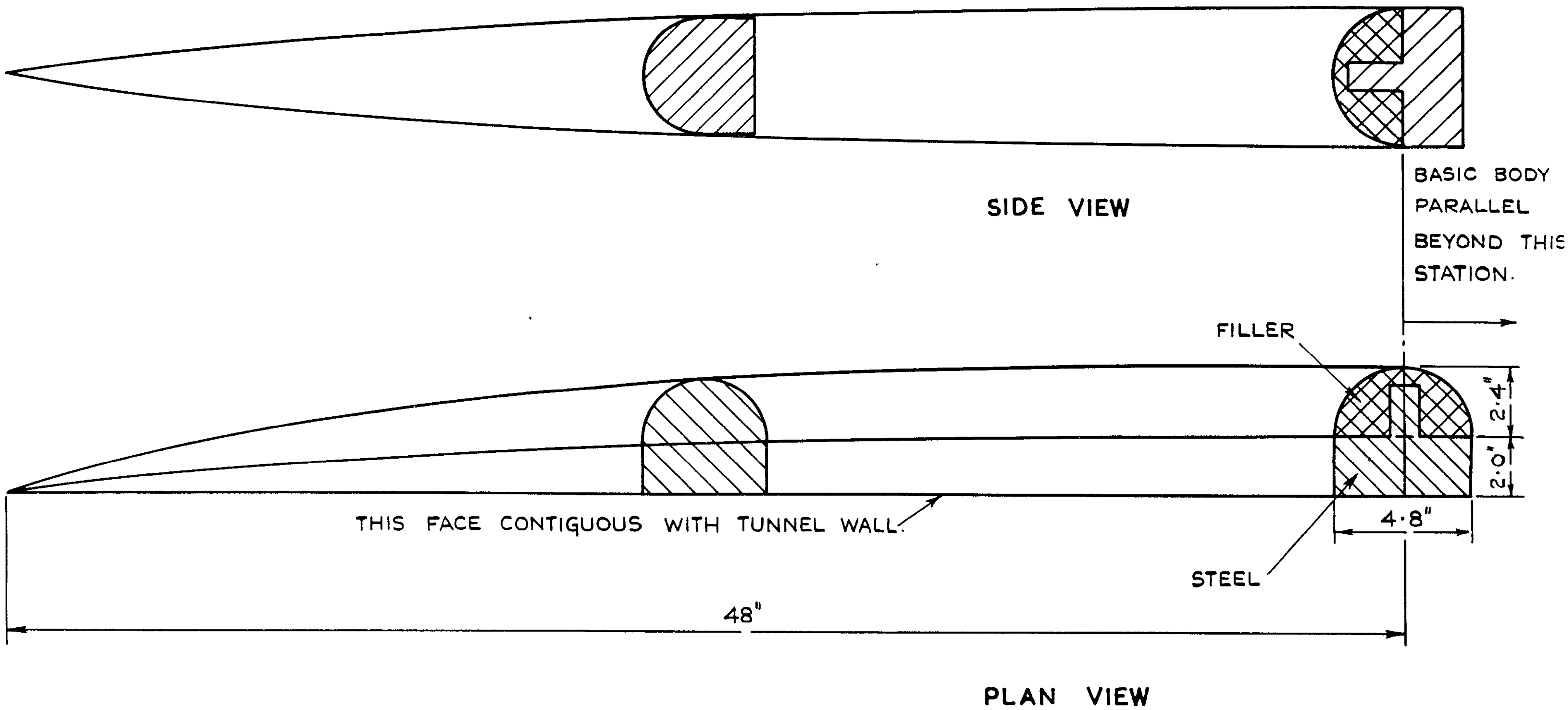

FIG. 5. VIEWS OF NOSE OF BODY SHOWING SECTION SHAPE.

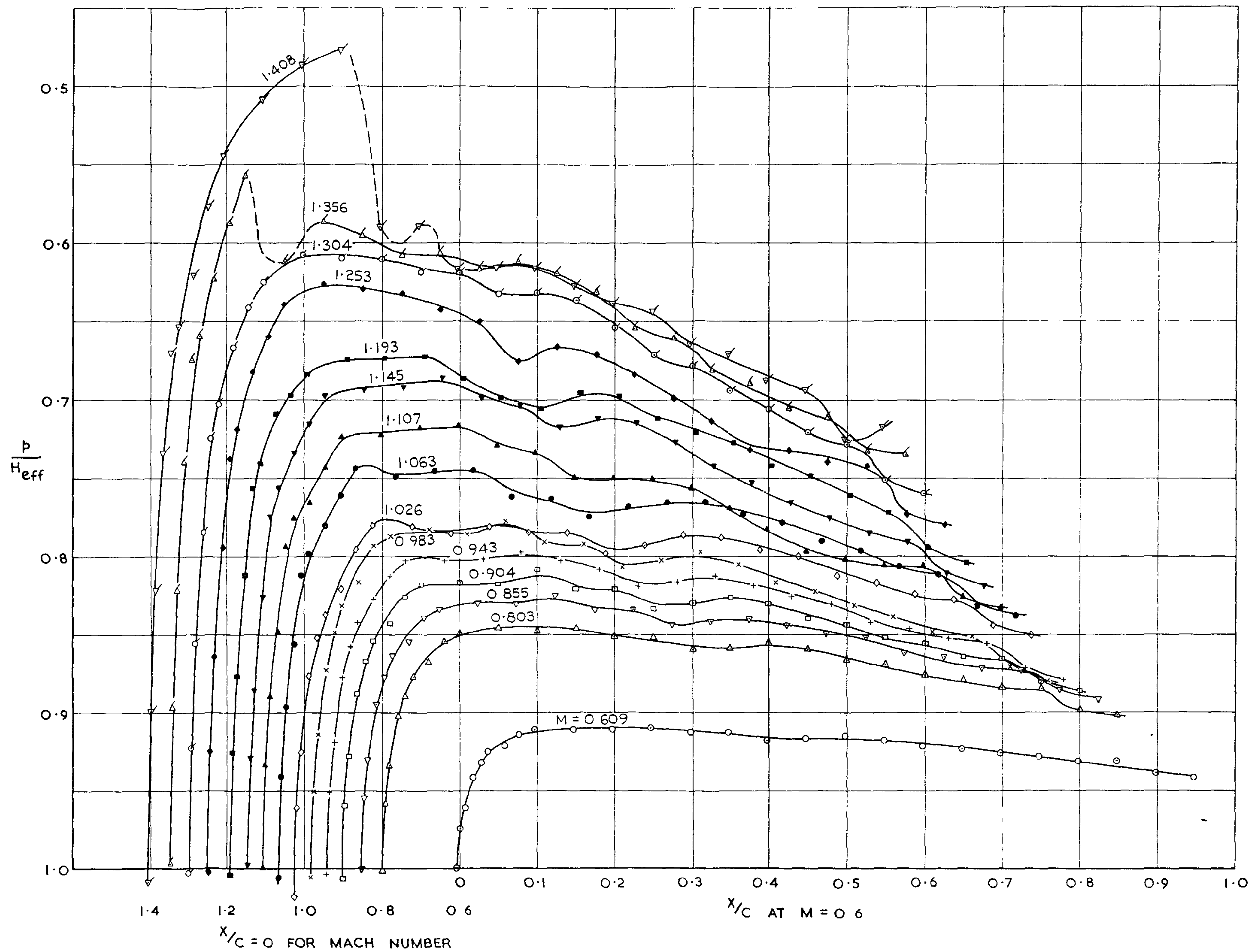

FIG. 6. UPPER SURFACE PRESSURE DISTRIBUTIONS AT VARIOUS MACH NUMBERS.
$\alpha_E = 0^\circ$; STAGNATION PRESSURE 30 INS. MERCURY.

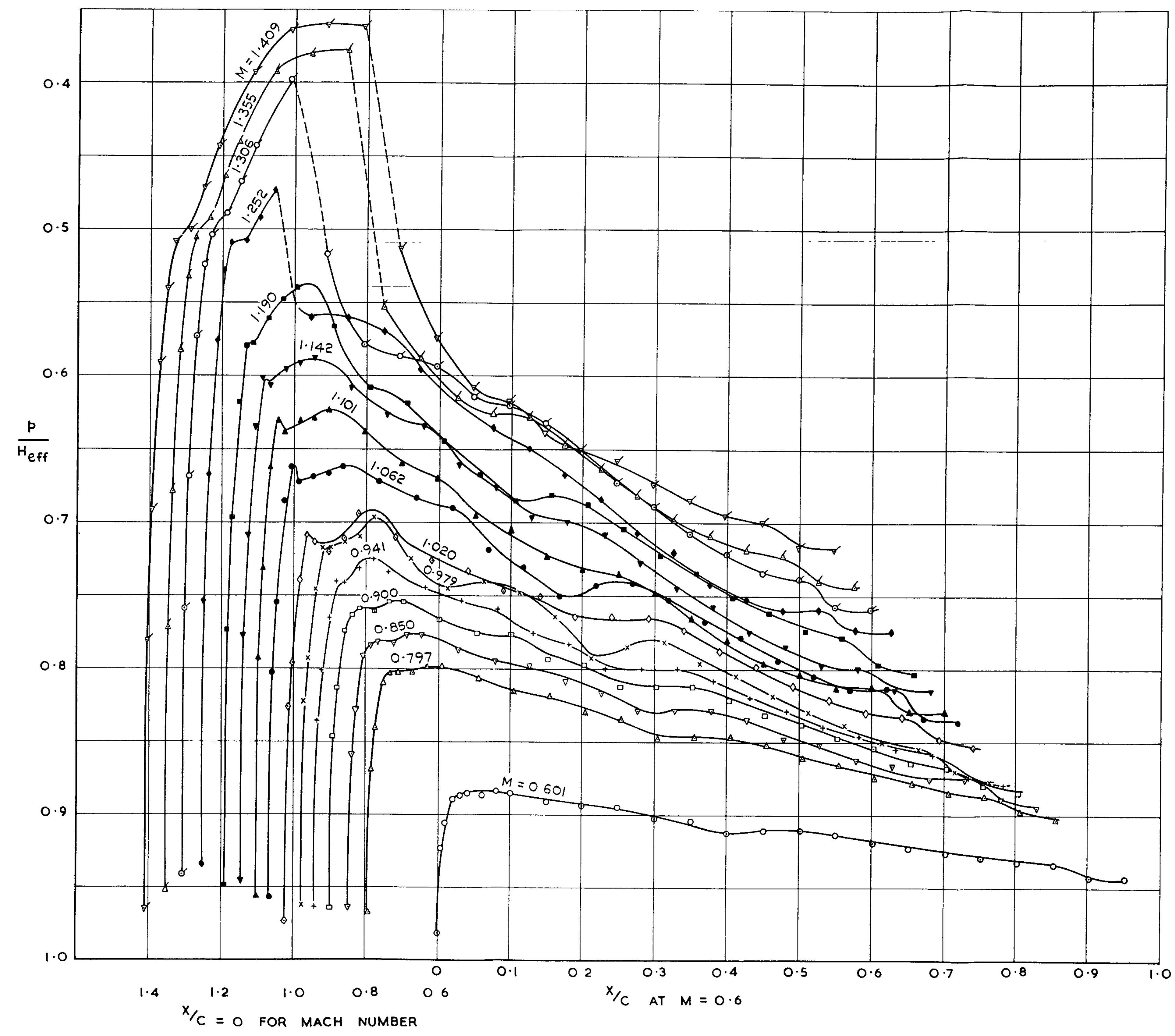

FIG. 7. UPPER SURFACE PRESSURE DISTRIBUTIONS AT VARIOUS MACH NUMBERS.
$\alpha_E = 2{\cdot}0^{\circ}$; STAGNATION PRESSURE 30 INS. MERCURY.

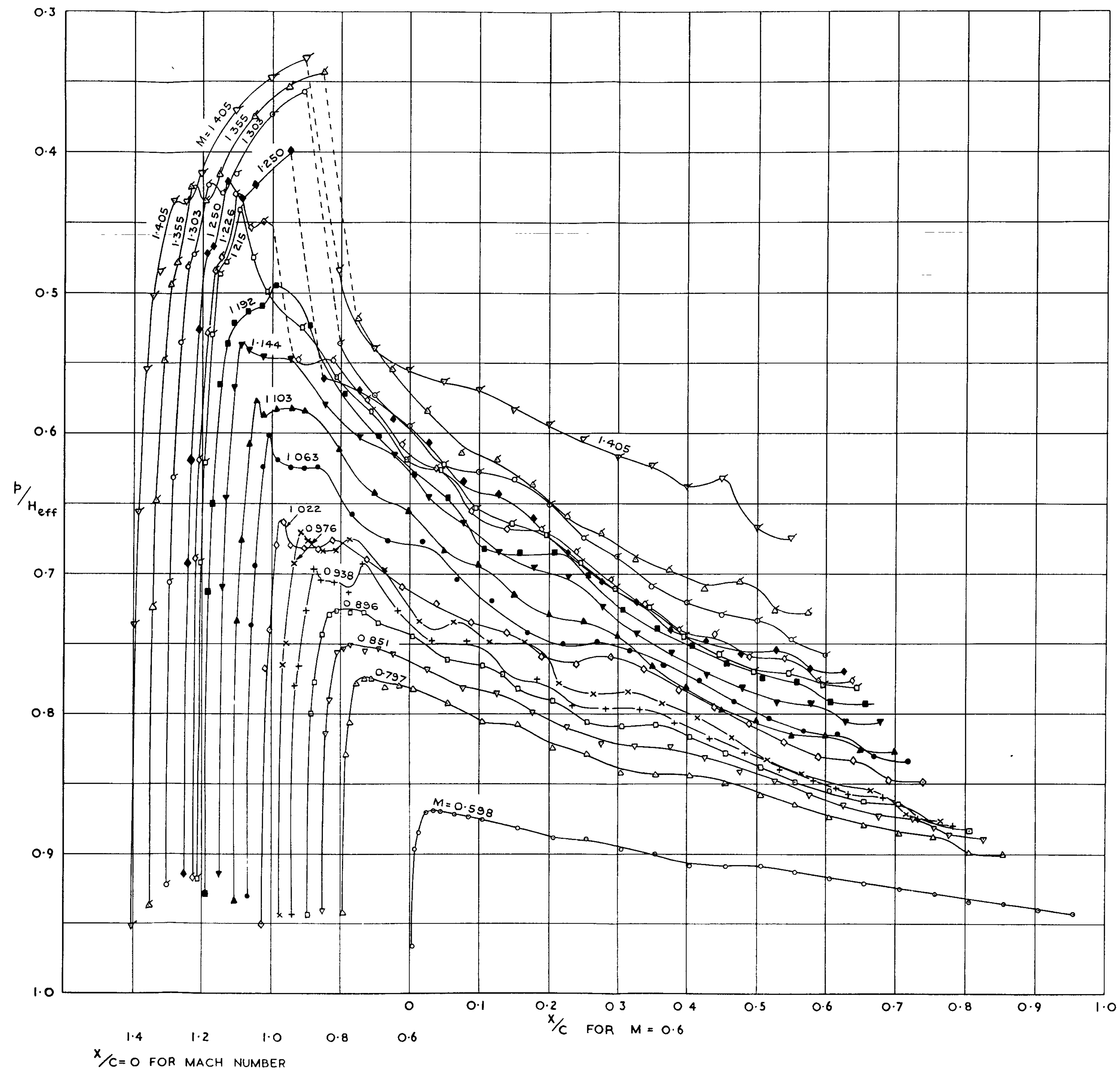

FIG. 8. UPPER SURFACE PRESSURE DISTRIBUTIONS AT VARIOUS MACH NUMBERS
$\alpha_E = 2{\cdot}6^\circ$; STAGNATION PRESSURE 36 INS. MERCURY. (30 INS. FOR M = 1·405).

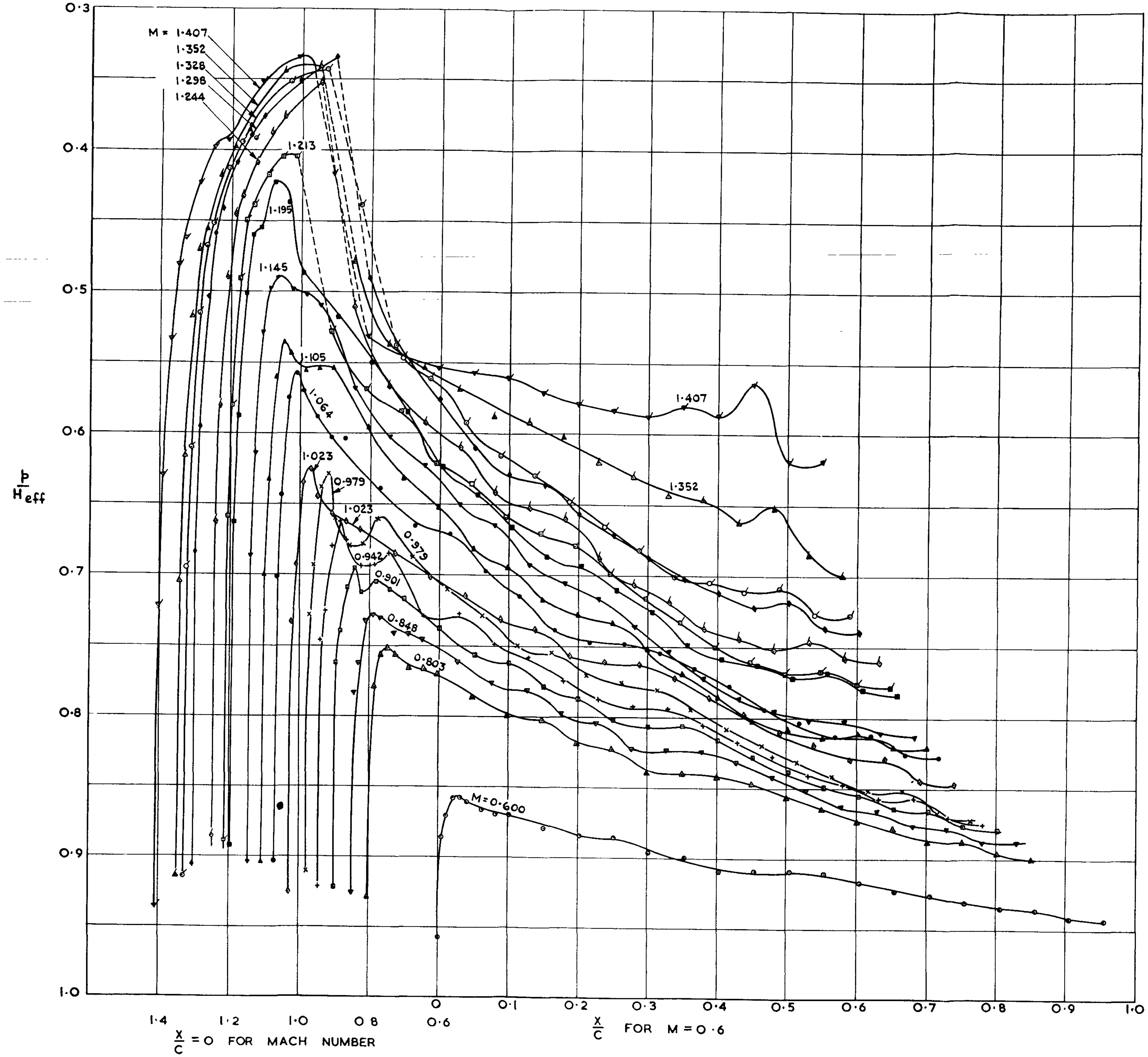

FIG. 9. UPPER SURFACE PRESSURE DISTRIBUTIONS AT VARIOUS MACH NUMBERS.
$\alpha_E = 3 \cdot 0^{\circ}$; STAGNATION PRESSURE 30 INS. MERCURY.

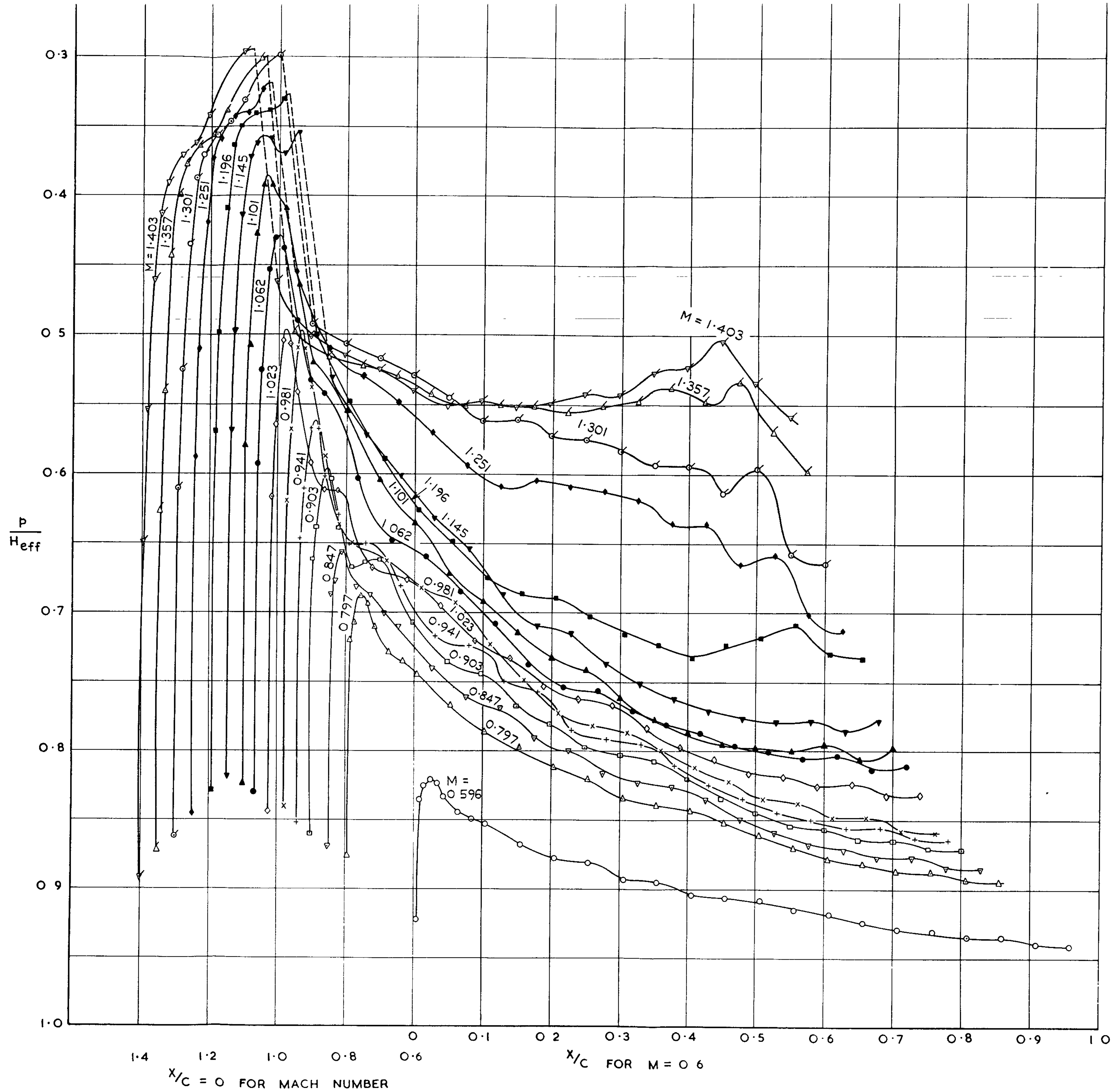

FIG. 10. UPPER SURFACE PRESSURE DISTRIBUTIONS AT VARIOUS MACH NUMBERS.
$\alpha_E = 4·0°$; STAGNATION PRESSURE 30 INS. MERCURY.

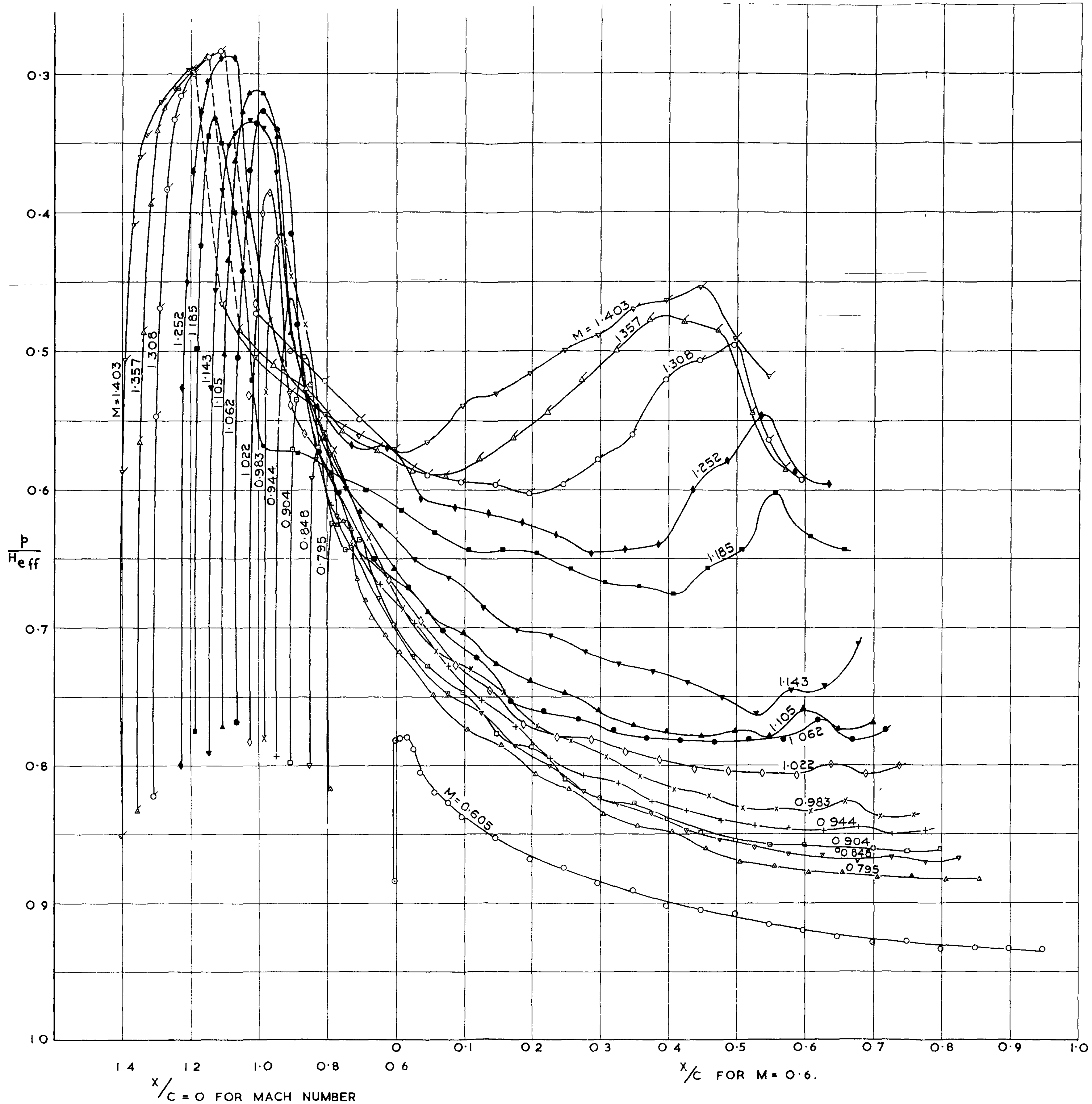

FIG. 11. UPPER SURFACE PRESSURE DISTRIBUTIONS AT VARIOUS MACH NUMBERS.
$\alpha_E = 5 \cdot 0^{o}$; STAGNATION PRESSURE 30 INS. MERCURY.

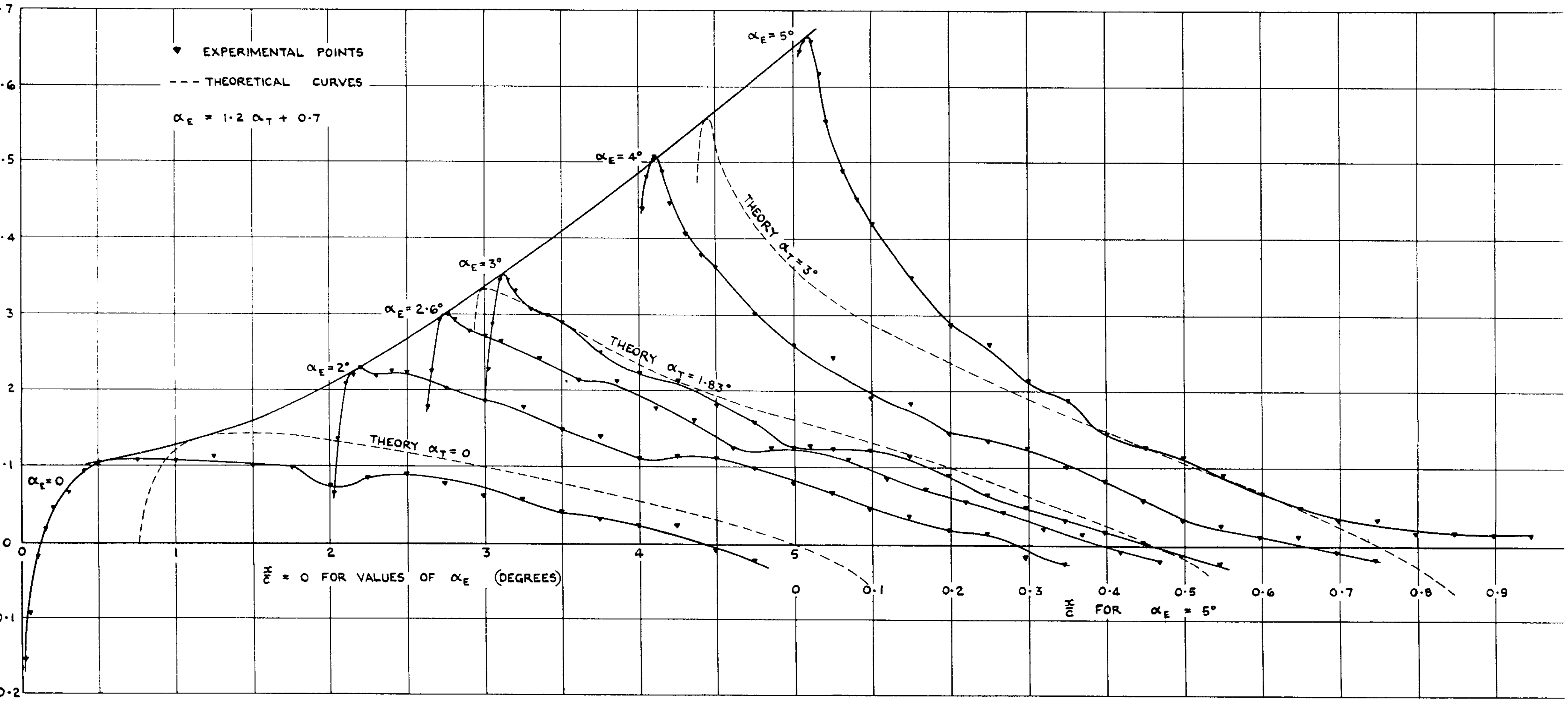

FIG. 12 CARPET PLOT OF C_P vs. $\frac{x}{c}$ AND α_E, UPPER SURFACE, $M_0 \doteqdot 0 \cdot 6$

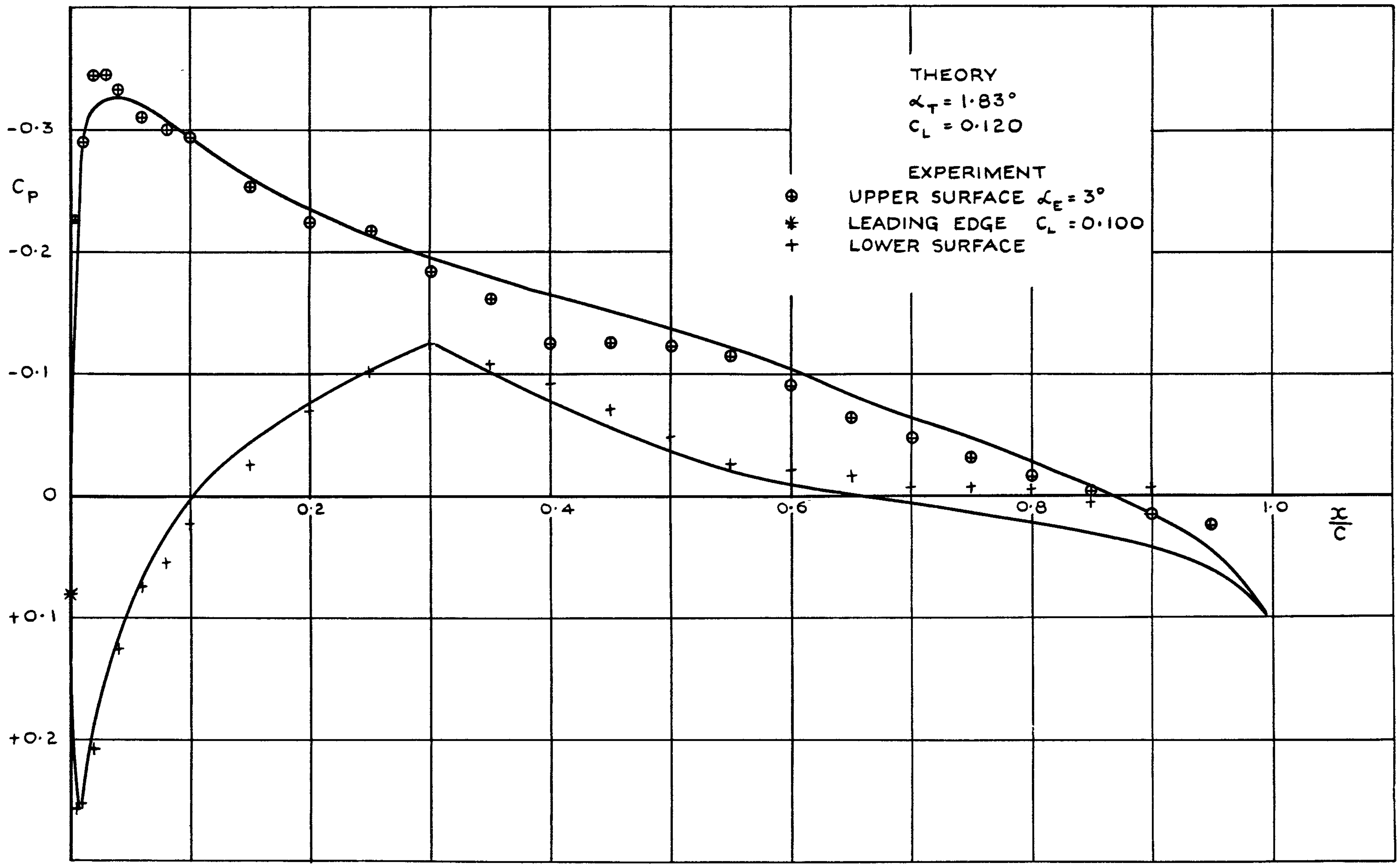

FIG. 13. COMPARISON OF THEORETICAL AND EXPERIMENTAL PRESSURE DISTRIBUTIONS AT SIMILAR VALUES OF PEAK SUCTION, $M_0 = 0\cdot600$.

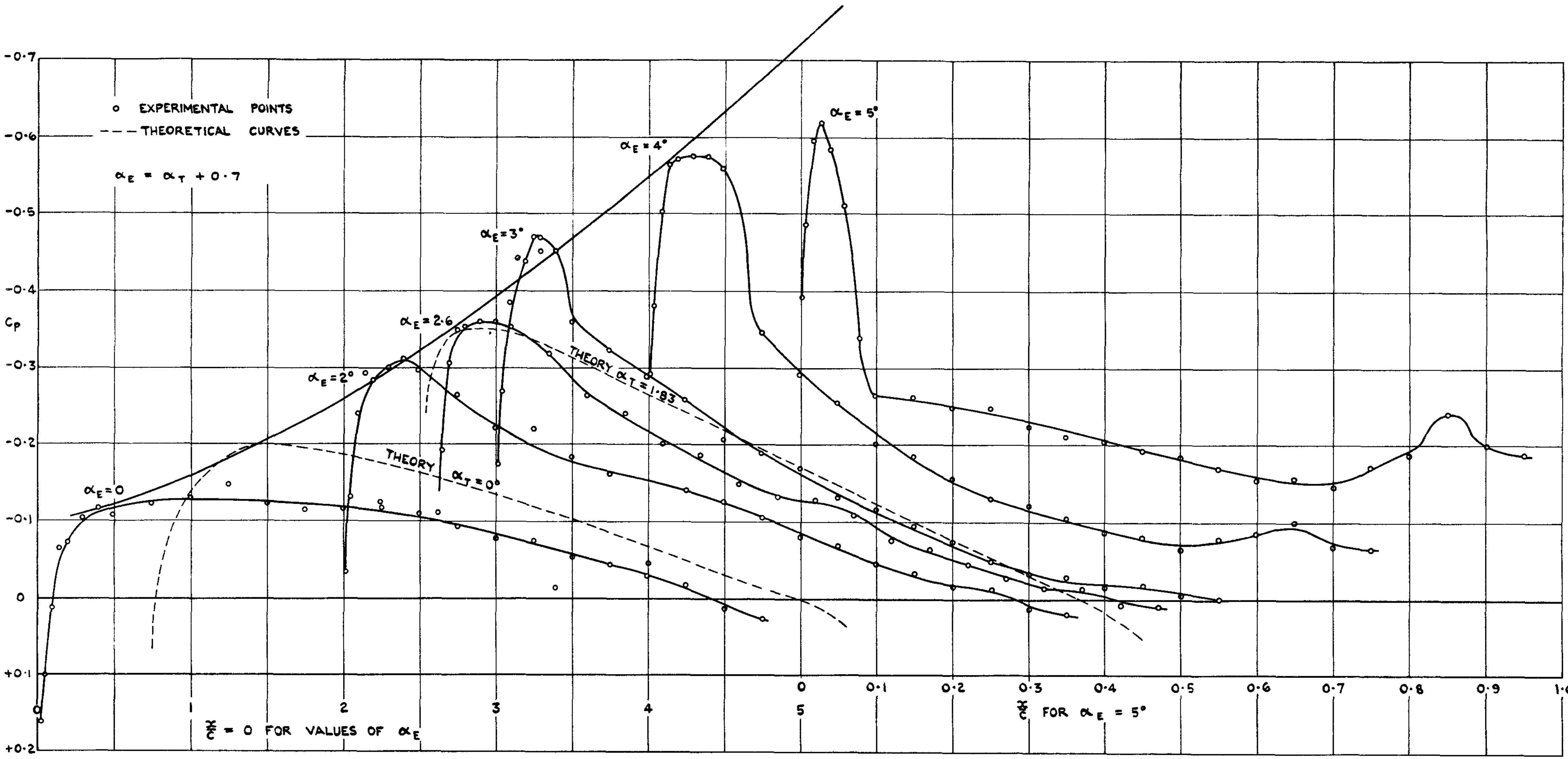

FIG.14 CARPET PLOT OF C_p vs. $\frac{x}{c}$ AND α_E, UPPER SURFACE, $M_0 \doteqdot 1{\cdot}20$

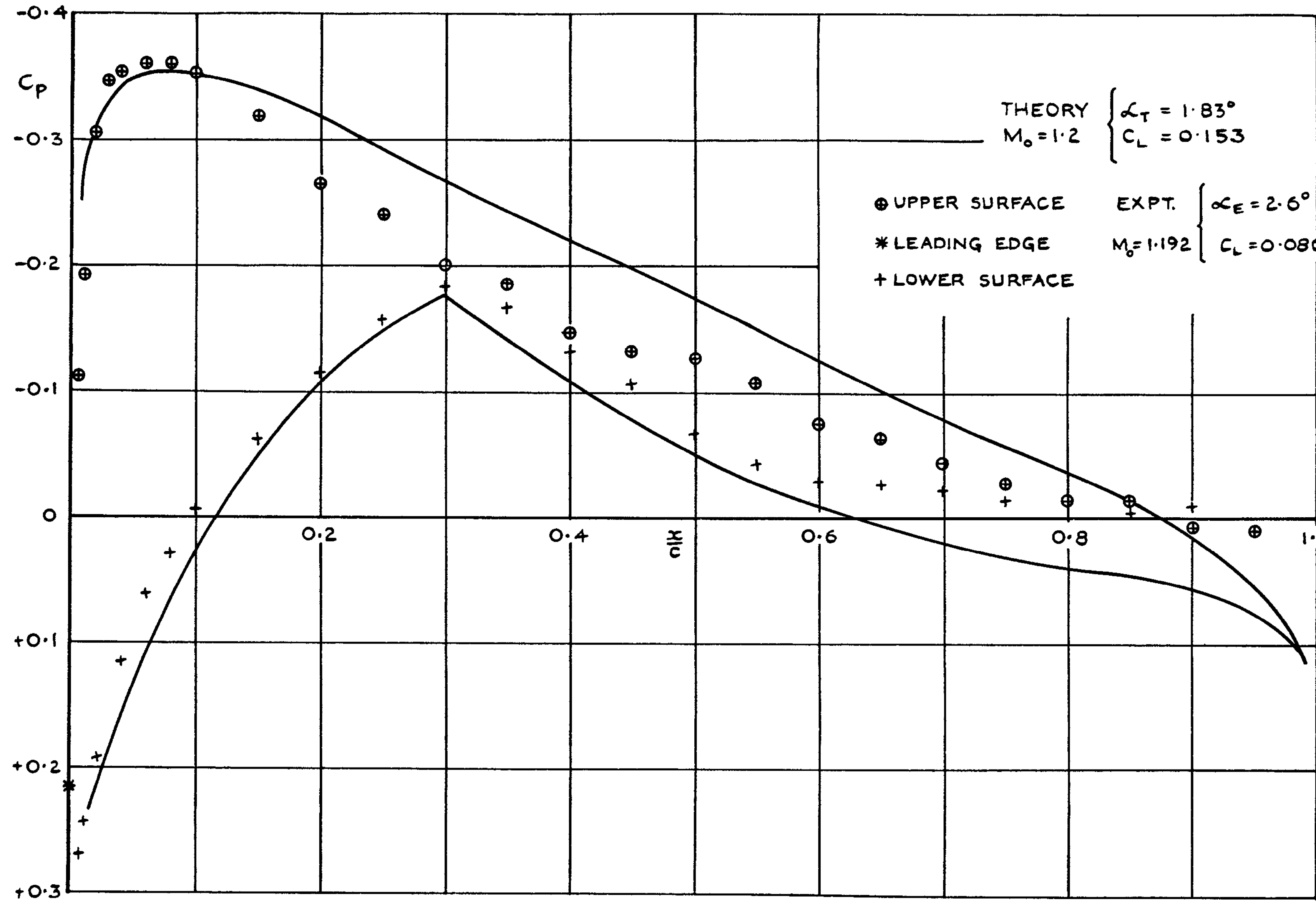

FIG. 15. COMPARISON OF THEORETICAL AND EXPERIMENTAL PRESSURE DISTRIBUTIONS AT SIMILAR VALUES OF PEAK SUCTION, ($M_o = 1·20$.)

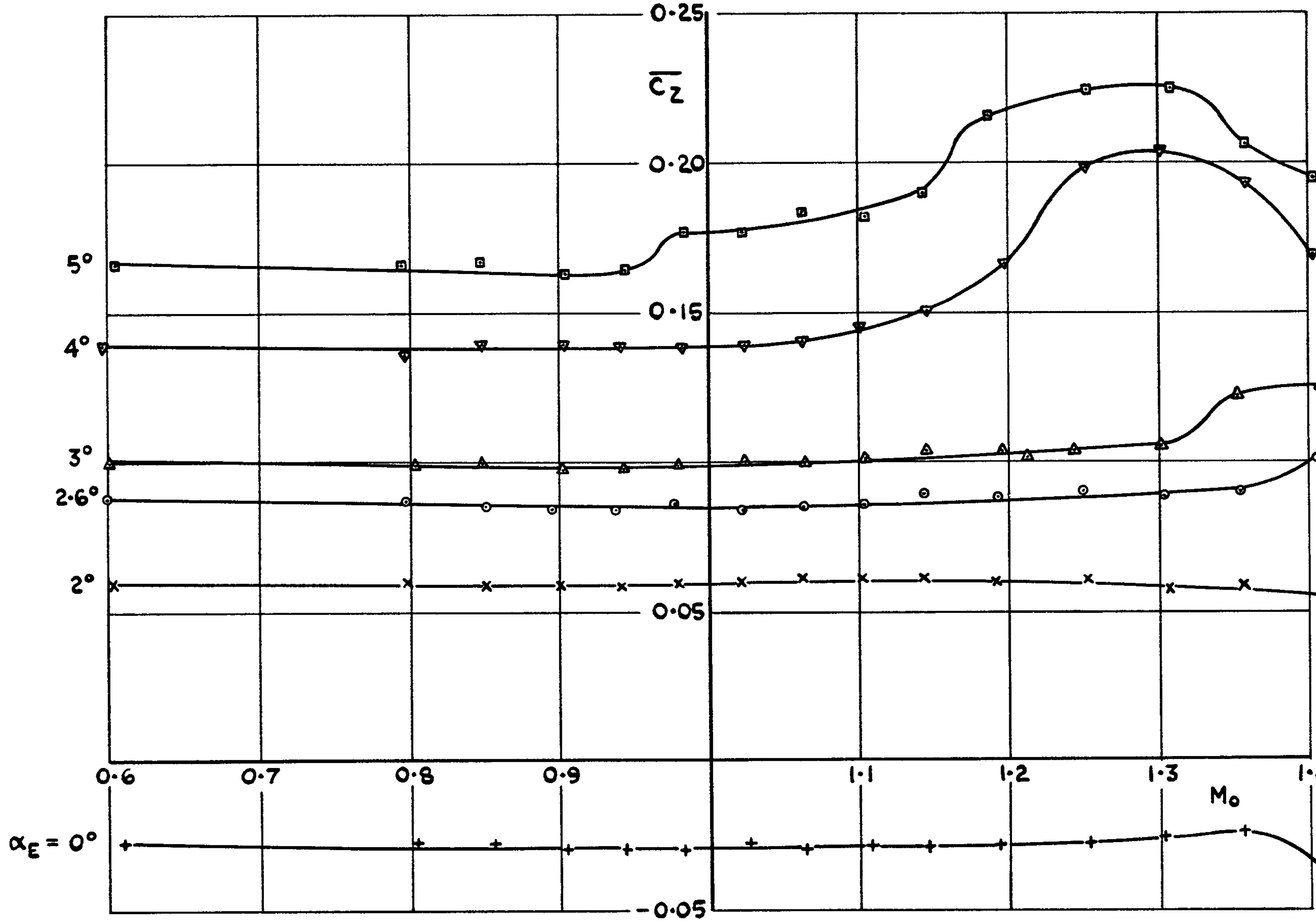

FIG.16 NORMAL FORCE COEFFICIENT vs. M_O FOR VARYING α_E
(NO "TUNNEL CORRECTIONS").

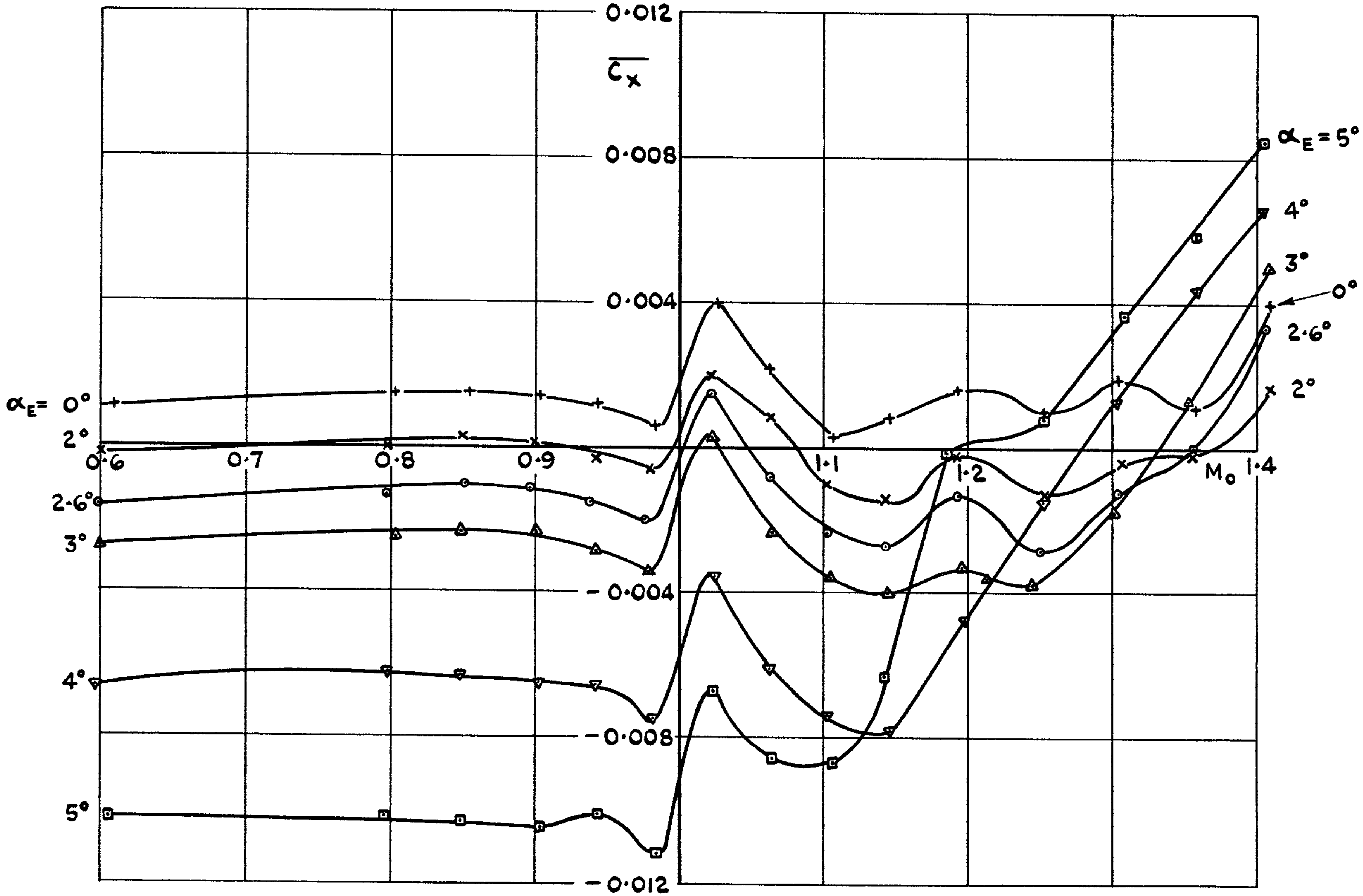

FIG.17 CHORD FORCE COEFFICIENT vs. M_0 FOR VARYING α_E
(NO "TUNNEL CORRECTIONS").

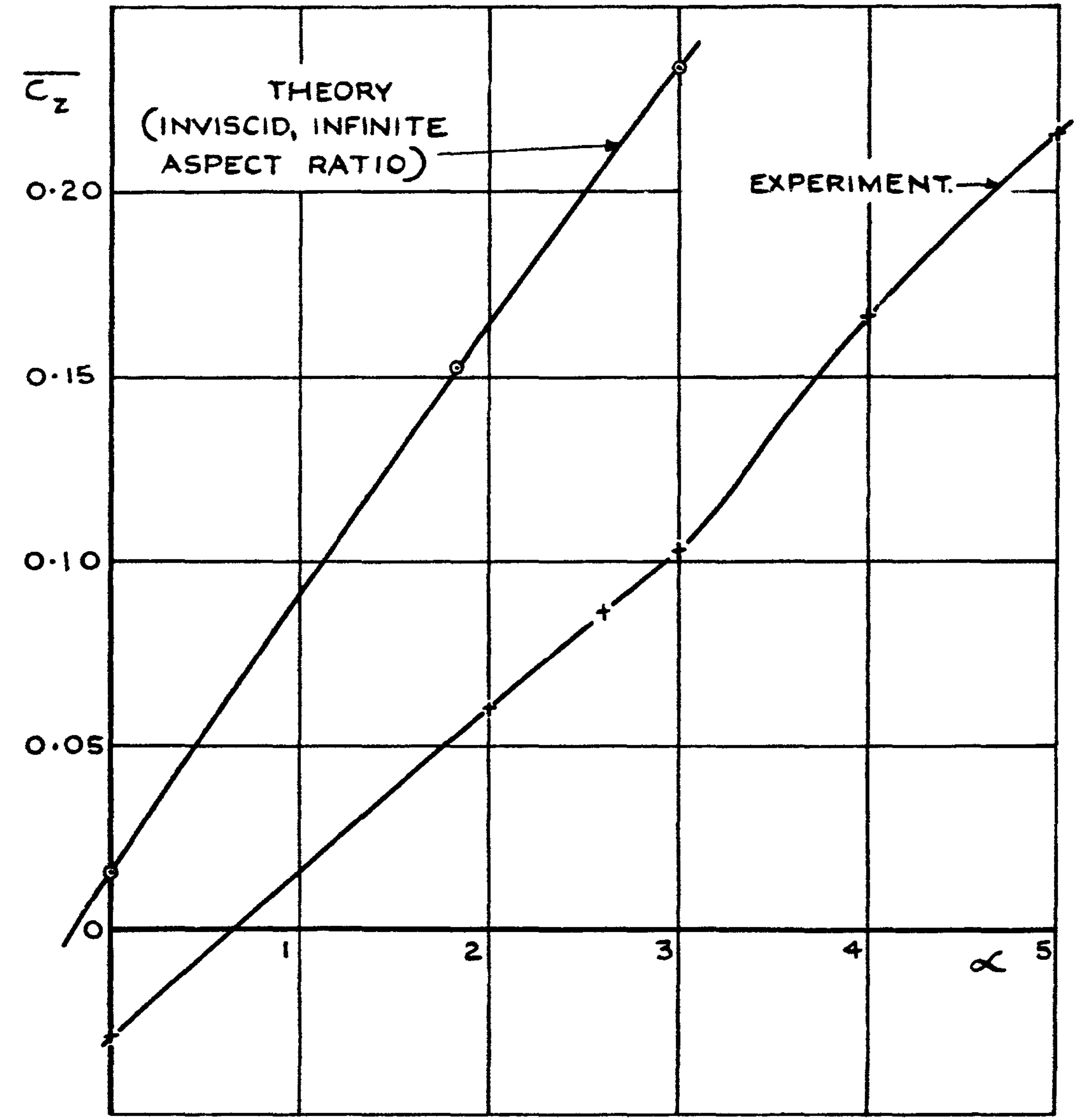

FIG.18. COMPARISON BETWEEN THEORETICAL AND EXPERIMENTAL NORMAL FORCE vs INCIDENCE CURVES AND ZERO LIFT ANGLES, $M_0 \approx 1{\cdot}2$.

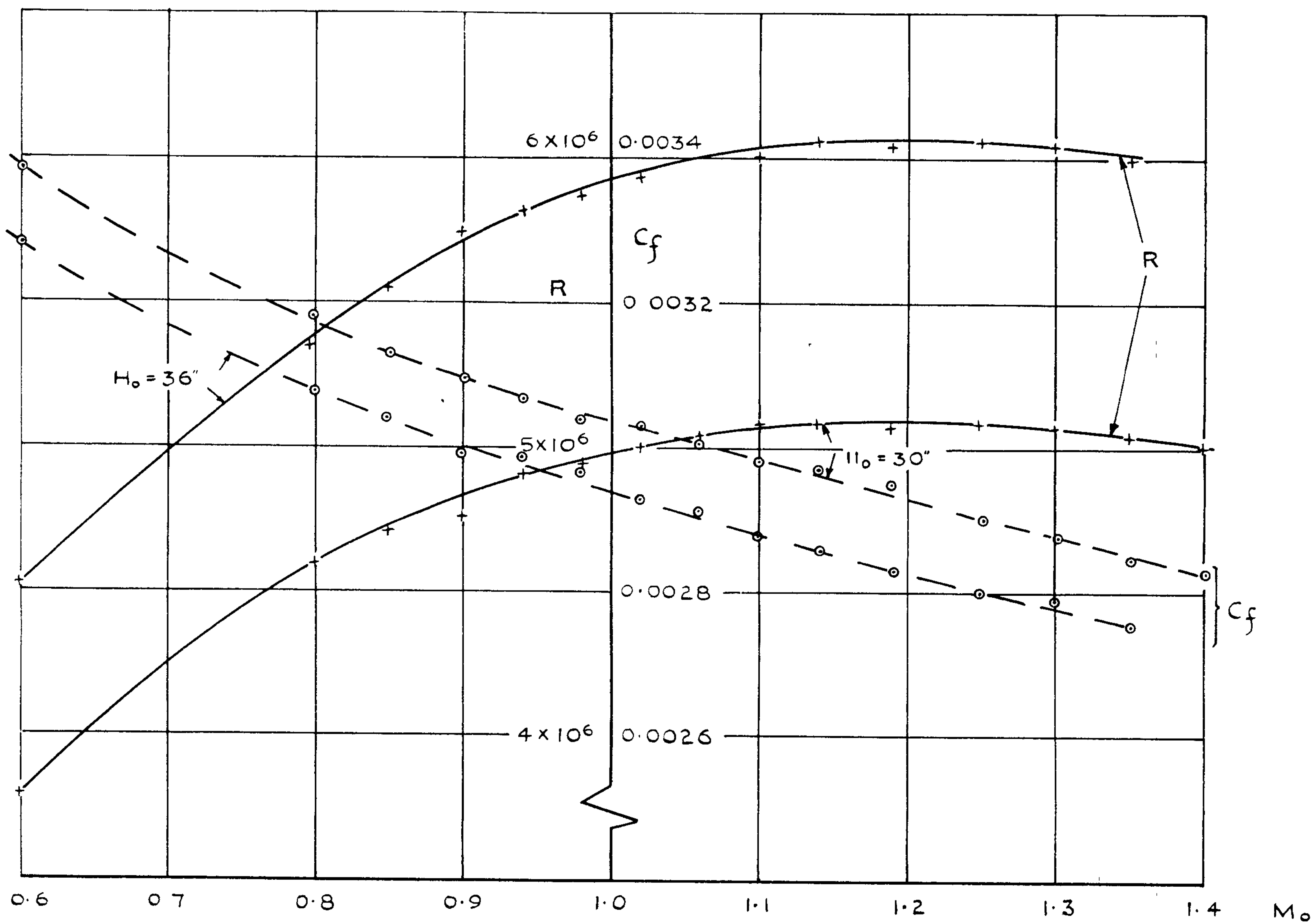

FIG .19. TEST REYNOLDS No. AND ASSUMED SKIN FRICTION COEFFICIENT vs MACH NUMBER.

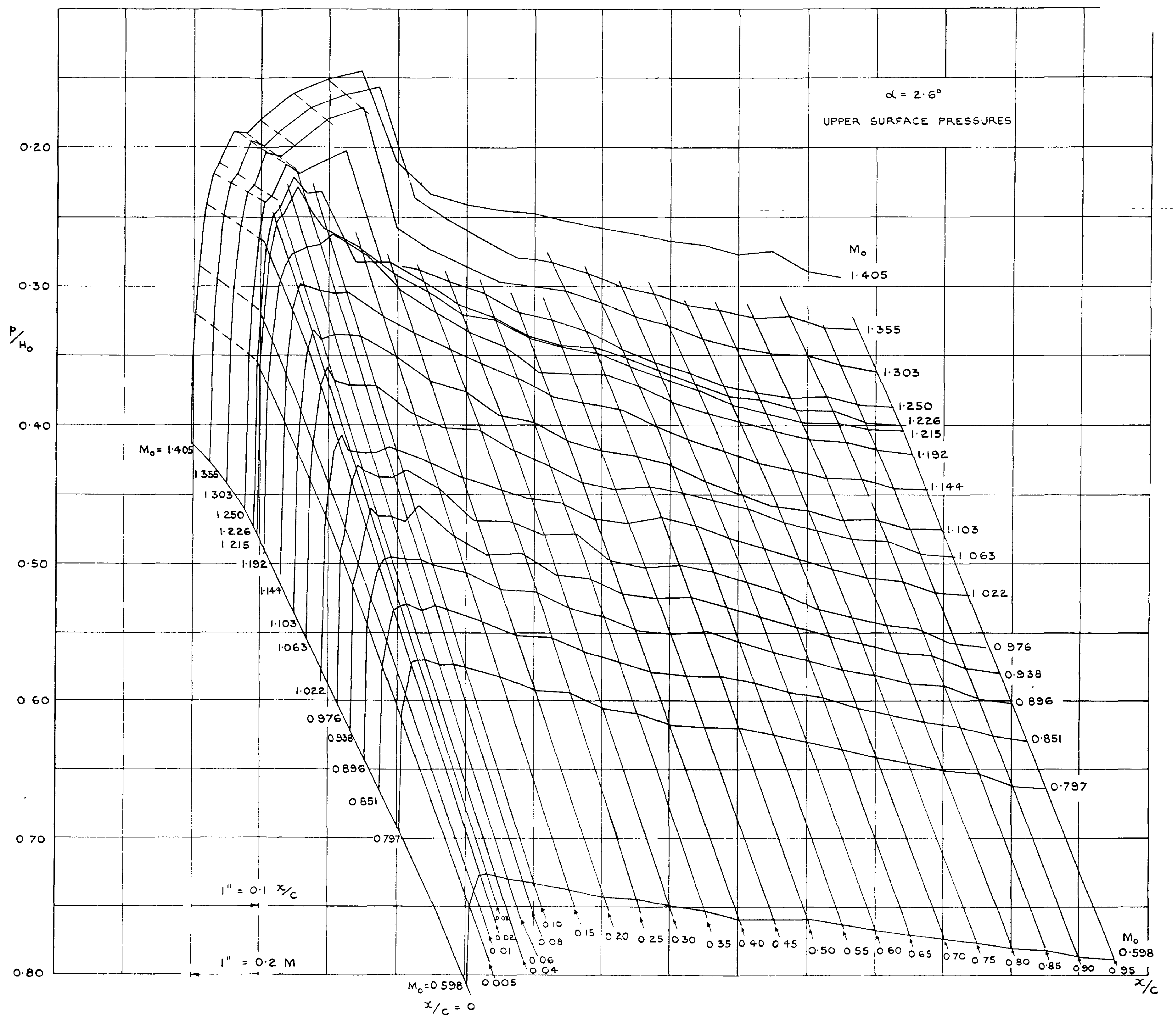

FIG. 20. CARPET PLOT OF $\frac{p}{H_0}$ VS. M_0 AND x/c, $\alpha_E = 2 \cdot 6^{\circ}$, UPPER SURFACE.

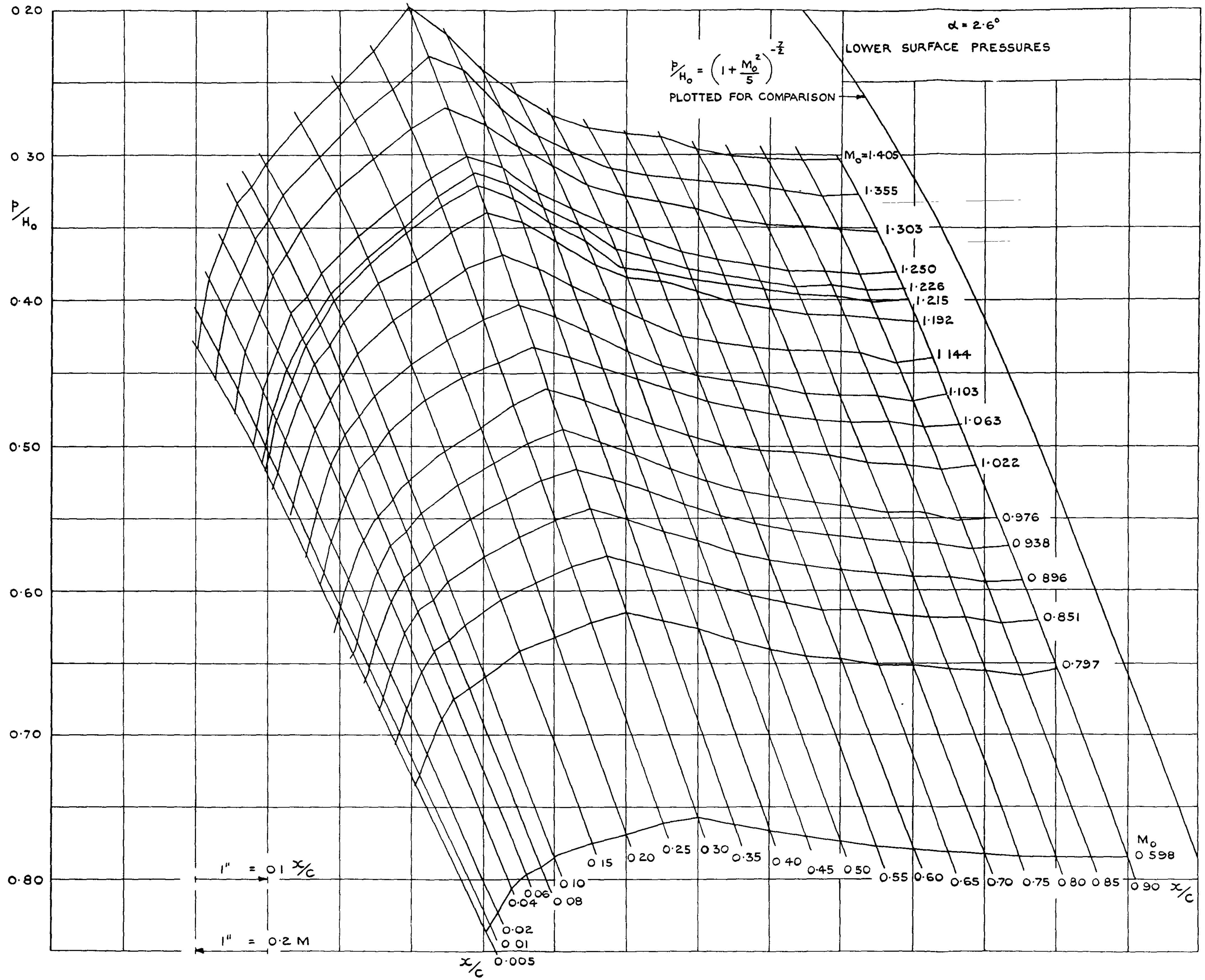

FIG. 21. CARPET PLOT OF $\frac{p}{H_0}$ VS. M_0 AND x/c, $\alpha_E = 2 \cdot 6^\circ$, LOWER SURFACE.

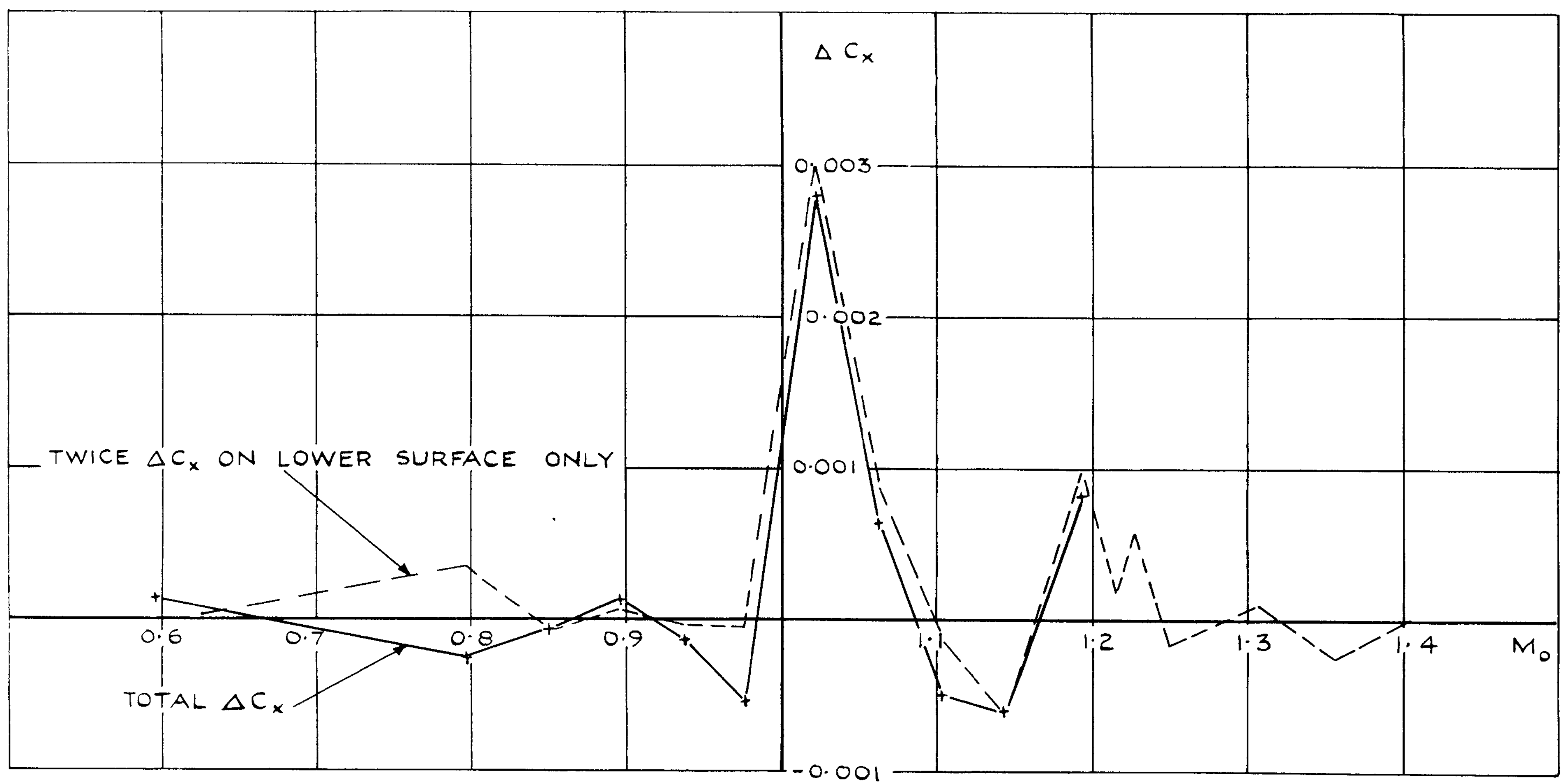

FIG. 22. CORRECTION TO CHORD FORCE COEFFICIENT vs M_o, $\alpha_E = 2 \cdot 6°$

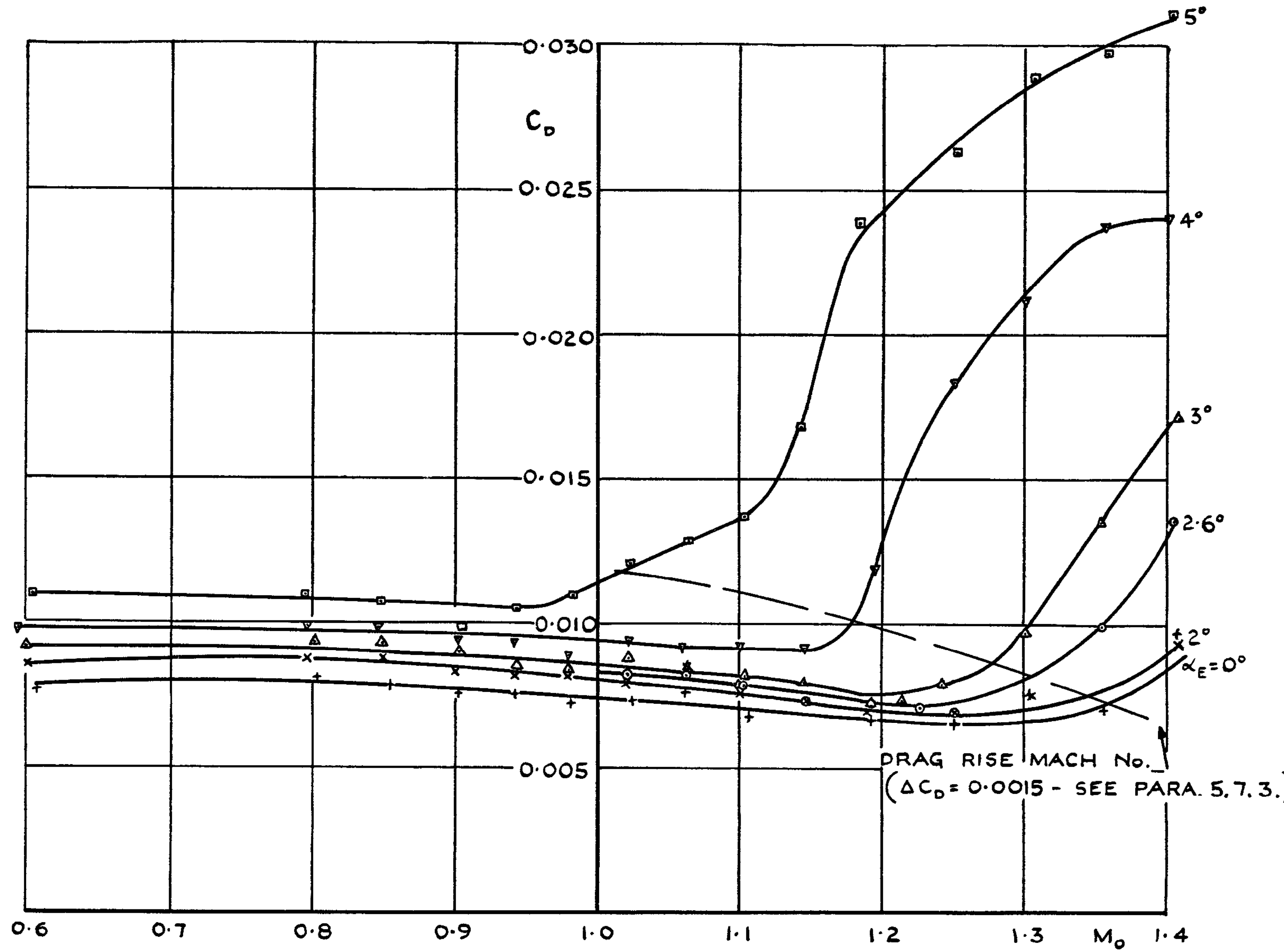

FIG. 23. SECTION DRAG COEFFICIENT vs MACH NUMBER FOR VARYING INCIDENCE (WITH "TUNNEL CORRECTIONS")

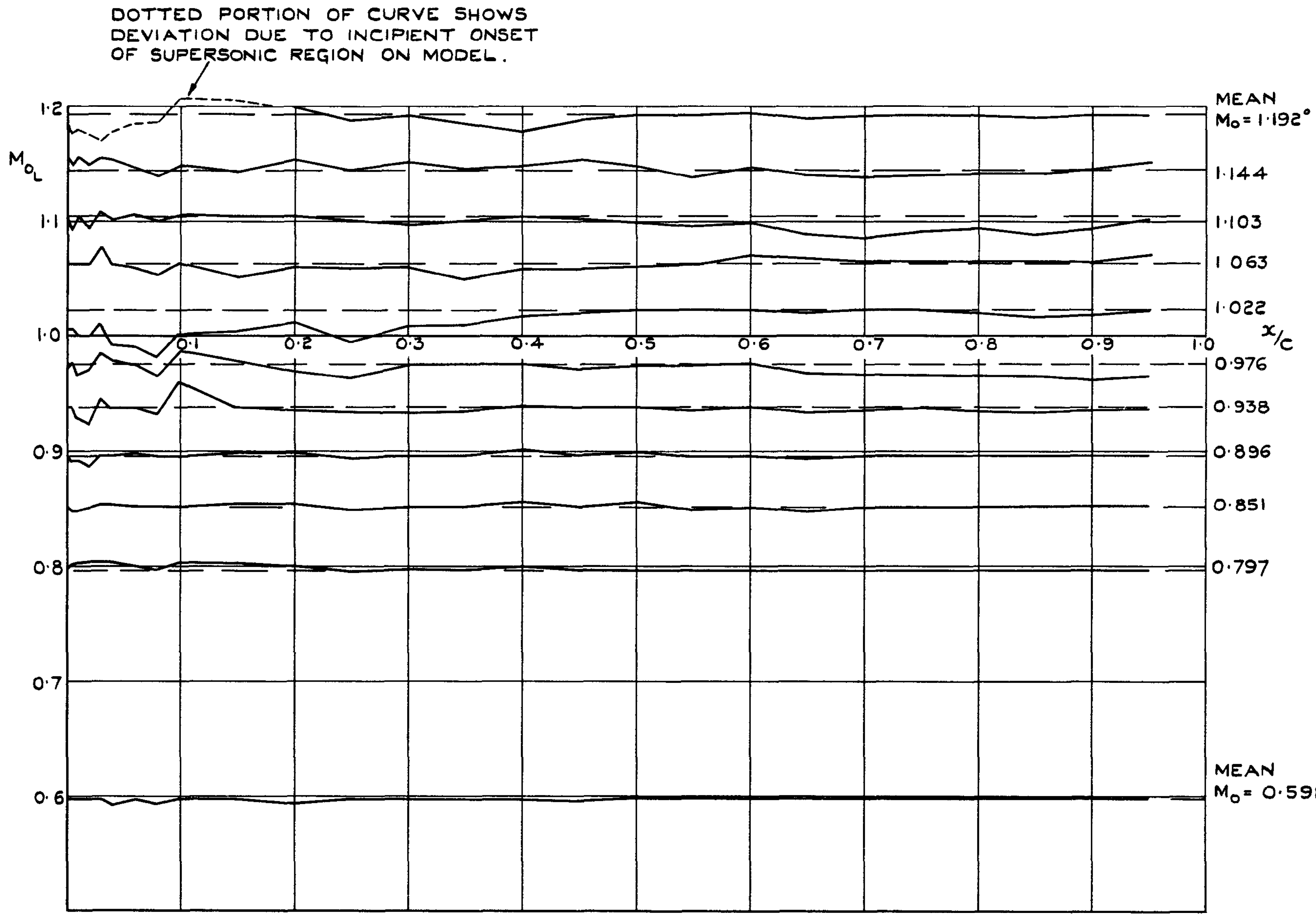

FIG. 24. TUNNEL MACH NUMBER DISTRIBUTION AT POSITION OF AEROFOIL.
(OBTAINED BY INTERPOLATION OF TEST RESULTS FROM UPPER SURFACE AT $\alpha_E = 2 \cdot 6^\circ$)

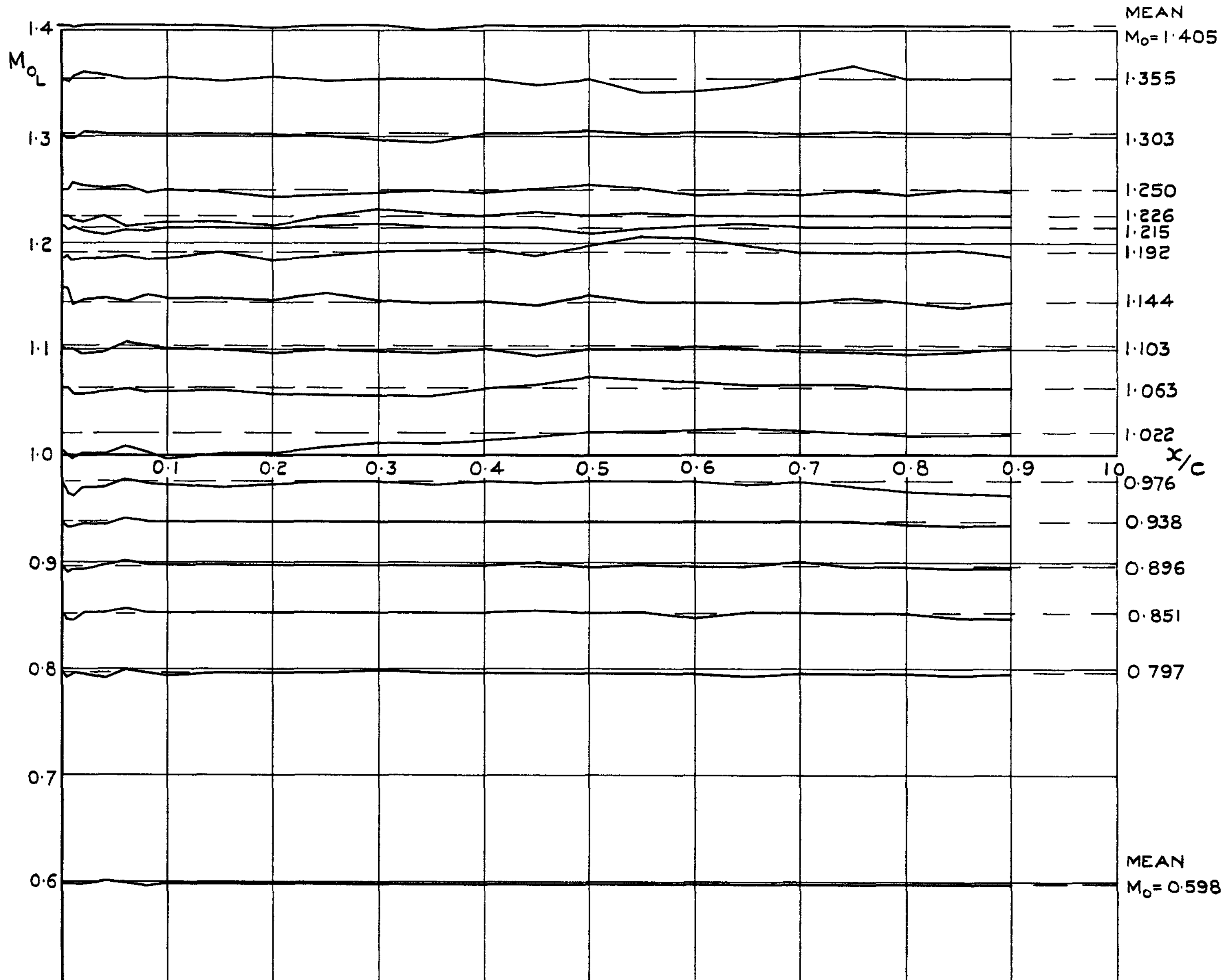

FIG. 25. TUNNEL MACH NUMBER DISTRIBUTION AT POSITION OF AEROFOIL.
(OBTAINED BY INTERPOLATION OF TEST RESULTS FROM LOWER SURFACE AT $\alpha_E = 2\cdot6^\circ$)

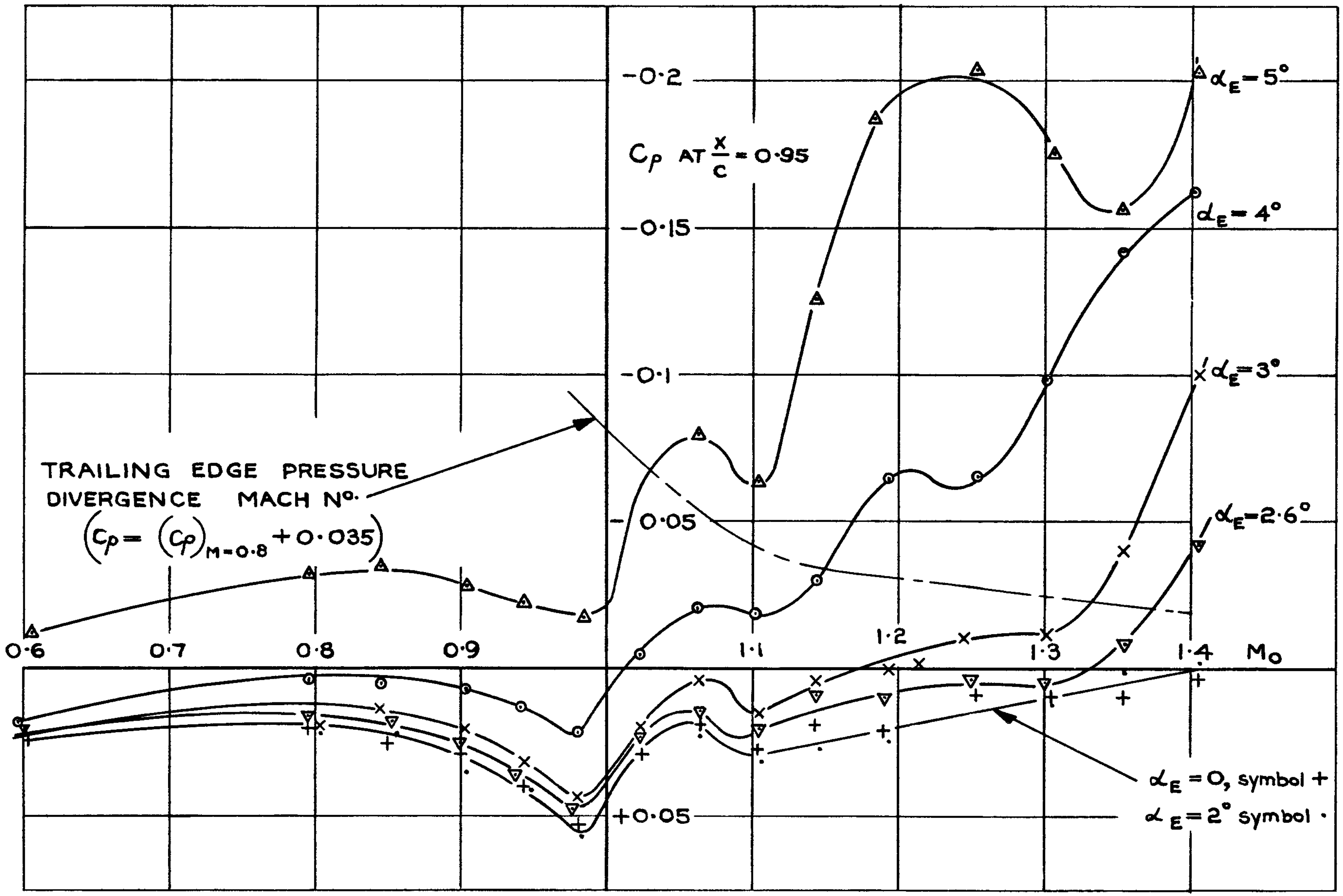

FIG. 26 PRESSURE COEFFICIENT AT 95% CHORD vs. MACH No. FOR VARYING INCIDENCE

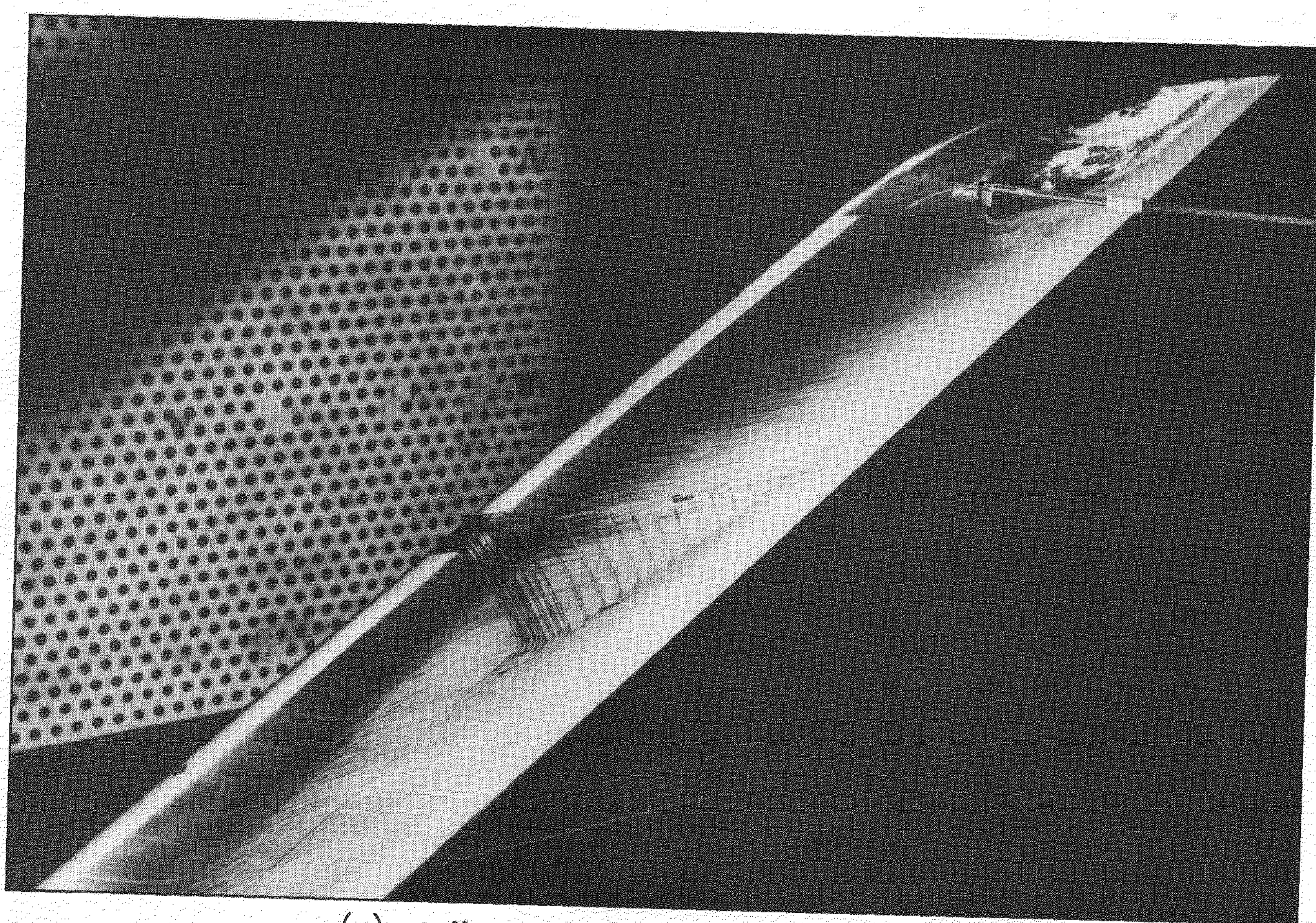

(a) $M_o = 1.25$, $\alpha_E = 2.6°$

a. OUTBOARD PART OF SPAN SHOWING PRESSURE MEASURING STATION

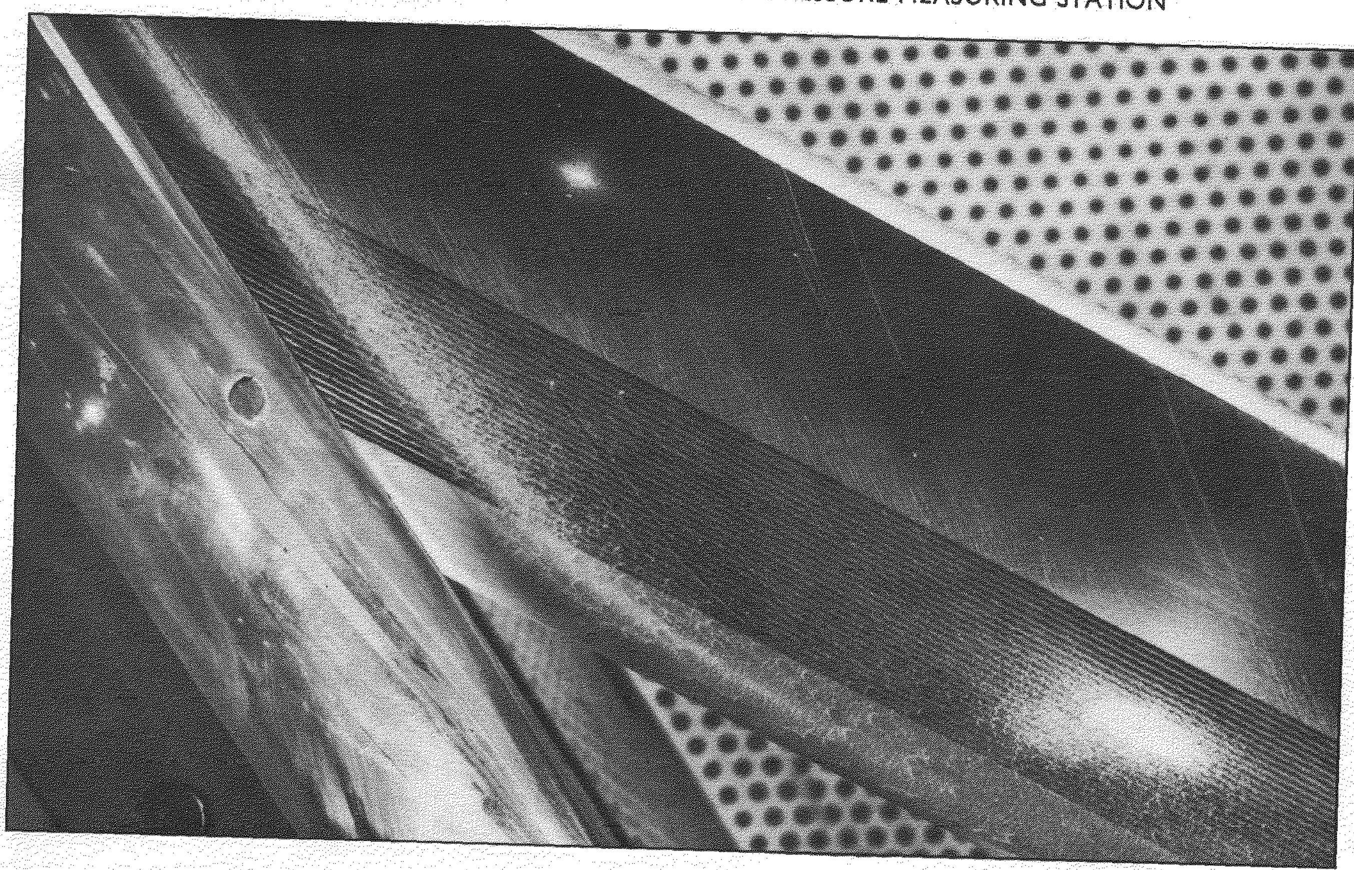

(b) $M_o = 1.25$, $\alpha_E = 2.6°$

b. WING BODY JUNCTION

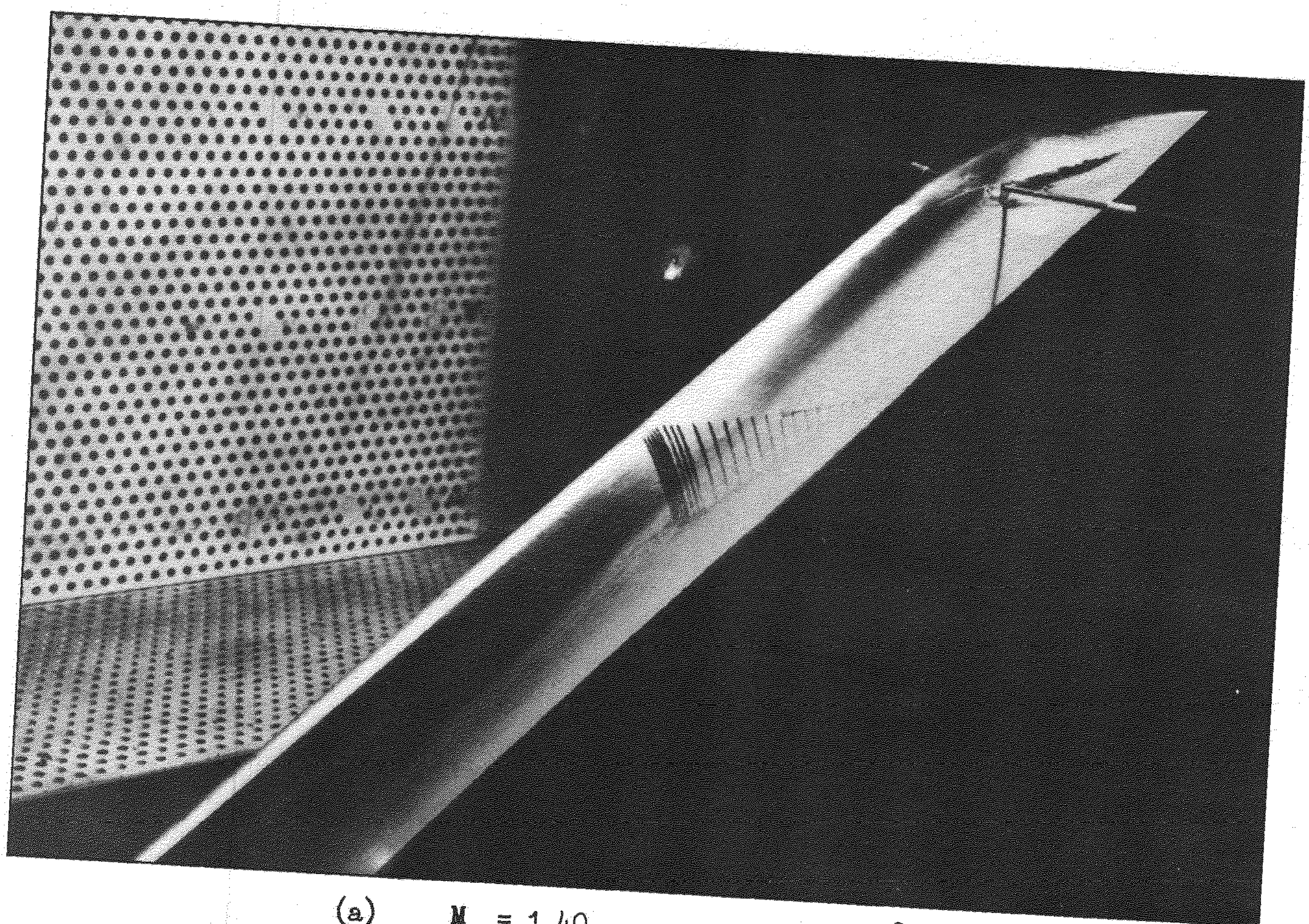

(a) $M_o = 1.40$, $\alpha_E = 2.6^\circ$

a. GENERAL VIEW OF WING

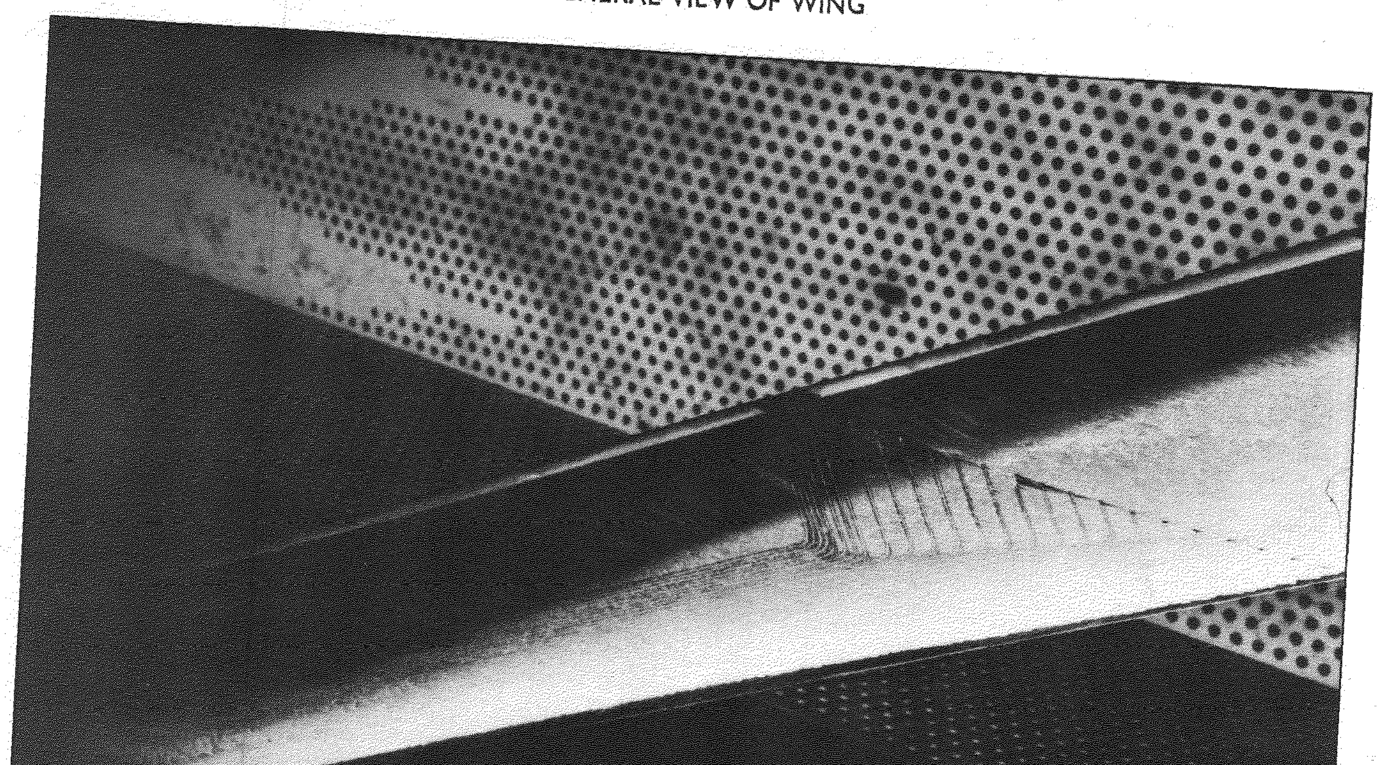

(b) $M_o = 1.40$, $\alpha_E = 2.6^\circ$

b. REGION NEAR PRESSURE MEASURING STATION

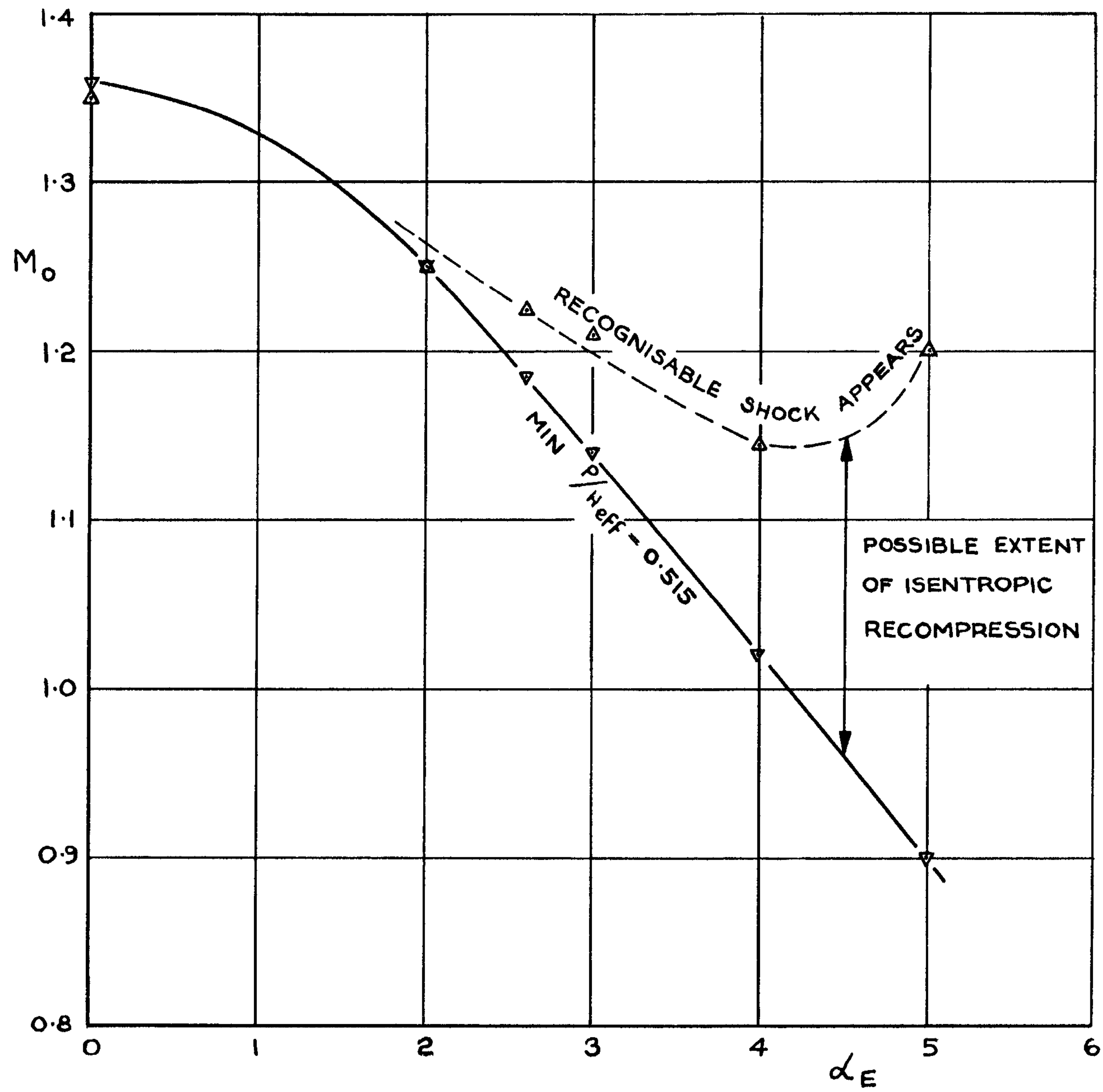

FIG. 29. MACH NUMBER FOR FIRST APPEARANCE OF SHOCK WAVE vs INCIDENCE; COMPARISION BETWEEN ESTIMATES BY METHOD OF REF. 14 AND OBSERVED VALUES (PARA. 5.7. 1.)

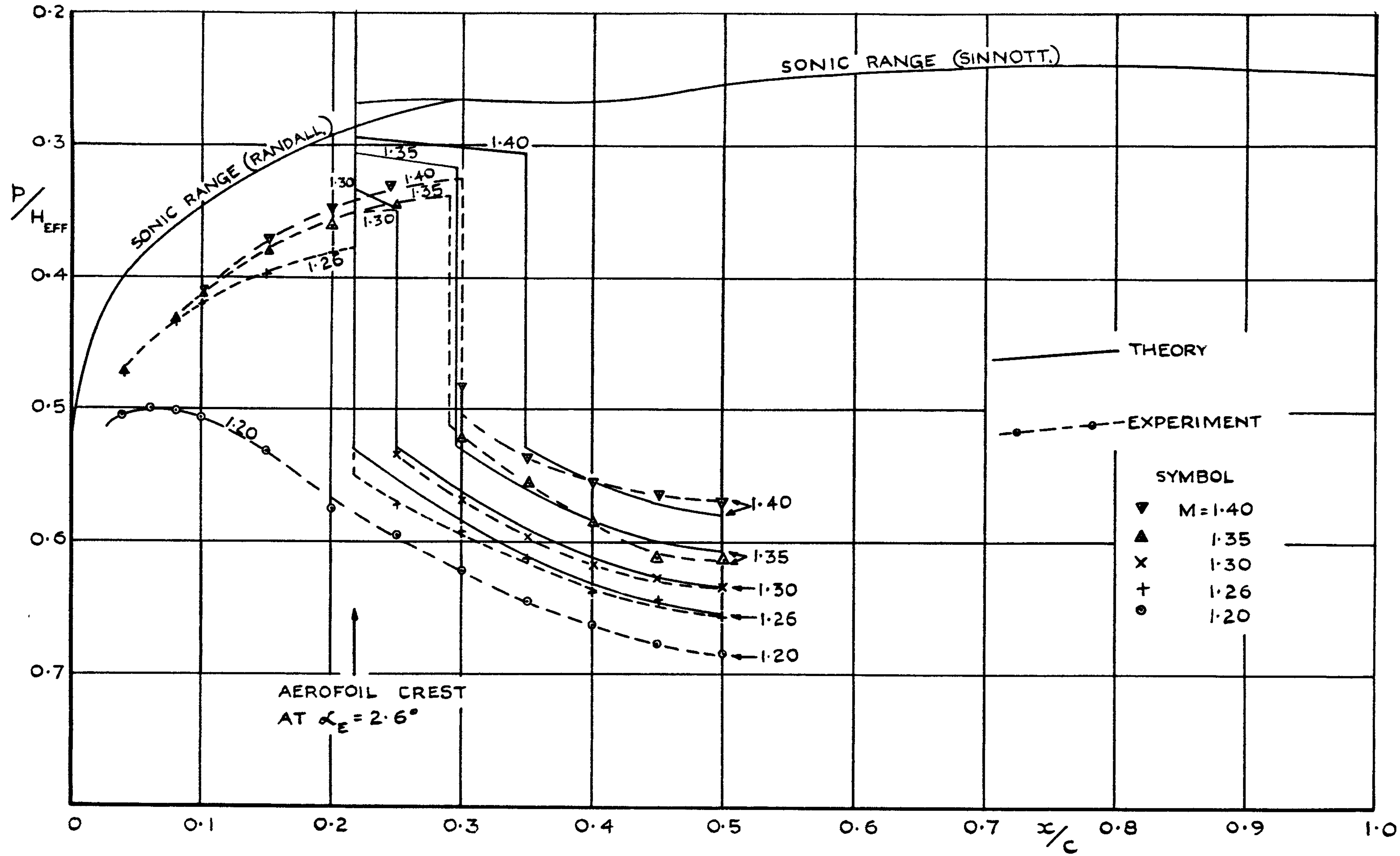

FIG. 30. COMPARISON OF THEORETICAL AND EXPERIMENTAL PRESSURE DISTRIBUTIONS WHEN THE SHOCK IS AFT OF THE AEROFOIL CREST ($\alpha_E = 2·6°$)

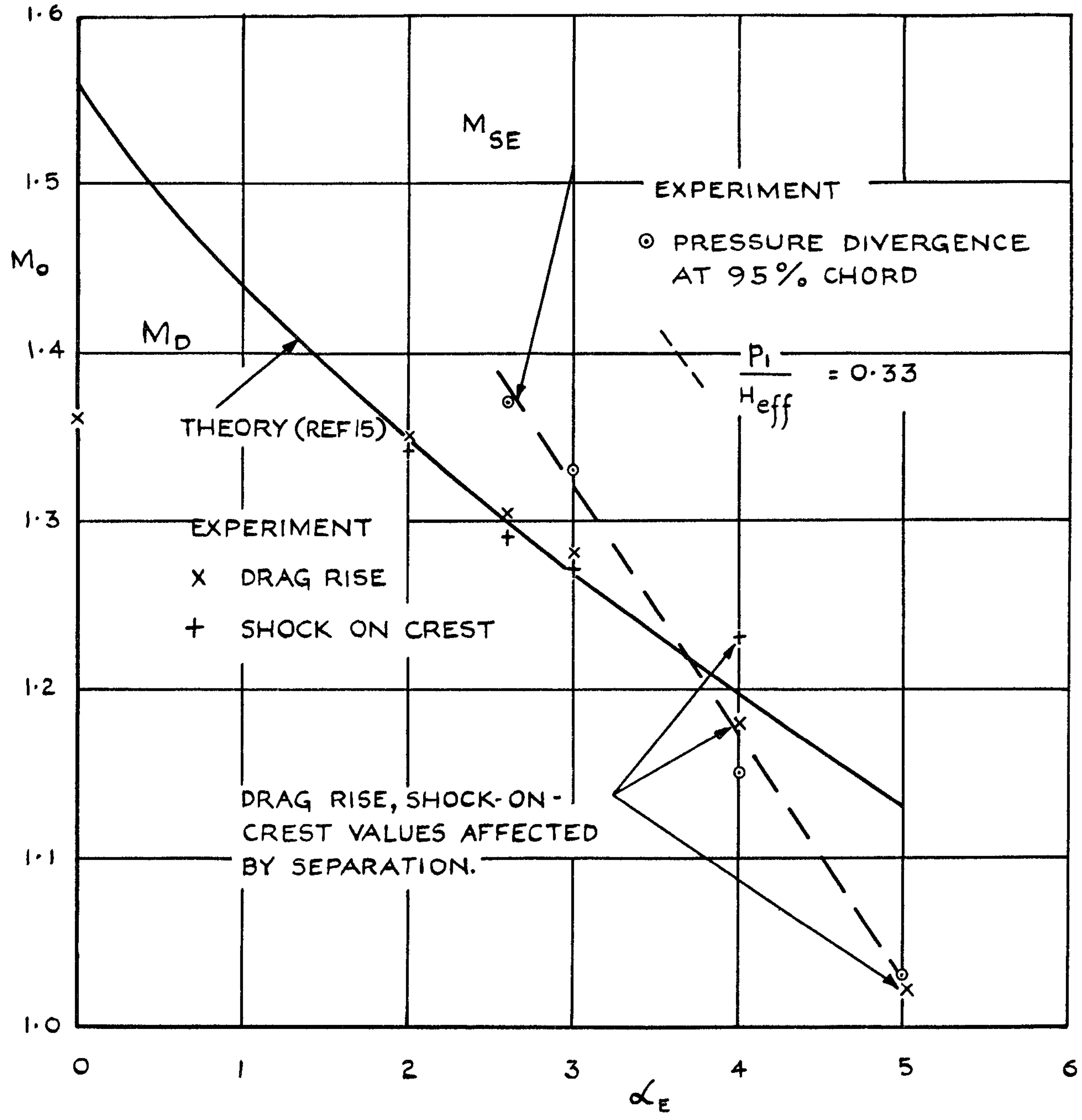

FIG. 31. MACH NUMBERS FOR DRAG RISE AND FOR ONSET OF SEPARATION EFFECTS vs INCIDENCE; COMPARISON BETWEEN THEORY AND EXPERIMENT.

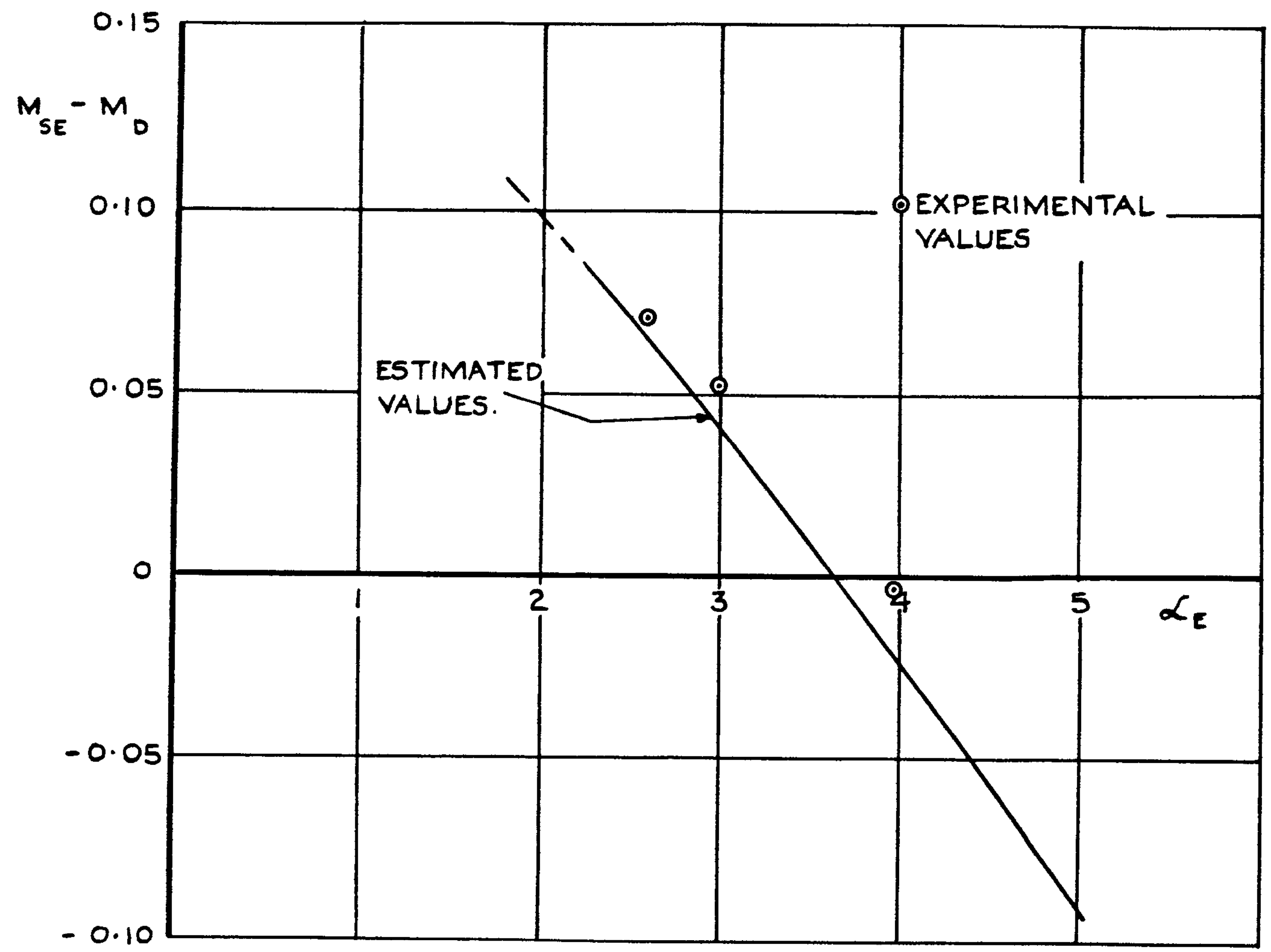

FIG. 32. VALUES OF MACH NUMBER MARGIN BETWEEN DRAG RISE AND ONSET OF SEPARATION EFFECTS vs INCIDENCE; COMPARISON BETWEEN THEORY AND EXPERIMENT.

A.R.C. C.P. No.582

533.692.1: 533.69.048.2:
533.693.1: 533.6.011.12:
533.6.011.35: 533.6.071.33
533.6.011.5:

WIND TUNNEL TESTS AT MACH NUMBERS BETWEEN 0.6 AND 1.4 OF A 60° SWEPT WING HAVING AN AEROFOIL SECTION DESIGNED FOR SUBCRITICAL FLOW AT A MACH NUMBER OF 1.2.
PART I: 9% THICK SECTION WITH "TRIANGULAR" PRESSURE DISTRIBUTION. Lawlor, E.F. May 1961.

Pressures have been measured at Mach numbers between 0.6 and 1.4 around one streamwise station on a 9% thick, 60° swept wing, cambered to have a subcritical type of upper surface pressure distribution of triangular shape at a Mach number of 1.2 and a lift coefficient of

P.T.O.

A.R.C. C.P. No.582

533.692.1: 533.69.048.2:
533.693.1: 533.6.011.12:
533.6.011.35: 533.6.071.33
533.6.011.5:

WIND TUNNEL TESTS AT MACH NUMBERS BETWEEN 0.6 AND 1.4 OF A 60° SWEPT WING HAVING AN AEROFOIL SECTION DESIGNED FOR SUBCRITICAL FLOW AT A MACH NUMBER OF 1.2.
PART I: 9% THICK SECTION WITH "TRIANGULAR" PRESSURE DISTRIBUTION. Lawlor, E.F. May 1961.

Pressures have been measured at Mach numbers between 0.6 and 1.4 around one streamwise station on a 9% thick, 60° swept wing, cambered to have a subcritical type of upper surface pressure distribution of triangular shape at a Mach number of 1.2 and a lift coefficient of

P.T.O.

A.R.C. C.P. No.582

533.692.1: 533.69.048.2:
533.693.1: 533.6.011.12:
533.6.011.35: 533.6.071.33
533.6.011.5:

WIND TUNNEL TESTS AT MACH NUMBERS BETWEEN 0.6 AND 1.4 OF A 60° SWEPT WING HAVING AN AEROFOIL SECTION DESIGNED FOR SUBCRITICAL FLOW AT A MACH NUMBER OF 1.2.
PART I: 9% THICK SECTION WITH "TRIANGULAR" PRESSURE DISTRIBUTION. Lawlor, E.F. May 1961.

Pressures have been measured at Mach numbers between 0.6 and 1.4 around one streamwise station on a 9% thick, 60° swept wing, cambered to have a subcritical type of upper surface pressure distribution of triangular shape at a Mach number of 1.2 and a lift coefficient of

P.T.O.

0.153. In spite of boundary layer effects which caused some loss of lift coefficient, subcritical flow conditions were achieved at the design Mach number of 1.2 with the design suction values over the forward part of the section. At all Mach numbers, the flow development was closely analogous to that over two dimensional aerofoils at subsonic speeds.

0.153. In spite of boundary layer effects which caused some loss of lift coefficient, subcritical flow conditions were achieved at the design Mach number of 1.2 with the design suction values over the forward part of the section. At all Mach numbers, the flow development was closely analogous to that over two dimensional aerofoils at subsonic speeds.

0.153. In spite of boundary layer effects which caused some loss of lift coefficient, subcritical flow conditions were achieved at the design Mach number of 1.2 with the design suction values over the forward part of the section. At all Mach numbers, the flow development was closely analogous to that over two dimensional aerofoils at subsonic speeds.

Published by
HER MAJESTY'S STATIONERY OFFICE

To be purchased from
York House, Kingsway, London w.c.2
423 Oxford Street, London w.1
13A Castle Street, Edinburgh 2
109 St. Mary Street, Cardiff
39 King Street, Manchester 2
50 Fairfax Street, Bristol 1
2 Edmund Street, Birmingham 3
80 Chichester Street, Belfast 1
or through any bookseller

Printed in England

S.O. CODE No. 23-9012-82

C.P. No. 582